Report Prepared by :

K. Lau
A. A. Sagüés
L. Yao

CORROSION PERFORMANCE OF CONCRETE CYLINDER PILES
Contract No. BC353 RPWO#10
Final Report to Florida Department of Transportation

A. A. Sagüés
Principal Investigator
Department of Civil and Environmental Engineering

University of South Florida
Tampa, FL, 33620
February 28, 2005

Technical Report Documentation Page

1. Report No.	2. Government Accession No.	3. Recipient's Catalog No.
BC353 - 10		

4. Title and Subtitle	5. Report Date
CORROSION PERFORMANCE OF CONCRETE CYLINDER PILES	February 28, 2005
	6. Performing Organization Code

7. Author(s)	8. Performing Organization Report No.
K. Lau, A. A. Sagüés, L. Yao	

9. Performing Organization Name and Address	10. Work Unit No. (TRAIS)
Department of Civil and Environmental Engineering University of South Florida Tampa, FL 33620	11. Contract or Grant No. BC353 - 10

12. Sponsoring Agency Name and Address	13. Type of Report and Period Covered
Florida Department of Transportation 605 Suwannee St. MS 30 Tallahassee, Florida 32399 (850)414-4615	Final Report 9/01/00 - 2/28/2005
	14. Sponsoring Agency Code

15. Supplementary Notes

Prepared in cooperation with the USDOT and FHWA

16. Abstract: Cylinder bridge piles that are produced by a centrifugally cast, vibrated, roller compacted process (also known as Raymond piles) have shown promising resistance to reinforcement corrosion in earlier FDOT surveys. This investigation examined additional FDOT bridges built with cylinder piles for evidence of similar corrosion resistance and considering updating guidelines for corrosion performance of these piles. Survey of three 40-year old marine bridges indicated in general minor or no corrosion distress of the spiral reinforcement in the piles, even though the concrete clear cover was on average only ~ 1.2 in (~30 mm). Chloride diffusivity was small with median value ~0.005 in^2/y (~1.10^{-13} m^2/s), lower than the typical results obtained in modern FDOT class V concretes for aggressive marine service. Other physicochemical concrete tests were also indicative of very low permeability. Thin concrete cracks not caused by corrosion were observed in some of the piles but preferential chloride penetration along the cracks was less pronounced than noted earlier in conventional marine substructure. Investigation of a 2 year old bridge with modern cylinder piles showed also excellent resistance of the bulk concrete to chloride penetration. Thin cracks (not caused by corrosion distress) were observed as well, with some evidence of enhanced chloride penetration, therefore continued monitoring of these spots as the bridge ages is recommended. The chloride threshold value for corrosion initiation in the older bridges is estimated to be above ~2 pcy (1.2 kg/m^3) and possibly considerably higher. The concrete in the new bridge piles had a desirably high pore water pH despite its high pozzolanic content, suggesting that chloride threshold in the new material will be normal. Simplified corrosion damage projections suggest that if concrete quality could be sufficiently assured, moderate relaxation of present cover requirements for new construction with cylinder piles could be made without severely compromising the requirements for minimum corrosion damage within a 75-year service life goal.

17. Key Word	18. Distribution Statement
Corrosion, Piles, Cylinder, Raymond, Steel, Chloride, Diffusion	No Restriction This report is available to the public through the NTIS, Springfield, VA 22161

19. Security Classif. (of this report)	20. Security Classif. (of this page)	21. No. of Pages	22. Price
Unclassified	Unclassified	115	

Form DOT F 1700.7 (8-72) Reproduction of completed page authorized

Table of Contents

NOTICE

Executive Summary

Cylinder bridge piles that are produced by a centrifugally cast, vibrated, roller compacted process (also known as Raymond piles) have shown promising resistance to reinforcement corrosion in an earlier FDOT field investigation. That work, performed on the twin Escambia Bay bridges, showed minimal corrosion damage after 30 years of service even though clear concrete cover over reinforcement was only 1.1 in (2.75 cm). Cylinder piles are encountering renewed applications in FDOT projects. However, present FDOT guidelines for reinforcement corrosion protection in aggressive marine service specify at least 3 in (7.6 cm) cover, which tends to constrain the manufacturing process and mechanical performance of cylinder piles. This investigation examined whether other FDOT bridges built with cylinder piles showed similarly high corrosion resistance and sought to establish any factors responsible for that performance, with a view to considering redefining cover guidelines for construction.

Cylinder piles of three ~40 year old FDOT bridges, and another one newly built, were examined to establish corrosion performance. Activities performed included visual surveys, coring to assess chloride penetration and steel condition, and other electrochemical as well as physicochemical concrete property measurements in the field and laboratory.

The results for the older bridges (Hathaway, Pensacola Bay, and Brooks - all in the Florida panhandle) indicated in general only minor, highly isolated or nonexistent corrosion distress of the spiral reinforcement in the piles (with exception of damage near pile caps likely reflecting original mechanical distress, and earlier repair patches for topical deterioration). This performance is noteworthy in view of the very thin concrete clear cover measured (~ 1.2 in (~30 mm) on average). Whenever exposed by coring, the deeper grouted strand was unaffected or showing only vestigial corrosion. The good corrosion performance in spite of low cover was consistent with the observation of very slow chloride ion penetration. An indicator of the chloride penetration rate, the apparent diffusion coefficient, had in the older bridges a median value of only ~0.005 in^2/y (~1.10^{-13} m^2/s). That value is significantly lower than the typical results obtained in a recent study of modern FDOT class V concretes for aggressive marine service. Other physicochemical concrete tests were also indicative of very low permeability. The results for the older bridges were also in general agreement with those obtained in the earlier Escambia Bay investigation. Thin (< 0.013 in(<0.3 mm)) concrete cracks were observed in some of the piles in the 40-year old bridges. However, preferential chloride penetration along the crack was less

pronounced than in cases recently noted in other FDOT bridges with conventional concrete substructure

The newer bridge (St. George Island) was in service for only a short time and chloride penetration rate measurements are consequently subject to significant uncertainty. Nevertheless, the results were also indicative of average excellent resistance of the concrete to chloride penetration, which is expected to improve as long term aging takes place. Physicochemical tests of the concrete also indicated very good performance. Concrete from one of the piles examined showed somewhat faster chloride penetration than elsewhere, but it is suspected that the pile section sampled was of a different mix design intended for higher elevations. As in the older bridges, thin cracks (not caused by corrosion distress) were observed here as well. Cores centered on those cracks showed some evidence of enhanced chloride penetration at shallow depths. Also average concrete resistivity of those cores was smaller than for sound adjacent concrete controls, suggesting some enhanced electrolyte transport from the crack presence. Continuing monitoring of these spots as the bridge ages is recommended. As expected from the early time in service, no corrosion distress from reinforcement corrosion was identified in this bridge.

The combined information from nearly corrosion-free condition in the older bridges, measurements of concrete cover, and chloride concentration profiles, was used to obtain an estimate of the lower bound of the prevalent range of effective critical chloride threshold values for corrosion initiation in the order of ~2 pcy (1.2 kg/m^3), although effective threshold values may be considerably higher. This lower bound is consistent with the reported high cement content of the concrete (650-800 pcy, (350 to 500 kg/m^3)) and the observation of pH values in extracted cores that approached (although not always) normally expected values. The concrete in the new bridge piles had a desirably high pore water pH despite its high pozzolanic content, suggesting that chloride threshold values in the new material will be in the normal range.

Simplified corrosion damage forecasts were made for the older and new piles using the apparent chloride transport parameters observed, actual and alternative cover values, threshold bound values, and informed assumptions for the other model parameters. The projections suggest that if concrete quality could be sufficiently assured, moderate relaxation of cover requirements for new construction (for example from 3 in (7.5 cm) to 2 in (5 cm) could be made without severely compromising the requirements for minimum corrosion damage within a 75-year service life goal. Recommendations of alternative cover guidelines are presented for consideration of manufacturing and quality control factors.

1 Introduction

1.1 Project Scope

Corrosion of steel in marine concrete structures can be envisioned as a two-stage process. In the first (initiation) stage chloride ions penetrate through the concrete cover until the concrete surrounding the steel is contaminated to a critical concentration threshold C_T that triggers active corrosion of the steel. In the second (propagation) stage the steel corrodes actively and expansive corrosion products damage the surrounding concrete, until externally visible signs of distress appear. Repair or rehabilitation is usually required at that moment. The corrosion-limited durability of a given portion of the structure can then be measured in terms of the sum of the times elapsed during the initiation t_i and the propagation t_p stages [1].

Durability design strategies adopted by the FDOT seek to extend t_i as much as possible, since control of corrosion after initiation is comparatively difficult. The time t_i becomes longer with greater concrete cover, and less permeable concrete. Increased C_T, and lower chloride levels at the concrete surface also extend t_i but are less amenable to control during design. As a result, the present FDOT design guidelines address minimum concrete cover and concrete quality as the principal means to obtain durability expectations of many decades. Concrete cover is particularly important since corrosion forecasting models indicate that, all else being equal, t_i is proportional to the square of the concrete cover thickness (for example, reduction of the cover from 3 to 1.5 in (7.5 to 3.8 cm) would shorten the initiation stage by 75%). Consequently, there is reluctance to reduce clear cover requirements unless exceptional circumstances arise. Indications of apparently exceptional corrosion resistance have been obtained in a 1997-8 assessment [1] of the substructure of the Escambia Bay Bridges (EBB), No. 580071 and 580058, located in highly aggressive estuary water with chloride concentrations exceeding 10,000 ppm at times. The substructure of these bridges was built in 1966 using circular Centrifugally Cast, Vibrated, Roller Compacted (CEN-VI-RO process) Raymond piles. There are 268 54-in (1.4 m) diameter and 1,218 36-in (0.9 m) diameter cylinder piles in water. The nominal clear concrete cover for the spiral hoop reinforcement of either size of pile is only 1 3/8 in (3.5 cm), and actual cover values as small as 3/4 in (1.9 cm) were recorded. Despite the low cover, aggressive environment, large number of cylinder piles and 30-year long exposure, no indication of significant corrosion damage was found in the cylinder piles. Detailed examination of

chloride penetration was performed in 17 cores extracted from the piles. Analysis of chloride concentration profiles yields a value of D, the apparent chloride diffusion coefficient of the concrete and an indication of its permeability to chlorides. The analyses indicated values of D that in most cases were less than 0.01 in^2/y ($2x10^{-13}$ m^2/s), among the lowest values ever determined for any FDOT bridge substructure examined to date [2].

Although D was small, the concrete cover was thin, which allowed appreciable chloride buildup at the hoop reinforcement depth. In the tidal zone, that chloride concentration had already exceeded commonly accepted C_T values for plain steel bars. In the absence of corrosion damage, that indicated that either corrosion was already in progress but at a very slow rate (a large value of t_p), or that the value of C_T for the spiral steel/concrete combination was higher than encountered in conventional reinforced concrete. Chloride concentrations close to commonly accepted C_T values were observed in the splash-evaporation zone, suggesting that corrosion there could begin in the relatively near future.

A corrosion degradation forecast model was developed for the EBB [1] based on the corrosion assessment data and information on the performance of structures elsewhere. The model parameters included assumed values for C_T and t_p that reflected the present condition of the structure. The forecast functions projected significant but still moderate corrosion damage development over the next 60 years of service. The damage projections were used together with cost data for repair procedures to estimate life-cycle costs over that period. The life cycle cost estimates for the next 60 years indicated that keeping the present substructure in service was preferable to demolition and erection of a new bridge.

The present condition and favorable durability projections for the EBB have encouraged consideration of the use of the same type of pile for new FDOT bridges in aggressive environments. Because cylinder pile construction is optimized for relatively low concrete covers, there is considerable interest in establishing whether normal cover requirements (presently 3 in (7.6 cm) [3]) could be relaxed for that type of pile, if possible, to thicknesses comparable to those used in the EBB. The feasibility of reliably constructing 36-in (0.9 m) or 66-in (1.7 m) diameter cylinder piles with 3 in (7.6 cm) covers has been questioned [4], and there is also concern that cracks may develop more easily when the cover is thick. Unfortunately the information available from the 1997-8 survey, although encouraging, is too limited to fully substantiate the use of concrete covers much thinner than present specifications for a 75-year design service life goal. Only a limited number of cylinder piles was examined in detail, and as indicated before the deterioration models had to assume critical parameter values in lieu of limited or absent information on the same.

The present investigation is intended to expand the knowledge on the present performance, and its future prognosis, of cylinder piles in FDOT structures. It was examined whether other FDOT bridges built with cylinder piled showed corrosion resistance comparable to that encountered in the EBB. It was also sought to establish any factors responsible for that performance, with a view to considering redefining cover guidelines for cylinder pile construction.

The performance of cylinder piles in major structures worldwide was briefly reviewed. Cylinder piles of three ~ 40 year old FDOT bridges, and another one newly built, were examined to establish corrosion performance. Activities performed included visual surveys, coring to assess chloride penetration and steel condition, and other electrochemical as well as physicochemical concrete property measurements in the field and laboratory.

A brief review of documented cylinder pile performance is presented in the following. Methodology and findings of the field and laboratory investigations are detailed in the subsequent sections.

1.2 Performance of Cylinder Piles

Cylinder pile manufacturing has been reviewed in detail elsewhere [5- 9]. Based on the available records reported in literature [8,10-14], personal communication with DOT personnel and Bayshore Concrete Products Corporation (BCP), it is conservatively estimated that at least 75 bridges have been built as of 2002 with Raymond Piles in the United States. As shown in Table 1.2, Raymond piles are used in coastal states such as Florida, Georgia, Alabama, Mississippi, Louisiana, South Carolina, North Carolina, Virginia, Maryland, New York, New Jersey, and Rhode Island.

A number of investigations have documented cracks in Raymond Piles [11-13]; however, most of the cracks were found to be minor or moderate without severe chloride buildup in adjacent areas [11-12]. The cracks were not likely caused by the expansion of corrosion products but rather by elastic rebound of prestress ducts, differential shrinkage, frost damage, or damage from hammering [12]. Fuller [8] discussed durability issues of Raymond Piles structures in severe environments (Table 1.1). A brief survey of Raymond Pile bridges as of 2002 was prepared under this study and a sampling of findings it is listed in Table 1.2. The results are indicative of generally good corrosion performance, with the caveat that thin cracking, usually longitudinal and normally neither a cause nor a consequence of corrosion, has been reported in many instances.

Table 1.1 Performance of Structures on Raymond Piles [8]

Location	Structures	Year of construction	Year of Examination	Performance
Gulf of Mexico	six offshore platforms	1950	1955	very satisfactory
Eugene Island	offshore structures	1955	1975	very good
Quarantine Bay, La*	Gulf Oil Company platform	1950	1968	prestressed wires in the concrete was clean and rust-free
Black Bay	Offshore platform	1952	1968	no evidence of corrosion; surface of piles were free of defects
Pass Christain, Mississippi	a breakwater	1958	1978	no signs of any concrete deterioration
Lake Pontchartrain, LA	Lake Pontchartrain causeway	1964	1977	in excellent condition
Lower Chesapeake Bay, VA	The Lower Chesapeake Bay-tunnel	1955 (old); 1969 (new)	1978	in excellent condition
Lake Maracaibo, Venezuela	several platforms, piers, bridges, breakwater and bulkheads	1956	1978	no evidence of concrete corrosion was found on piles and no evidence of internal steel corrosion.

* The piles were broken by a hurricane in 1965; those damaged piles were then exposed in marine environments for three years before examination.

Table 1.2 Sampling of Bridges Built with Circular Piles and Performance Notes- 2002 summary. See also Table 1.1.

State/ No.	Bridge Name	Location	Year Built	Appx. Length	Pile Diam.(in)	Performance
Florida						
1	Escambia Bay (EB)	Escambia Bay	1966	13597'	54&36	no significant corrosion damage found on piles in 1997(1)
2	Escambia Bay (WB)	Escambia Bay	1966	13597'	54&36	no significant corrosion damage found on piles in 1997(1)
3	Brooks	Okaloosa	1964	1318'	36	substructure was in satisfactory condition in June, 2001(2)
4	Pensacola Bay	Pensacola Bay	1960	15640'	54	substructure was in satisfactory condition in June, 2001(2)
5	Hathaway	Panama City	1960	3358'	54	substructure was in fair condition in February, 2001(2)
6	Lake Underhill	Orlando	1974	N/A	36	N/A
7	St.George Island	St. George Island	2003	3.1mile	54	under construction in 2002
Louisiana						
1	Lake Pontchartrain Causeway	New Orleans	~1955	24 mile	54	vertical hairline cracks were found on some piles in 1995 (3) some localized damage to transverse joint epoxy seal (4)
2	Lake Pontchartrain Causeway	New Orleans	~1965	24 mile	54	vertical cracks were found on some piles in 1995 (3)
3	4500700651 (EB)	Baton Rouge	N/A	N/A	54	moderate damage and hairline cracks were found
4	4500700652 (WB)	Baton Rouge	N/A	N/A	54	on some piles in 1998 (5)
5	4500614951 (EB)	Baton Rouge	N/A	N/A	54	N/A
6	4500614952 (WB)	Baton Rouge	N/A	N/A	54	hairline cracks on some piles (1998) (5)
7	4501400001 (EB)	New Orleans	N/A	N/A	54	hairline cracks on some piles (1998) (5)
8	4501400002 (WB)	New Orleans	N/A	N/A	54	hairline cracks on some piles (1998) (5)
9	US 11 bridge	New Orleans	N/A	4.76 mile	54	N/A
10	west pearl bridge	N/A	N/A	N/A	N/A	hairline crack over post-tensioning duct (4)
11	Wax Lake Outlet bridge	New Orleans	N/A	N/A	N/A	hairline crack over post-tensioning duct (4)
Georgia						
1	Elba Island	Elba Island	N/A	1780'	54	N/A
2	State Road 303 Turtle River	Glymm Co.	1963~1965	2968'	54&36	N/A
3	South Bronswick River	Glymm Co.	1963~1964	1160'	54&36	N/A

Table 1.2 (Continued)

State/ No.	Bridge Name	Location	Year Built	Appx. Length	Pile Diam.(in)	Performance
New York						
1	Loop Parkway	Nassau Co.	~1999	N/A	66	N/A
2	Peconic River Bridge	N/A	N/A	N/A	54	N/A
3	Lake Chautauqua Bridge	Chautauqua Co.	N/A	N/A	36 or 54*	N/A
4	Cooper & Wando Rivers Bridge	N/A	N/A	N/A	36	N/A
5	Ponquogue Ave. Bridge	Long Island	N/A	N/A	54	N/A
6	Sag Harbor Bridge	N/A	N/A	N/A	36	N/A
7	Wantagh Parkway over Goose Creek	N/A	N/A	N/A	54	N/A
8	NYDOT Pedestrian	N/A	N/A	N/A	36	N/A
9	Cross Bay Boulevard	N/A	N/A	N/A	54	N/A
Virginia						
1	James River	Newport News	1980	23200'	54	In good or fair condition (7)
2	Monitor –Merrimac Bridge Tunnel (#2236)	Newport News	1990	16685'	54	In good or fair condition (7)
3	Monitor –Merrimac Bridge Tunnel (#2237)	Newport News	1990	16636'	54	In good or fair condition (7)
4	Hampton Roads Bridge Tunnel (EB)	Norfolk	1974	5925'	54	In good or fair condition (7)
5	Hampton Roads Bridge Tunnel (WB)	Norfolk	1957	6151'	54	In good or fair condition (7)
6	City of Norfolk (#1865)	Lafayette River	1994	1755'	36	In good or fair condition (7)
7	City of Norfolk (#1866)	Lafayette River	1970	1755'	36	In good or fair condition (7)
8	Coleman Bridge	Yorktown	1952	3750'	54	N/A
9	Chesapeake Bay Bridge Tunnel	Chesapeake Bay	1960~1964	17.6 mile	54	vertical cracks found on some piles (1988) (5.6)

Table 1.2 (Continued)

State/ No.	Bridge Name	Location	Year Built	Appx. Length	Pile Diam.(in)	Performance
Maryland						
1	William Preston Lane Memorial (WB)	Annapolis	~ 1973	4.3 mile	54	severe cracks found on piles; cracks were epoxied (5)
2	Patuxent River Bridge	N/A	N/A	N/A	54	N/A
3	Severn River Bridge	Anne Arundel	N/A	N/A	54	N/A
4	Bridge over Bear Creek	N/A	N/A	N/A	36	N/A
5	Miles River Bridge	Rt. 370	N/A	N/A	54	N/A
6	Choptank River Bridge	Dorchester Co.	N/A	N/A	54	N/A
7	Sassafras River Bridge	N/A	N/A	N/A	42	N/A
8	Nanticoke River Bridge	Dorchester Co.	N/A	N/A	66	N/A
9	Back River Bridge	N/A	N/A	N/A	54	N/A
10	Deal Island Bridge	Somerset Co.	N/A	N/A	54	N/A
11	Bohemia River	Cecil Co.	N/A	N/A	N/A	N/A
North Carolina						
1	Nelson's Bay	Carteret Co.	1982	1480'	54	piles were in satisfactory condition in 1999(8)
2	Lake Drummond Canal (Bridges #43)	Camden Co.	1982	2132'	54	piles were in satisfactory condition in 1999(8)
3	Lake Drummond Canal (Bridges #44)	Camden Co.	1982	2132'	54	piles were in satisfactory condition in 1999(8)
4	Bonner Bridge	Dare Co.	1962	12,865'	66	piles were in acceptable condition in 1999(8)
5	Sneads Ferry	Onslow Co.	1993	2781'	54	piles were in poor condition and repaired in 2000 (8)
6	Oregon Inlet Bridge	NC 12	N/A	N/A	66	piles were in good condition in 2000(8)
7	Chowan River Bridge	Bertie Co.	1996~2000	9500'	66	N/A

Table 1.2 (Continued)

State/ No.	Bridge Name	Location	Year Built	Appx. Length	Pile Diam.(in)	Performance
New Jersey						
1	Great Egg Harbor Inlet	Ocean City	2001	3450’	54	Under construction(9)
2	Watson’s Creek	Rt. 29, 10B	1990	1500’	36	Acceptable(9)
3	Watson’s Creek	Rt. 29, 10B	1991	1000’	54	Acceptable(9)
4	Risley’s Channel	Rt. 152, 1B	1989	1425’	54	Acceptable(9)
5	Crosswick’s Creek	Rt.295	1994	1400’	54	Acceptable(9)
6	Watson’s Creek	Rt. 295, 17H	1991	700’	36	Acceptable(9)
7	Watson’s Creek	Rt. 295, 17H	1991	700’	54	Acceptable(9)
8	Navasink River	Rt.35	2000	1000’	54	Acceptable(9)
9	Barnegat Bay (WB)	Rt.37	1974	4750’	N/A	Acceptable(9)
10	Absecon Inlet Bridge	N/A	N/A	N/A	36 or 54*	N/A
11	Middle Thorofare Bridge	Cape May Co.	N/A	N/A	36	N/A
South Carolina						
1	Cooper River Bridge	Charleston	~ 1992	5.1 mile	54	N/A
Rhode Island						
1	Jamestown-Verrazzano Bridge	N/A	N/A	7350’	36	N/A
California						
1	San Diego-Coronado Bridge	San Diego	1967~1969	11,179’	54	cracks appeared on piles during construction and delivery in 1969(5)
Mississippi						
1	Bayou Bernard	Harrison Co.	2000	1378’	66	N/A
2	west pearl bridge	N/A	N/A	N/A	54	N/A
Alabama						
1	Mobile Bay Causeway Bridge	N/A	N/A	N/A	54	Vertical hairline cracks randomly distributed on the piles (5)

Table 1.2 (Continued)

Location/ No.	Bridge Name	Location	Year Built	Appx. Length	Pile Diam.(in)	Performance
Puerto Rico						
1	Arecibo River Bridge	N/A	N/A	N/A	36	N/A
2	Rio LaPlata Bridge	Toa Baja	~ 1984	2541'	54	N/A
3	Victor Rojas (Rehabilitation)	N/A	N/A	N/A	54	N/A
4	Santo Domingo	N/A	N/A	N/A	54	N/A
5	Deigo Expressway	N/A	N/A	N/A	36	N/A
6	Rio Grande De Loiza	N/A	N/A	N/A	54	N/A
Saudi Arabia						
1	Ju'Aymah Trestles	Saudi Arab	1977~1979	6 mile	54&66	marine mollusk borers attacked the piles in 1982(10); vertical cracks were found on the piles(11)

Table 1.2 Notes

(1) A..A. Sagüés et al, "Assessment of Rehabilitation Alternatives for Bridge Substructure Components", Draft Report, Jan. 1998, SPN: 58002-1445, WPI: 3148533

(2) FDOT bridge management system comprehensive inventory data report

(3) Guy F. LeMieux, "Underwater inspection of the world's longest overall bridges, part I", Concrete International, Feb.1998 pp67-70

(4) Ahn, Woosuk, et al. "A study on corrosion resistance of prestressed marine concrete piles." Corrosion 2003. March 16, 2003.

(5) R.R. Avent and D.J. Mukal, "Investigation of Cracks in Cylindrical Spun-Cast Concrete Piles in a Marine Environment", Final Report for Louisiana Transportation Research Center, 1998

(6) Donald R. Garder, "Inspection of substructure of the Chesapeake bay bridge-tunnel above and below the waterline", Transportation Research Record, pp130-137

(7) Jack Meredith, Virginia DOT

(8) Laura E. Sutton, North Carolina DOT
this bridge was subjected to extreme scour; the pile condition didn't necessarily reflect the adequacy of the piles.

(9)Jack Mansfield from New Jersey DOT provided this information

(10) R. K. Snow, "Attack by Lithophaga and Cliona on Marine Concrete Structures: Some Prevention and Control Measures", Oxford &IBH Publishing Co. PVT. Ltd, 1988

(11) Ben C. Gerwick, "International Experience in the Performance of Marine Concrete", Concrete International, May 1990, pp47-53.

2 Investigation Methodology

2.1 Bridges Investigated

Cylinder piles of three ~40 year old FDOT marine bridges, and another one newly built (Table 2.1), were examined to establish corrosion performance. The newly built bridge, constructed in 2003, was examined to compare corrosion performance of cylinder piles representative of current FDOT building guidelines to that of piles several decades old. The cylinder piles in all bridges in the study showed joints indicative of segmented construction characteristic of Raymond Piles. Further evidence of Raymond Pile construction was observed from the presence of grout around strands exposed by coring in the Hathaway and Pensacola Bay Bridge. Personal communications[1] confirmed Raymond Pile construction for the Hathaway Bridge.

Table 2.1 Surveyed Bridges

Bridge	Number	Year Built	Inspection Date	Location	Water Chloride Content (ppm)[2]	Length	No. of Bents/ Cylinder Piles	Pile Diameter
Hathaway	460012	1960	Dec. 2002	Panama City, FL	25 560	3 359 ft. (1 024 m)	34 / 74	54 in. (1.37 m)
Pensacola Bay	480035	1960	March 2003	Pensacola, FL	7 374	15 640 ft. (4 767 m)	257 / 916	54 in. (1.37 m)
Brooks	570034	1964	March 2003	Ft. Walton Beach, FL	9 833	1 318 ft. (402 m)	14 / 80	36 in. (0.91 m)
St. George Island (SGI)	490003	2003	March 2004	St. George Island, FL	8 875	21 615 ft. (6 588 m)	~165 / ~646	54 in. (1.37 m)

[1] Don Theobald, V.P. Engineering, Gulf Coast Prestress, Inc. and Bob Bruce, Ph.D., Catherine and Henry Boh Chair in Civil Engineering, Tulane University, formerly of Raymond International.
[2] FDOT records.

The Escambia Bay Bridges, also in the Florida Panhandle coast and built with Raymond Piles, were surveyed in 1997 in a manner similar to that used here. The results of that investigation have been reported elsewhere [1] and are used here for comparison whenever appropriate

2.2 Methodology

Field activities involved in the inspection of the concrete cylinder piles were coordinated among personnel from the Corrosion Laboratory of the FDOT Materials Office and the Corrosion Engineering Laboratory of the University of South Florida (USF). Subsequent laboratory experiments were conducted by USF personnel at the Corrosion Engineering Laboratory at the University of South Florida and at the FDOT Materials Office; some chloride analyses were contracted to A&S Laboratories, Clearwater, FL.

2.2.1 Field investigation methods

Field bridge evaluation included visual surveying for corrosion distress, concrete core sampling, testing of probable corrosion status, and concrete internal relative humidity measurements. Prior accounts of bridge deficiencies as documented by FDOT inspections can be found in the FDOT Bridge Management System bridge inspection reports [15-17]. All accessible marine piles in each bridge were visually examined, except for the newly constructed St. George Island (SGI) Bridge where only selected piles installed at the beginning of construction were addressed. A general survey of the piles was taken first by boat from approximately 6 feet (~ 2 m) away, systematically progressing along both sides of pile group bents. Attention was focused on the tidal and splash zones of the piles where corrosion of steel reinforcement is expected to be most severe. Notation and photographic documentation of distress type and location were made. Piles that exhibited severe signs of corrosion distress were selected for examination at close range by docking the boat to the pile group bent. Hammer soundings were conducted on selected piles with severe rusting or other signs of distress to determine the presence and extent of concrete delamination (internal separation of concrete). The presence of concrete spalls (actual, partial or total loss of cover concrete) either pre-existing or as a result of hammer testing were noted as well. The type, width (measured with a CTL crack comparator gage), and probable cause of observed cracking were assessed. For those piles where reinforcement steel had been exposed during coring, half-cell potentials were measured with a saturated copper/copper sulfate reference

electrode (CSE). Electrical continuity between the steel reinforcement hoop wire and strands was tested when possible.

Concrete internal relative humidity (IRH) measurements using a procedure described elsewhere [18] were made when permitted by time constraints. A Vaisala humidity/temperature probe was inserted into a sealed cylindrical cavity, bored to a depth of 1.25 in (~ 3.2 cm) from the pile external surface (Figure 2.1), effectively sampling the humidity of air in equilibrium with the concrete at the bottom of the cavity. A closed-cap stabilization time of ~ 20 hours was typically allowed after drilling/installing the fitting and the first IRH measurement; the fittings were left in place for future monitoring. The internal relative humidity was sampled at elevations approximately 6 in (~ 0.15 m) and 5 feet (~ 1.5 m) above high tide (AHT).

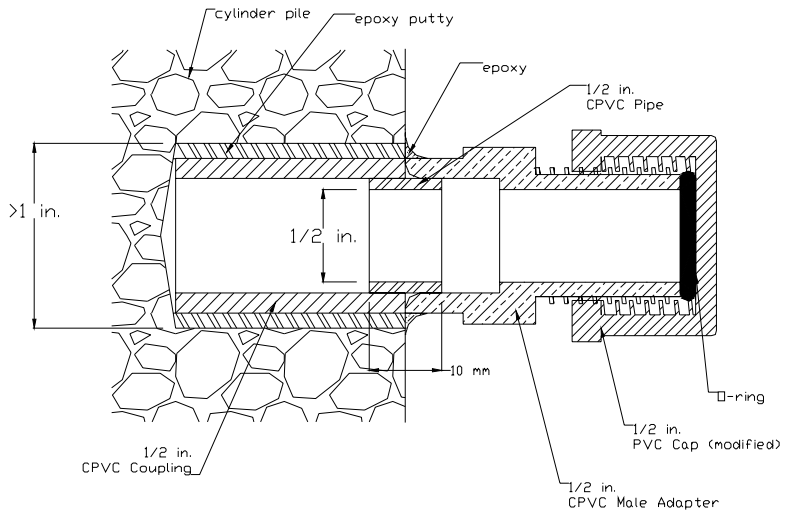

Figure 2.1 Schematic of concrete internal relative humidity set-up

Concrete core samples were extracted from the piles at the tidal and splash zones as well as at higher elevations. A nominally 2 in (~ 5 cm) diameter cylindrical core drill bit was used resulting in cores ~ 1.75 in (~ 4.5 cm) in diameter. Coring of concrete samples was made to depths ~3.5 in (8.9 cm) or upon reaching post-tension strands. The intersecting spiral wire and spacing rebars were typically severed by coring in the older bridges in the study; they were not severed in the SGI Bridge. The strand assembly was not severed, but may be nicked by the coring drill bit. The bit was continuously cooled with fresh water while drilling. Core sample elevations ranged from -6 in to 5 feet (~ -0.15 to ~ 1.5 m) AHT. The cores were typically extracted in pairs along the same

elevation 6 in (~ 0.15 m) apart on center. If a noticeable vertical concrete crack was observed, two pairs of concrete cores were extracted around a given elevation. One core from each pair was centered on the crack, and the four cores formed the corners of a square 6 in (~ 0.15 m) on the side.

Additional samples including 3.5 in (8.9 cm) diameter concrete cores of piles that have not been placed in service were gathered from cutoff pile segments from construction of the SGI Bridge.

2.2.2 Laboratory experimental methods

For chloride analysis selected cores were wet cut with a fine blade tile saw, cooled with fresh water, to obtain thin slice sections. Thinner sections were cut near the external concrete surface to better assess the rapid change of chloride concentration near the external surface. The thin sections were ground into powder for analysis. The initial ~ 0.08 in (2 mm) of the concrete core was directly powdered by shaving in a lathe and carefully collecting the powder. The concrete cores extracted from the SGI Bridge piles, which had very narrow chloride concentration profiles, were sampled for near surface chloride concentration using profile grinding [19]. A $9/16^{th}$ in (1.4 cm) diameter carbide-tipped T-slot cutter was used to mill layers from the concrete core as thin as ~ 0.04 in (1 mm). Thinner and more frequent layers were milled at the external surface of the concrete core. Thicker sections were subsequently sampled from portions deeper into the concrete by milling larger depths and cutting thin slices with a fine blade tile saw.

Some of the 3.5 in (8.9 cm) diameter concrete cores from unused pile sections of the SGI Bridge were used to make specimens for ponding with salt solution following a modified Nordtest method [20], to measure chloride penetration parameters. Cut samples, approximately 1.5 in (3.8 cm) in length, were sealed with epoxy leaving only the cut surface exposed to ~ 2.8 M NaCl solution by means of a dam constructed for each individual sample. The salt solution was filled to a depth 0.5 in (1.3 cm) and was periodically changed with new solution. Ponding was conducted for an extended period (~ 22 months) in consideration of the anticipated high quality of the concrete. Profile grinding was conducted by the milling procedure described above.

The sampled concrete powder was normally analyzed for total chloride content following the regular FDOT procedure [21]. Samples of concrete cores where chloride penetration had been significant due to longer exposure to seawater were contracted for chloride analysis to a certified FDOT provider (A&S Laboratories, Clearwater, FL). For concrete cores where near-surface chloride

penetration was sampled by profile grinding the FDOT procedure was modified to use a smaller amount of powder per test (typically 1.5 g instead of 3 g). Control tests with concrete samples of known chloride content showed no significant loss in accuracy; the homogeneity of the powder sample was addressed by thoroughly mixing the sample and making duplicate measurements. In all cases the concrete powder was oven dried ~105^{o}C and digested with boiling nitric acid solution. The dissolved chlorides were filtered from the undissolved remnants such as sand. Potentiometric titration, with a silver ion selective electrode and $AgNO_3$ titrant, was conducted to measure the chloride content of each sample. Results are reported in Section 2.4.1 as a ratio of chloride mass to dry concrete mass, mg Cl^- per g of dry concrete $(\frac{mg}{g})$.

An apparent chloride diffusivity D, chloride surface concentration C_s, and native chloride concentration C_o were obtained by fitting the measured chloride content and depth profile to an idealized diffusion profile described by Eq.1 [22].

$$C(x,t) = C_s - (C_s - C_o)\ \mathrm{erf}\ \frac{x}{2\sqrt{Dt}} \qquad (1)$$

where t is the time of service in seawater upon extraction and x is the depth from the concrete core external surface. It is noted that this profile results from assuming ideal Fick's 2nd law diffusion behavior with time- and space-invariant diffusivity in a homogeneous medium, as well as a constant surface concentration and uniform initial concentration [22]. The resulting fit parameters are consequently only nominal values.

Additional tests aimed at assessing concrete permeability were conducted by conditioning selected cores in 100% relative humidity chambers. Concrete water absorption was monitored upon reaching constant saturated weight. Electrical resistivity was measured with a CNS Electronics RM MKII Wenner-array probe or a Nilsson Model 400 resistivity meter set up with a 4-point electrode configuration. The terminal wet resistivity, corrected for core geometry [23] is reported as ρ_{wet}. Internal concrete relative humidity for selected core samples was monitored for ambient and conditioned environments. A sealed cylindrical cavity was bored from the original surface of concrete samples collected from the unused portion of the SGI Bridge piles. Similar to field measurements, a Vaisala humidity/temperature probe was inserted into the cavity sampling the humidity of the air in equilibrium with the concrete. The IRH of the concrete was initially recorded in ambient conditions and subsequently measured as the samples were being conditioned in 100% relative humidity chambers. Concrete permeability was also tested by density, absorption, and porosity measurements following ASTM C 642 standard procedures [24].

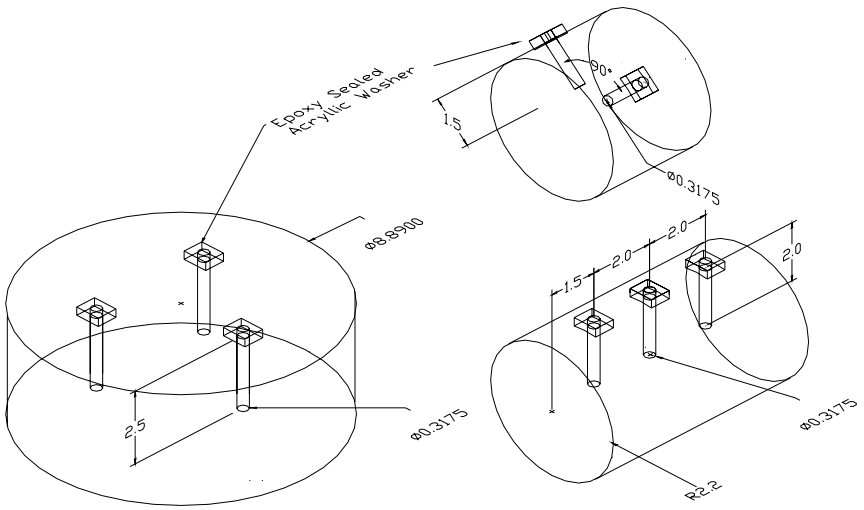

Figure 2.2 Schematic of ISL concrete samples. (dim. in cm)

Other concrete cores and cable grout samples similar to those used to grout pre-stressing steel were conditioned in 100% relative humidity and used to measure the pH of pore water solution using the in-situ leaching technique (ISL) [25]. Different sample configurations (Figure 2.2) were made depending on the geometry of the specimens. Acrylic washers and rubber stoppers were used to seal residue-free equidistant cavities drilled with a 1/8th in (3.2 mm) masonry drill bit to depths as shown in Figure 2.2. Distilled water was pippetted into the cavities depending on the size of the cavities and in consideration for time required for equilibrium between the surrounding pore water and the cavity water. For the 3.5 in (8.89 cm) and 1.75 in (4.44 cm) diameter cores, and core fragments with shorter lengths, the amounts of distilled water used were 0.15 mL, 0.10 mL, and 0.08 mL respectively. If the water in the cavities dried up, the pH measurements were repeated by introducing new distilled water into the cavities. Measurements were made with a micro-pH electrode calibrated with certified pH buffer solutions.

3 Field Investigation Results

3.1 Hathaway Bridge

A detailed review of the survey results is included in Appendix I Table A1a. Cylinder piles, all 54-in diameter, were typically configured four to a bent and located in the approach spans. As a naming convention for this report, the bents were numbered from the west and the piles were numbered from the south. Throughout this report individual piles are named as in the following example: H-8-2 for Hathaway Bridge bent 8, pile 2. Center span piers[3] numbered 15 to 28 were comprised of square piles and will not be considered here. A total of 76 piles were examined.

3.1.1 Concrete Observations

The majority of the piles showed no visual signs of corrosion distress. Seven piles had rust stains typically ~ 1 foot (~ 0.30 m) below pile cap in the atmospheric exposure zone where severe chloride-induced corrosion is less common. These stains are likely to result from rust of steel exposed due to mechanical damage from pile driving. Three piles had rust stains at intermediate elevations, and only four piles showed rust stains at low elevations (splash zone). Few cracks were noted.

Coring in this bridge was conducted in one pile each from bents 8 and 29. Pile H-8-2 was one of those exhibiting rust stains in the tidal/splash zone as well as some concrete delamination. Six cores were extracted in pairs at elevations below high tide, within splash zone, and at atmospheric exposure zone. The core samples were labeled H-8-2-1 through H-8-2-6. Pile 3 of bent 29 (H-29-3) had a hairline crack ~ 0.013 in (~ 0.3 mm) thick, but no rust was observed. Four cores were extracted in pairs from the splash zone and at atmospheric exposure zone, labeled H-29-3-1 to H-29-3

[3] Numerical labels of center span piers are continuous with approach span bents as convention for report.

3.1.2 Steel Condition Observations

The coring of the piles sampled exposed steel that was cut and removed with the core or steel that showed at the bottom of the core hole where the core broke off. Most of the exposed steel was ¼ in (6.3 mm) diameter spiral hoop reinforcement. Post tensioning strand was exposed at the bottom of two of the cores. One of those cores, H29-3-3 clearly showed grout and the trace of the duct opening around the strand. A spacing rebar ½ in (~ 1.27 cm) diameter was cut in one core.

Visual condition of the exposed steel and clear concrete cover values are detailed in Appendix III, Table A3. For this and the other older bridges, the exposed steel in most instances could be broken cleanly from the surrounding concrete and had a dull to lustrous gray mill scale appearance, with no discernable rust. This no-corrosion condition, exemplified in Figure A4, is denoted by NC in the following. In a few instances the exposed hoop steel or spacing bar showed faint rust-colored discoloration on part of the exposed surface, as illustrated in Figure A5. Also in a few cases the exposed strand showed similar minor discoloration together sometimes with tiny rusty dots or stringers on the matching strand imprint on the surrounding grout (Figure 3.3). No cross sectional steel loss of any significance was observed associated with these cases, and it was not clear whether the discoloration represented corrosion that took place in service, or prior to casting. These light corrosion situations are denoted by LC in the following.

All steel exposed by coring in this bridge fell under the NC or LC categories. Despite the presence of an external rust stain on the concrete in the pile cored in Bent 8, both the steel reinforcement and strand exposed there had an NC visual appearance. In the Bent 29 pile the core revealing a strand and a spacing rebar was drilled centered on a vertical hairline crack, and both steel surfaces had an LC rating. However, as shown later there was no evidence of significant enhanced chloride penetration from analysis of that core.

The cumulative distributions of clear cover values for this and the other bridges investigated are shown in Figure A2, and the results are summarized in Table A2. The average cover value for spiral reinforcement in the cores from this bridge was 1.20 in (3.1 cm). While this value represents measurements from only two columns in the bridge, it is close to the 1½ in (~ 3.8 cm) cover value inferred from the construction drawings for this bridge archived in the FDOT District 3 Structures Office. There the cover to the strand duct opening is listed as 1¾ in (4.4 cm); subtracting the ¼ in thickness of the hoop wire assumed to be place immediately next to the opening yields 1.5 in.

As expected, there was electrical continuity between spiral hoop reinforcement exposed at the perimeter or bottom of different core holes of the same pile. The one spacing rebar exposed was also continuous with the spiral wire. The two exposed strands were found to be not continuous to the other steel in the same pile, which is consistent with the construction method of Raymond piles where the strand is placed and grouted afterwards.

3.1.3 Field Measurements of Steel Potential and Concrete Moisture

Half-cell potentials as function of elevation are listed in Appendix III Table A5 and a summary is shown in Figure 3.1. Potential levels of -200 mV and -350 mV CSE are traditionally associated with indications of unlikely to likely ongoing corrosion, respectively, in atmospherically exposed concrete [26]. While the potential readings more negative than -350 mV CSE in Figure 3.1 are not a reliable indicator of corrosion in progress in wet concrete [27], values more positive than -200 mV CSE as seen at elevations above 1 to 3 ft (0.3 to 0.9 m) strongly suggest that the steel above those elevations was in the passive condition at the time of the measurements. The potential of the spacing rebar with surface rated as LC in the core drilled on a crack 5 feet (~ 1.52 m) AHT in H-29-3 was -96 mV vs. CSE at that elevation, suggesting that active corrosion was not in progress there when tested.

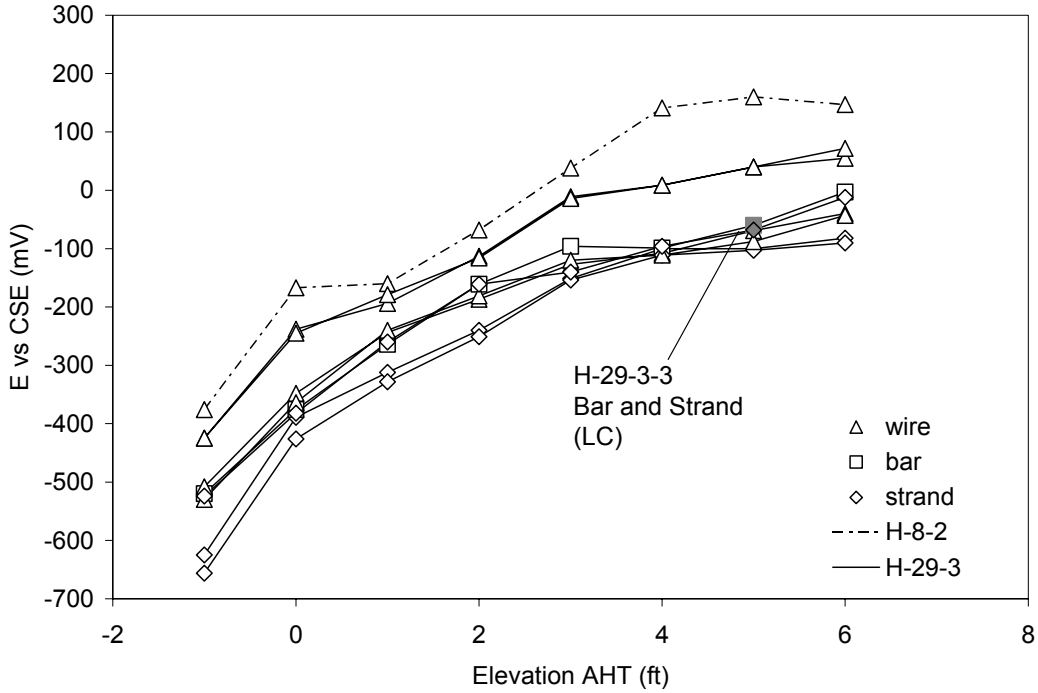

Figure 3.1 Hathaway Bridge half-cell potential measurements. ■ near steel under LC rating.

Concrete internal relative humidity measurements were taken from the same two piles (H-8-2 and H-29-3). Measurements were taken at elevations within the tidal/splash zone and atmospheric exposure zone as listed in Appendix III Table A7. IRH measurements were made approximately 18 hours after the test fittings, described in Section 2.2.1, were installed and sealed. IRH measurements were made for approximately 1 hour after inserting the Vaisala probe into the fitting. Figure 3.2 shows the measured IRH as function of time upon insertion of the Vaisala probe into the fitting. These tests show that concrete IRH was generally higher at the tidal/splash zone (expected to have a higher water content) than at higher elevations. Ambient conditions upon completion of testing were ~85% RH and ~15^{o}C

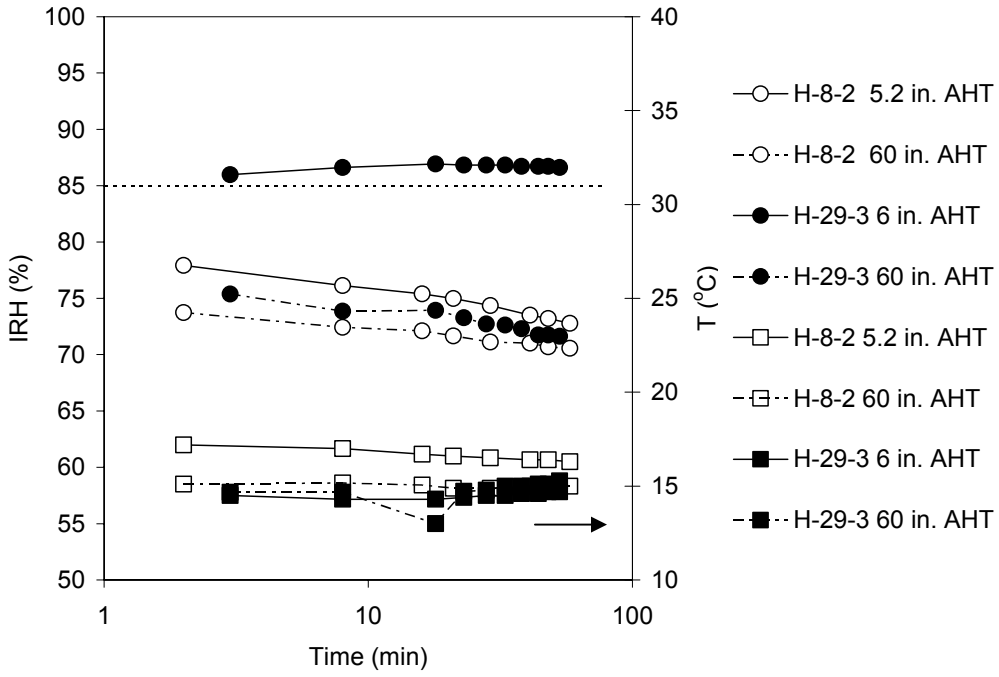

Figure 3.2 Hathaway Bridge concrete internal relative humidity. Measurement readings as function of time after probe insertion, 18h after fitting installation. ○ ● IRH. □ ■ Temperature.

3.2 Pensacola Bay Bridge

A detailed review of the inspection survey is included in Appendix I, Table A1. Bents in the approach spans of the Pensacola Bay Bridge are typically arranged by four (normal piers) or six (tower piers, typically every 15 bents) cylinder piles, all 54-in diameter. The bents are numbered from the north and piles from the east. Bents 256 and 257 were not surveyed due to accessibility

issues. Piles from piers 112-145 from the center span column piers were below tidal zone and were not inspected. A total of 908 circular piles were examined.

3.2.1 Concrete Observations

A cumulative count of deterioration features is shown in Figure A3 in Appendix II. The most commonly observed features, seen on ~ 25% of the piles examined, were rust stains typically one per affected pile and only a few square in (1 in^2 ~ 6.3 cm^2) in size. The stains were larger, of the type shown in Figure A1, in only 15 of the 908 piles examined. Repair patches were the next most common feature, often located just below the pile cap and occasionally at intermediate elevations ~ 1 to 3 feet (~ 0.3 to 0.9 m) AHT. Nearly all of the patches were in the south approach spans, and ~ 40% of the observed rust stains in the south approach spans were on preexisting repair patches. As shown in Figure A3, rust stains not on repair patches were nearly evenly distributed along the bridge.

Concrete spalls already in place and associated with rust stains were observed only on six piles, each deteriorated area on separate piles. Those spalls were all small and in four instances (not further examined) only of thumbnail size and very shallow. As shown below, later hammer sounding revealed delaminations and created new spalls at nine other rust stain areas from eight other piles. Thin vertical cracks were occasionally observed but nearly always not together with any corrosion damage. The cumulative deterioration counts in Figure A3 (b) were roughly evenly distributed along the bridge.

Sixteen piles (fourteen among those that exhibited sizable rust stains and two with thin cracks ~ 0.013 in (0.3 mm) in width but no rust stains, Appendix I, Table A1b) were selected for closer inspection. Twelve of those piles, with severe rust stains not associated with repair patches or preexisting spalls, were hammer sounded to detect delamination. In four of the twelve the concrete was found to be sound despite signs of external rust staining. Delaminations were detected in the remaining eight and hammering continued to remove the affected cover concrete. The delaminated areas were not very large, ranging in size from ~ 4 in^2 to 81 in^2 (~ 26 cm^2 – 523 cm^2), and the depth of the newly created spalls was typically only ~0.5 in (10 mm) with no steel directly exposed. Coring was performed on the center of the spall in pile P-185-2 and on the center of the top spall in pile P-185-4, revealing in both cases clearly corroded spiral wire immediately below the bottom of the spall. The sixteen piles included also the two piles with significant preexisting spall cases, which showed no directly exposed steel. Coring was performed on the center of one of those spalls (P-110-2-2), revealing steel ~ 0.25 in (6 mm) with an LC surface appearance below.

Hammer sounding of the piles with longitudinal cracks (P-4-1 and P-213-4) revealed no delamination, and coring on the cracks showed steel with no visual signs of corrosion.

3.2.2 Steel Condition Observations

Spiral reinforcement steel exposed by coring at most locations in this bridge was rated NC, and the surface of the spiral steel on the core drilled through the delamination/spall at 14 in (0.36 m) AHT on P-110-2-2 was only rated LC. However, the cores on spalled or delaminated areas in piles P-149-2, P-185-4 drilled 26 and 32 in (0.66 and 0.81 m respectively) AHT respectively revealed steel with localized but appreciable corrosion loss of metal. The damage is illustrated in Figure A6 (representative of both cases), showing that as much as ¼ of the wire cross section was lost near one end of the wire segment cut out by the core. With the exception of damage near the pile caps noted earlier, these two cases were the only direct observations of severe corrosion in all the field inspections and are denoted by SC in the following. All spacing bars exposed in this bridge, including one next to the SC steel in P-185-4 were rated NC.

Pressurized grout post-tensioned strands have been identified in four core locations (Table A3). The strands exposed from P4-1-4 and P110-2-2 were rated LC (Figure 3.3), and the other two (237-1-2, and 252-1-1) were rated NC. Surrounding grout was clearly visible in all cases strand was exposed. The grout around the NC strand from cores P237-1-2 and P252-1-1 appeared to have partial (<~ 0.40 in (10 mm)) voids suggesting partial consolidation (Figure 3.4). No evidence of corrosion was found associated with these voids, but good grout consolidation is an important quality control issue for future construction.

There were signs of other steel (possible spacing rebar) exposed at the bottom of the core hole at three other coring locations, but residual concrete there prevented detailed observation other than noting absence of any signs of rust.

The distribution of measured clear cover of spiral hoop steel is shown in Figure A2, Appendix II. As shown in Table A2 the average concrete clear cover to hoop reinforcement was thin — 2.33 cm which is ~ 20% lower than in the other older cylinder pile bridges investigated. All spiral wire observed was ¼ in (0.64 cm) diameter. Clear cover over strand ranged from 1.85 to 2.5 in (4.7 to 6.4 cm).

Exposed spiral reinforcement was found to be electrically continuous to each other. Strand was found not to be continuous with the spiral wire.

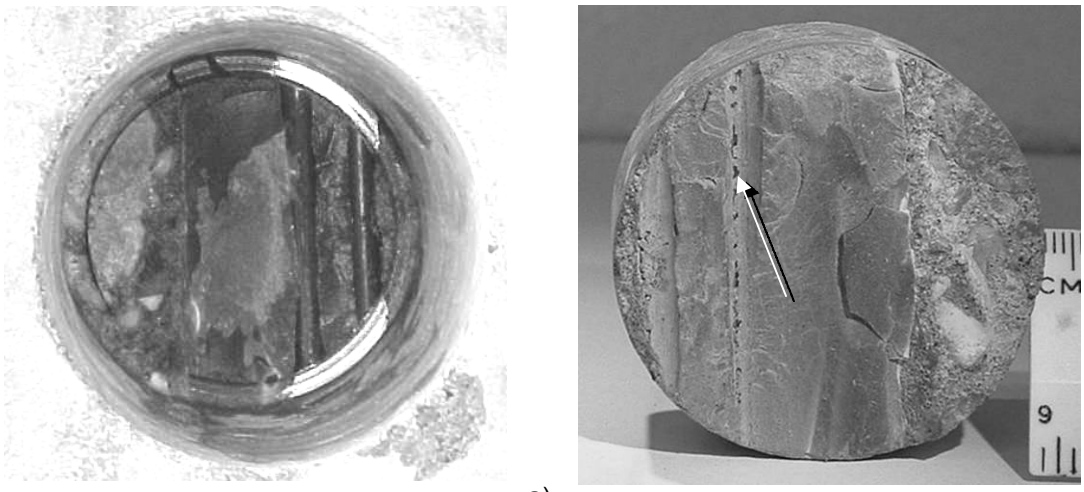

a)

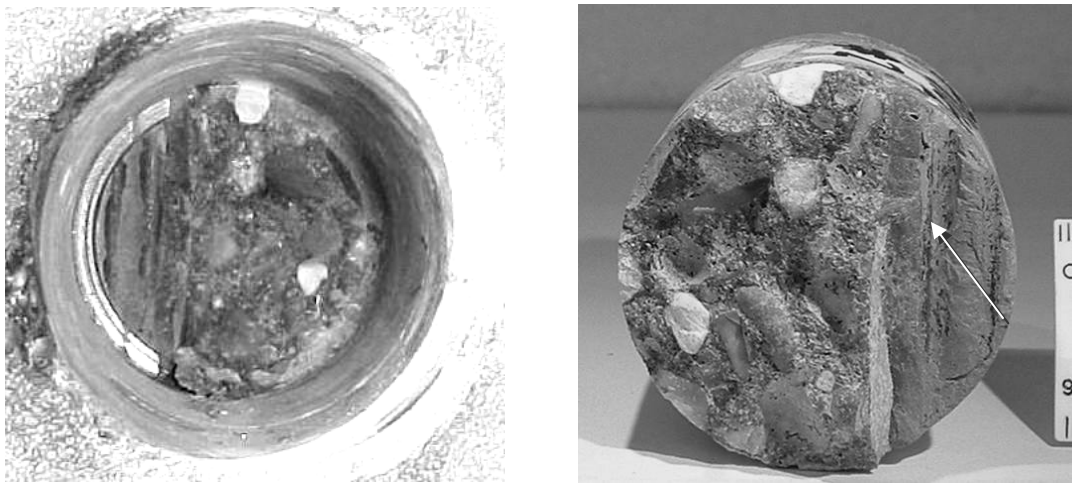

b)

Figure 3.3 Observation of surface rusting on strand, Pensacola Bay Bridge. Faint rust on strand. Traces of rust on grout imprint, indicated by the arrows, shown in the right of the figure. a) P4-1-4. b) P-110-2-2.

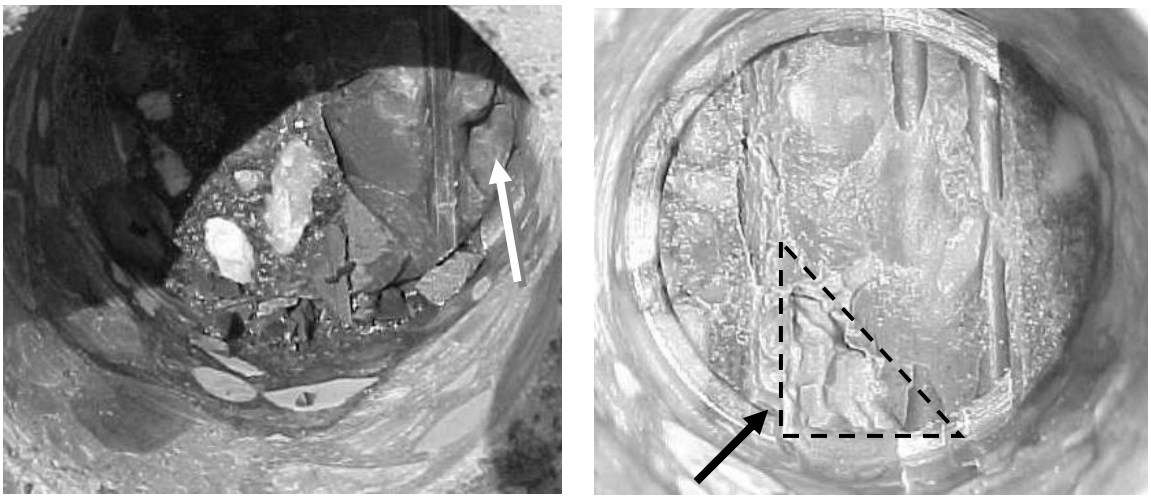

a) b)

Figure 3.4 Pressurized grout consolidation, Pensacola Bay Bridge. Voids indicated by the arrows. a) P237-1-2. b) P252-1-1 (triangular region).

3.2.3 Field Measurements of Steel Potential and Concrete Moisture

Half-cell potential measurements were made for exposed steel reinforcement in eight of the piles. Results are shown in Figure 3.5 and are listed in Table A5. Four locations having LC and SC ratings are indicated by black symbols in the figure below: P110-2, P110-2-2, P149-2, and P185-4. Duplicate measurements are shown where available. Notably, those corrosion locations had potentials more negative than -200 mV. While most reinforcement in delaminated or previously spalled concrete showed highly negative potentials suggestive of ongoing active corrosion risk, half-cell potential in the delaminated/spalled concrete of P252-1 located ~ 3 feet (~ 1 m) AHT, was only ~ -150 mV vs CSE. This may indicate that the spall/delamination there was not caused by corrosion of the spiral wire/bar or that the spiral wire/bar located 3 feet (1 m) AHT is not continuous with the reinforcements located 1 foot (0.3 m) AHT. However as mentioned above, limited electrical continuity checks from other piles showed that spiral wires severed by coring were electrically continuous to one another.

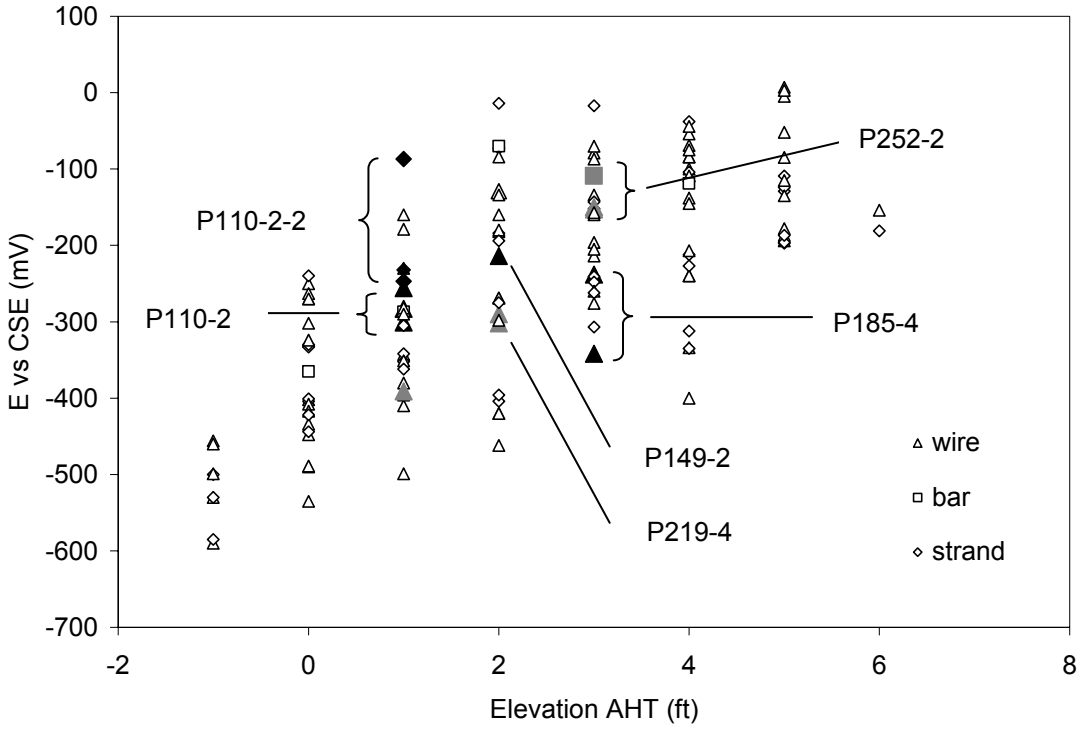

Figure 3.5 Pensacola Bay Bridge half cell potential measurements. ■ near corroded reinforcement. ■ near rust stained/delaminated concrete.

Concrete internal relative humidity measurements were made for P-110-2 at 14 in (35.6 cm) and 5 feet (1.5 m) AHT. IRH measurements were made starting approximately 22 hours after the fittings had been installed, and monitored for approximately 1 hour. Consistent with measurements from the Hathaway Bridge, the IRH is higher within the splash zone than that measured in the atmospheric exposure zone. This is likely due to the higher degree of water saturation near the surface of the tidal zone. Ambient conditions were ~ 65% RH and ~ 18^{o}C.

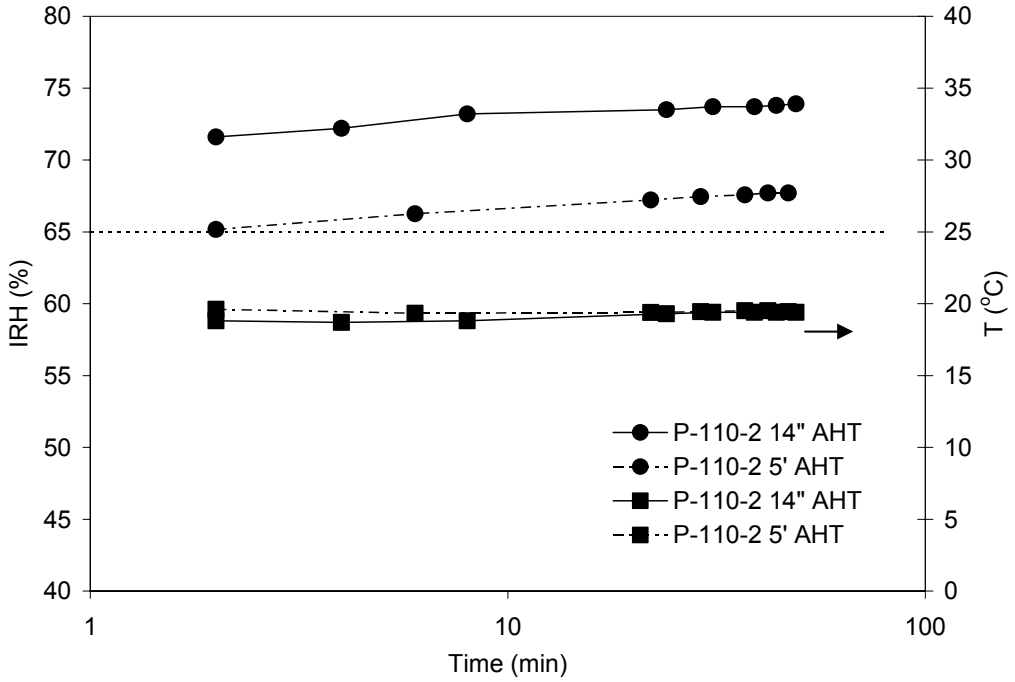

Figure 3.6 Pensacola Bay Bridge concrete internal relative humidity as function of time since probe insertion, 22 hrs after test fitting installation. ● IRH. ■ Temperature. Horizontal line represents ambient humidity.

3.3 Brooks Bridge

The Brooks Bridge approach spans have 36-in (91 cm) diameter cylinder piles with a ten pile bent configuration. The bents are labeled numerically from the south and the piles are labeled from the west. Bents 2 and 10-13 were constructed on shore and were not examined. End bents 1 and 14 at the face of the back wall as well as piers 5 – 8 were not examined. View of bent 9 was limited to the southern face due to boat accessibility. It should be noted that pile bents 3 and 9 were in shallow water. A total of 30 circular piles were examined.

3.3.1 Concrete Observations

Superficial rust staining was observed on Br-3-4 and Br-3-8. Shallow concrete spalling (with no reinforcement exposed) was noticed on two piles in bent 9, consistent with recent FDOT bridge inspection reports. Thin longitudinal cracks were common on many of the piles. Upon closer inspection of Br-3-2, two

parallel longitudinal cracks ~ 10 in (~ 25.4 cm) apart from one another were documented. The width of both cracks was ~ 0.008 in (0.2 mm).

3.3.2 Steel Condition Observations

Upon coring, an LC condition was observed on the spiral wire and spacing rebar in Br-3-2-5, located 6 in (15.2 cm) AHT. An NC condition was observed on a spiral wire in Br-3-2-6, located 6 in (15.2 cm) AHT. As shown in Table A2, the concrete clear cover to hoop reinforcement there was ~ 1 – 1.25 in (~ 2.5 – 3.2 cm), comparable to that noted for the Hathaway bridge and consistent with the design drawings for that bridge. The cover for the bar in Br-3-2-5 was 1.5 in (3.8 cm). Strand was not exposed in any of the corings of this bridge. All spiral wire was ¼ in (0.64 cm) diameter. Direct continuity measurements were not measured

3.3.3 Field Measurements of Steel Potential and Concrete Moisture

Half-cell potential measurements were made at elevations from high tide to 4 ft (1.2 m) AHT as well as below the waterline on piles Br-3-2-5 and Br-3-2-6. Potential measurements were taken for reinforcements exposed by coring from a crack line and the companion core hole 6 in (15.2 cm) horizontally apart on center. Potential mapping of the LC-rated wire and rebar in Br-3-2-5 showed highly negative values characteristic of corrosion activity. Continuity measurements are not available for this spot, but the reinforcements from the cracked concrete location had close potential values indicative of electrical continuity between hoop reinforcements and spacing rebar.

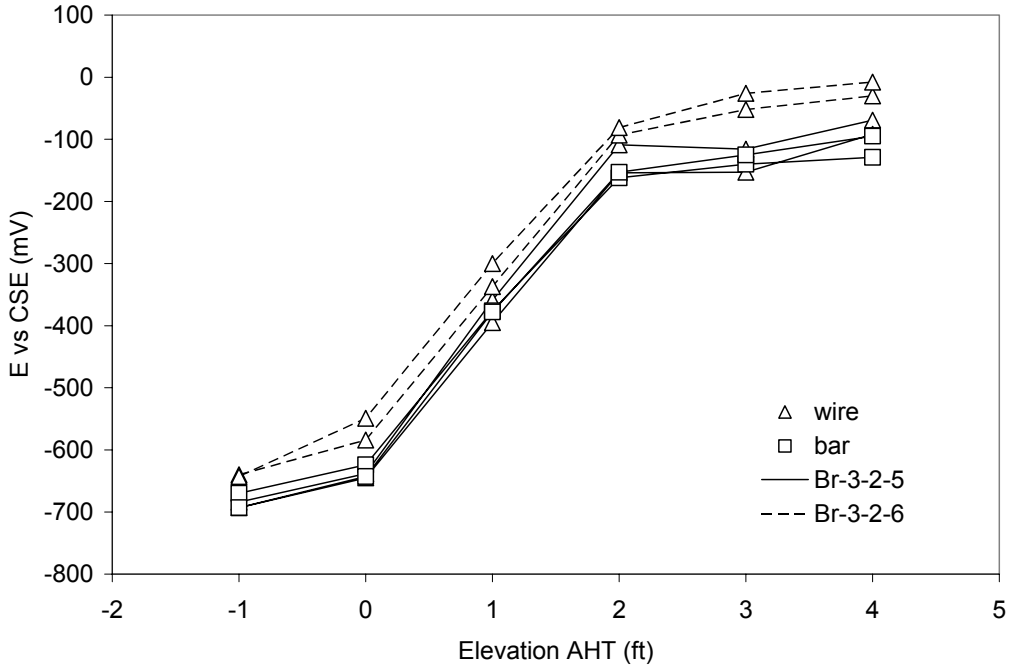

Figure 3.7 Brooks Bridge half-cell potential measurements as function of elevation.

3.4 St. George Island Bridge

The SGI Bridge was newly constructed (2003) at the time of the survey. Approach span bents contain each three 54-in (1.3 m) diameter piles. The bents are numbered from the south direction to the north direction, and the piles are identified by position and location in the pile bent: (E) east pile, (C) center pile, (W) west pile, (TP) test pile, and (N) north pile face, (S) south pile face. Not only is the bridge significantly newer than the other bridges in this study, but the cylinder piles in the bridge reflect current FDOT design specifications including design clear cover on the spiral reinforcement 3 in (7.6 cm) instead of ~0.75-1.5 in (1.9-4.4 cm) in the older bridges examined. Also, the concrete mixture proportions included ~22% fly ash cement replacement and ~8% microsilica cement replacement and a total cementitious content of ~840 pcy (~500 kg/m^3) for segments above tide level.

A limited survey of fifteen piles was conducted, twelve of which were being evaluated by FDOT operators for a construction-related assessment independent of the present investigation. Those twelve piles had superficial rust staining or fine longitudinal cracks and only visual appearance is reported here. The remaining three piles, among those earliest erected during construction, were investigated by coring as well. Piles 162-W-S and 163-W-S were selected for

closer inspection due to the presence and condition of thin longitudinal cracks measuring less than 0.002 in (0.051 mm) in width. Those piles were driven July 2001 and January 2002, respectively. A test pile, not part of the bridge but standing by itself next to bent 152 was inspected as well. It is thought that the test pile was driven at about the same time as the bent 152 piles (December 2001).

Core samples were extracted to hoop reinforcement depth, which was found at ~ 2.8 – 3.5 in (~ 7.2 -8.9 cm) (see Figure A2), consistent with design specifications. Hoop reinforcement exposed at the bottom of the cores was in all cases in the NC condition. Strand was not exposed during coring. As expected, the exposed hoop reinforcements were electrically continuous. Half cell potential measurements results for the exposed spiral wire are shown in Figure 3.9. It is noted that the core samples extracted from the test pile did not show any physical signs of concrete distress, yet the potential values were generally similar to those on the piles with longitudinal cracks.

Concrete cores from three unused pile cutoff sections labeled 878, 943, and 1404 from the SGI Bridge were retrieved as well.

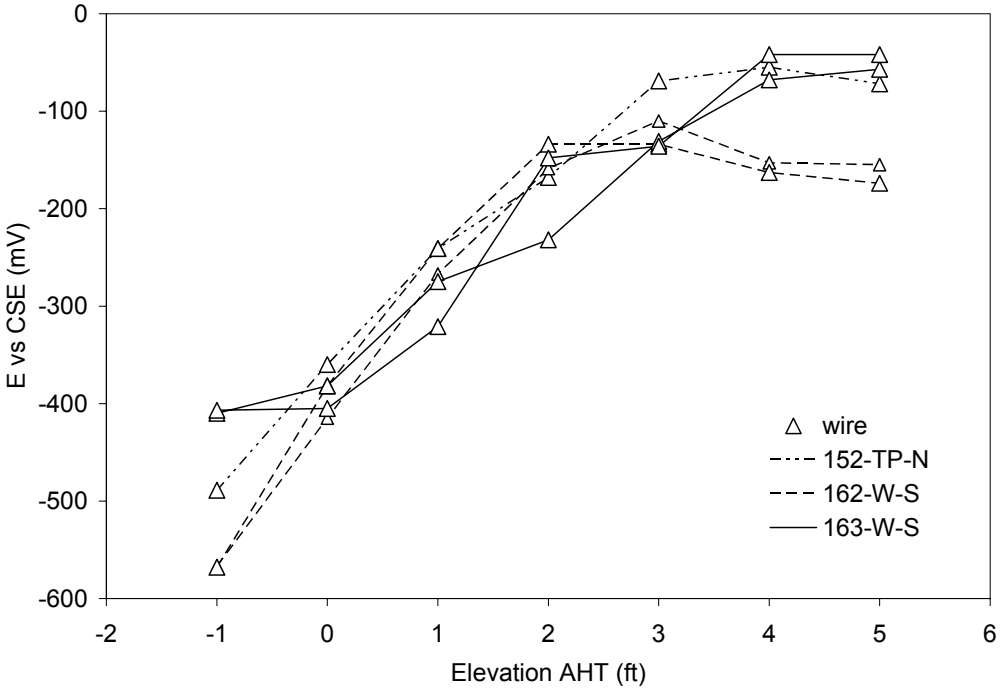

Figure 3.8 St. George Island Bridge half-cell potential measurements.

4 Laboratory Experiment Findings

4.1 Electrical Resistivity

Resistivity measurements were performed in field-extracted cores to obtain an additional indication of ionic permeability of the concrete. The tests involved simultaneous determination of moisture pickup (by mass gain) which was informative of the permeation properties of the concrete as well. It will be recalled that internal relative humidity in the piles was typically in the order of only ~70%. As shown in figures 4.1, 4.4, 4.7, 4.9, and 4.13 mass gain of most specimens tested in the 100% RH chambers began to show signs of stabilization (to a small value, ~ 1% of original specimen mass) after ~ 100 days of exposure, which was the normal test period. However, a few concrete cores that were exposed for extended periods showed continued mass gain in subsequent measurements made ~ 1 year later (figures 4.1, 4.4, and 4.13). The effect probably results from more accessible pores being saturated early, while the less accessible pores become eventually saturated at longer exposure times [28]. The modest and slow water pickup observed reflects the generally high quality of the concretes evaluated.

Resistivity measurements were successfully conducted per the specified procedures in most cases. However, it should be noted that the cores from the Hathaway Bridge and the Pensacola Bay Bridge contained fragmented edges, so geometric corrections [23] were only approximate. Also, several cores extracted from the Hathaway Bridge and Pensacola Bay Bridge had lengths less than 1.5 in (3.81 cm) so the effect of non-uniformities in the aggregate and cement distribution would become more notable with consequent variability in the results. Data from cores shorter and longer than 1.5 in (3.81 cm) are noted in Figures 4.2 to 4.6, which show some differentiation between the results of each class, although the overall trends are essentially the same. It is noted also that since moisture pickup takes place from the specimen surface inwards, the measured resistivity of specimens that are not terminally equilibrated is only an approximate spatial average of outer and inner regions of the specimen.

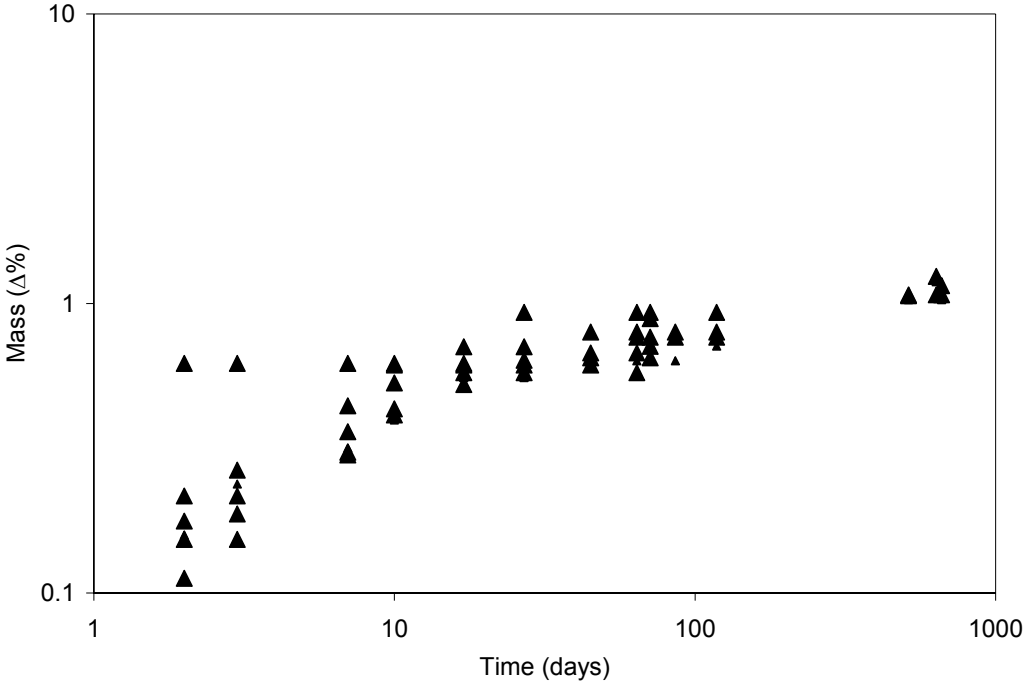

Figure 4.1 Hathaway Bridge core mass change as function of exposure time to 100% RH.

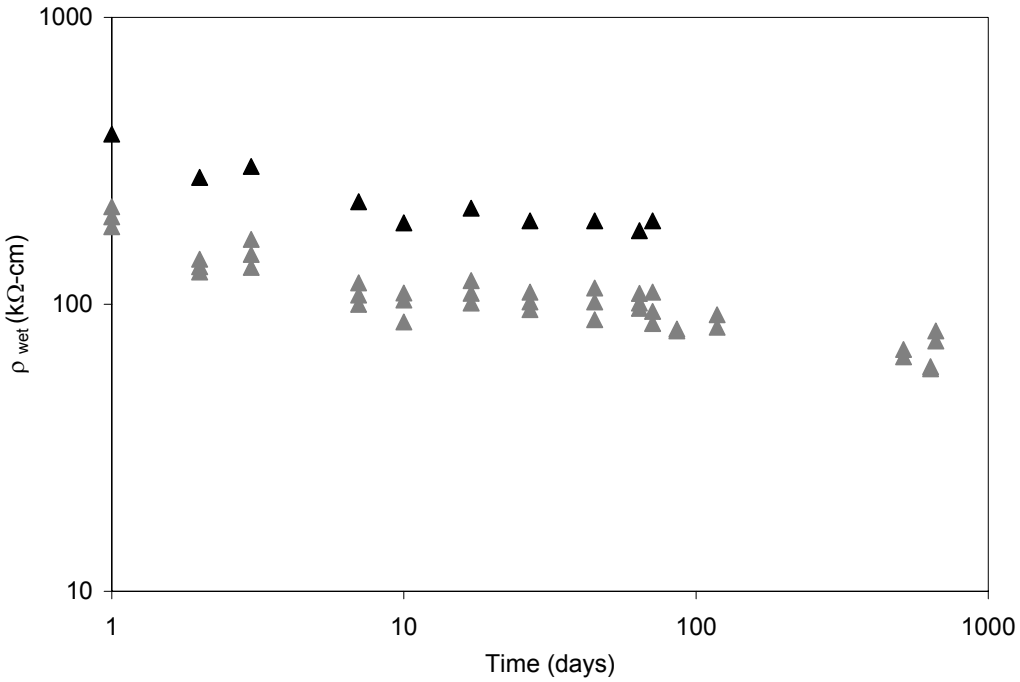

Figure 4.2 Hathaway Bridge core resistivity measurements as function of exposure time to 100%RH. ■ Cores > 1.75 inch (4.45 cm). ■ Cores < 1.5 inch (3.81 cm).

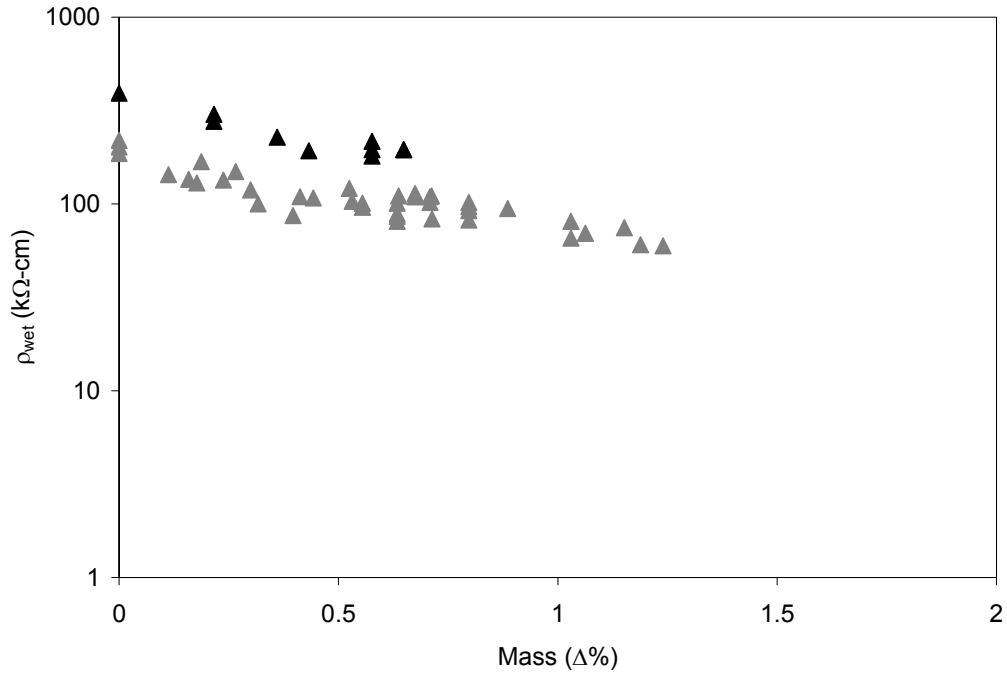

Figure 4.3 Hathaway Bridge core apparent wet resistivity as function of mass increase due to water absorption. ■ Cores > 1.75 inch (4.45 cm). ■ Cores < 1.5 inch (3.81 cm).

Hathaway Bridge specimens developed wet resistivity in the order of ~ 100 – 200 kΩ-cm after ~ 70 days and ~ 60 – 100 kΩ-cm after extended exposure of 635 days. Those are high values, characteristic of highly impermeable concrete. Water mass pickup and resistivity varied in inverse proportion as exposure time increased (Figure 4.1 and 4.3), as expected. The moisture mass gain was only 1% after ~600 days of conditioning in 100% RH which is also indicative of low pore connectivity.

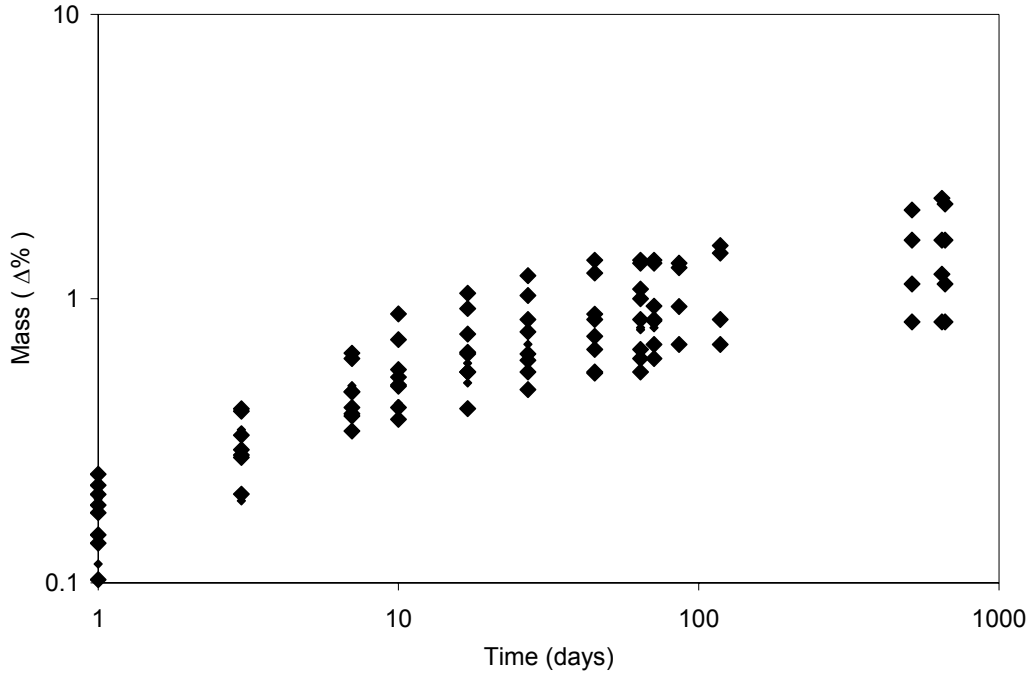

Figure 4.4 Pensacola Bay Bridge core mass change as function to exposure time to 100% RH.

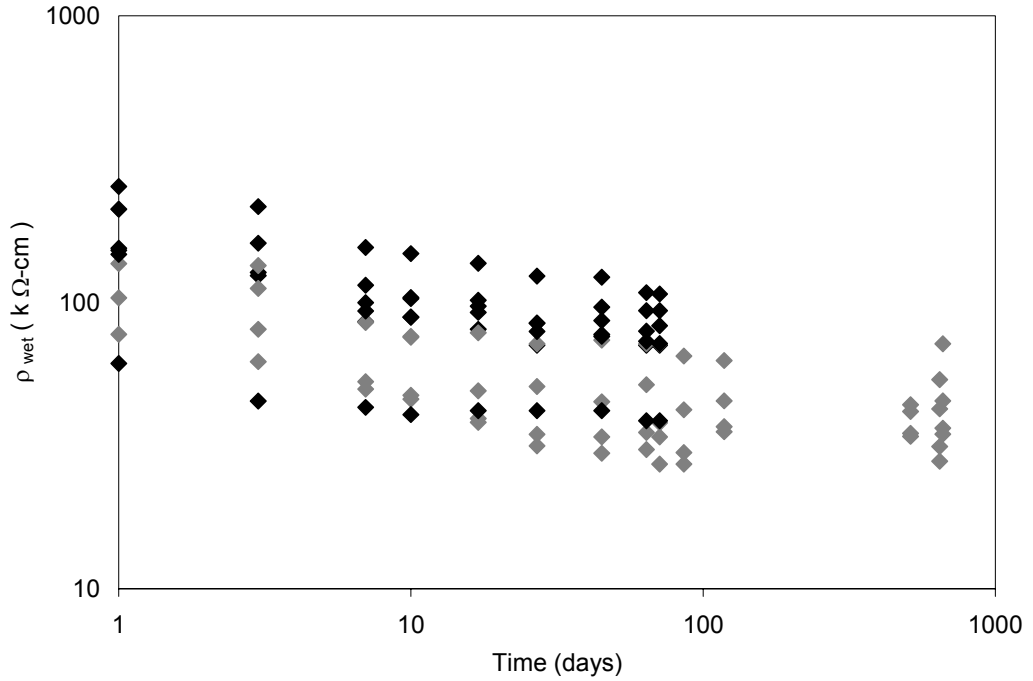

Figure 4.5 Pensacola Bay Bridge core wet resistivity measurements as function to exposure time to 100% RH. ■ Cores > 1.75 inch (4.45 cm). ■ Cores < 1.5 inch (3.81 cm).

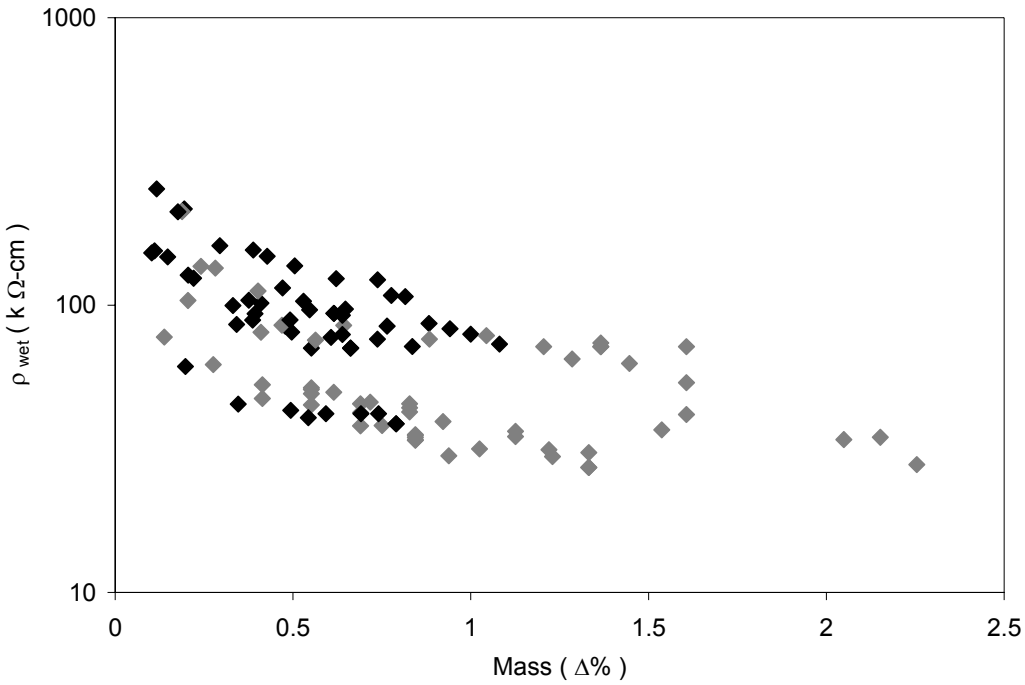

Figure 4.6 Pensacola Bay Bridge core apparent wet resistivity as function of mass increase due to water absorption. ■ Cores > 1.75 inch (4.45 cm). ■ Cores < 1.5 inch (3.81 cm).

The resistivity of some of the Pensacola Bay Bridge (Figure 4.5) cores reached values at ~70 days (~ 70 – 100 kΩ-cm) that were comparable to those of the Hathaway Bridge. Five other Pensacola Bay cores show a measured wet resistivity of only ~ 25 -50 kΩ-cm after ~ 70 days. Four of those cores were short and possibly subject to the test artifacts indicated earlier. Nevertheless, these resistivity values are still quite high for wet concrete and indicative of low permeability. The long term moisture mass gain was only 0.8% - 2%, also suggestive of low interconnected porosity. Mutual water pickup and resistivity trends were as expected (Figures 4.4 – 4.6).

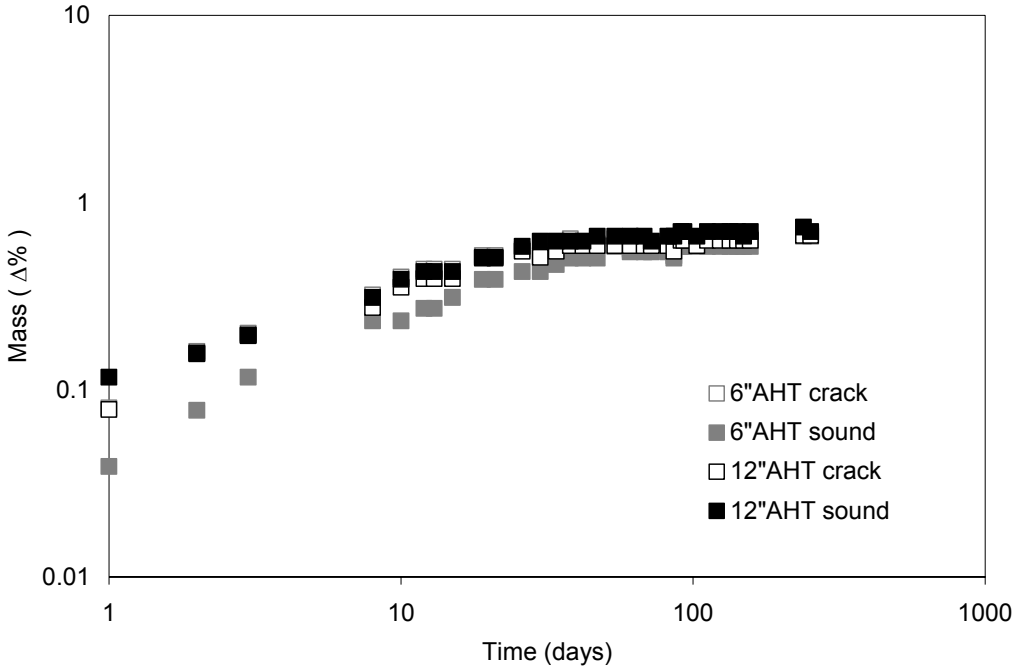

Figure 4.7 St. George Island Bridge (Pile 162) core mass change as function of exposure time to 100% RH.

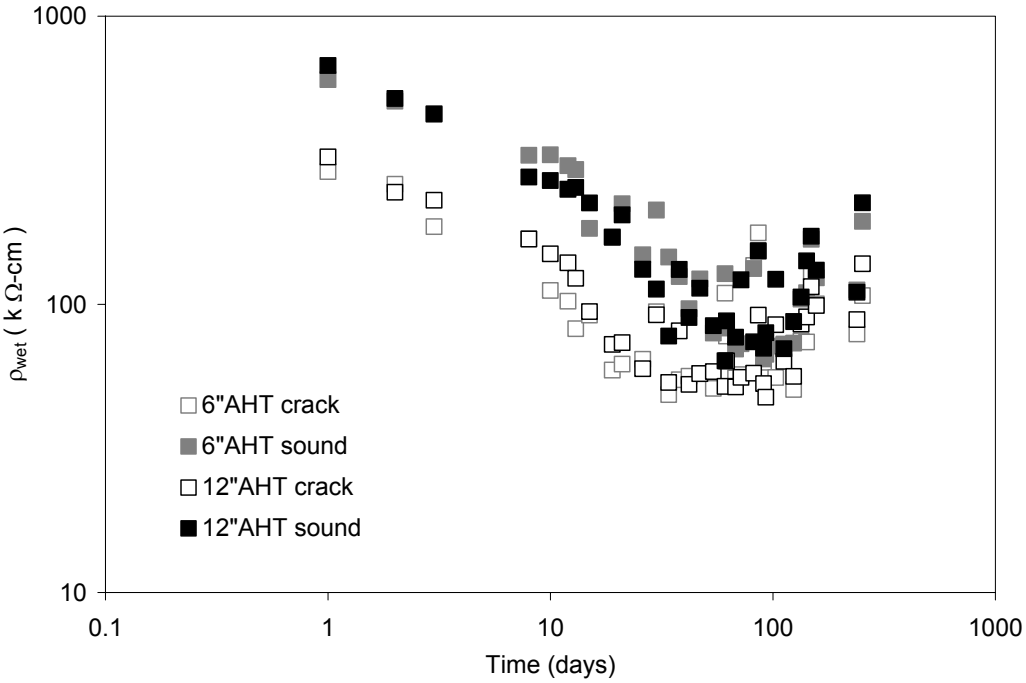

Figure 4.8 St. George Island Bridge (Pile 162) core wet resistivity measurements as function of exposure time to 100% RH.

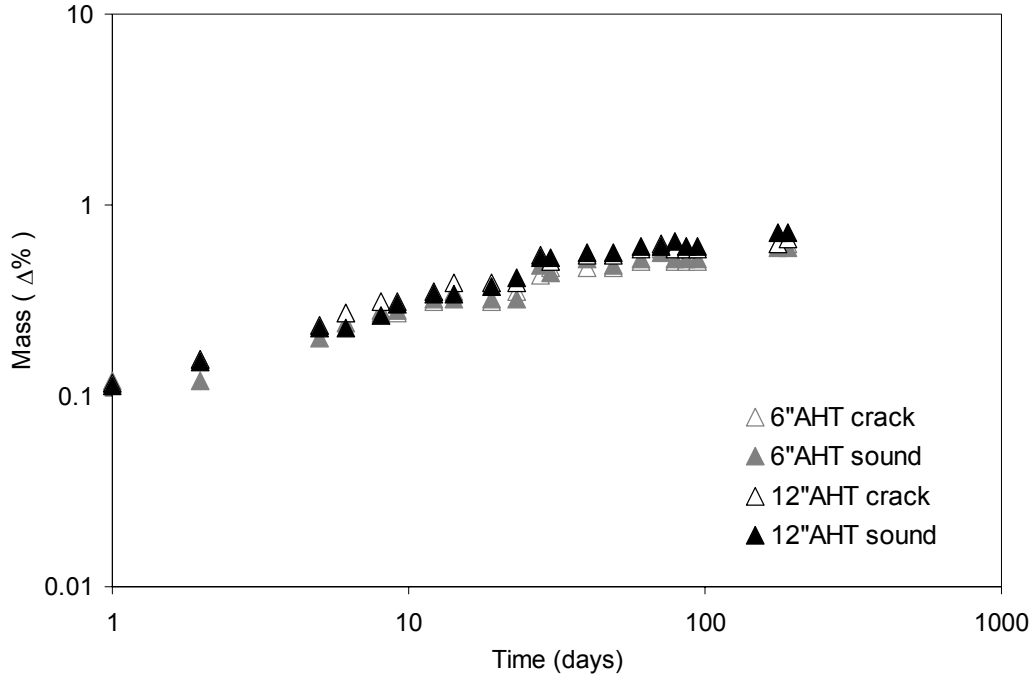

Figure 4.9 St. George Island Bridge (Pile 163) core mass change as function of exposure time to 100% RH.

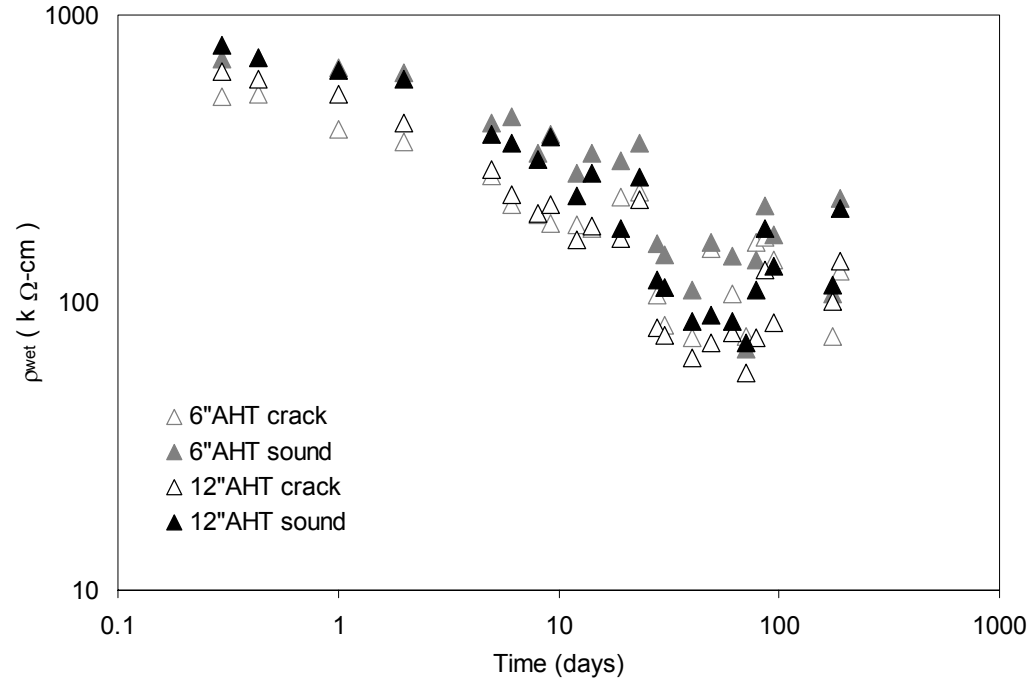

Figure 4.10 St.George Island Bridge (Pile 163) core wet resistivity measurements as function of exposure time to 100% RH.

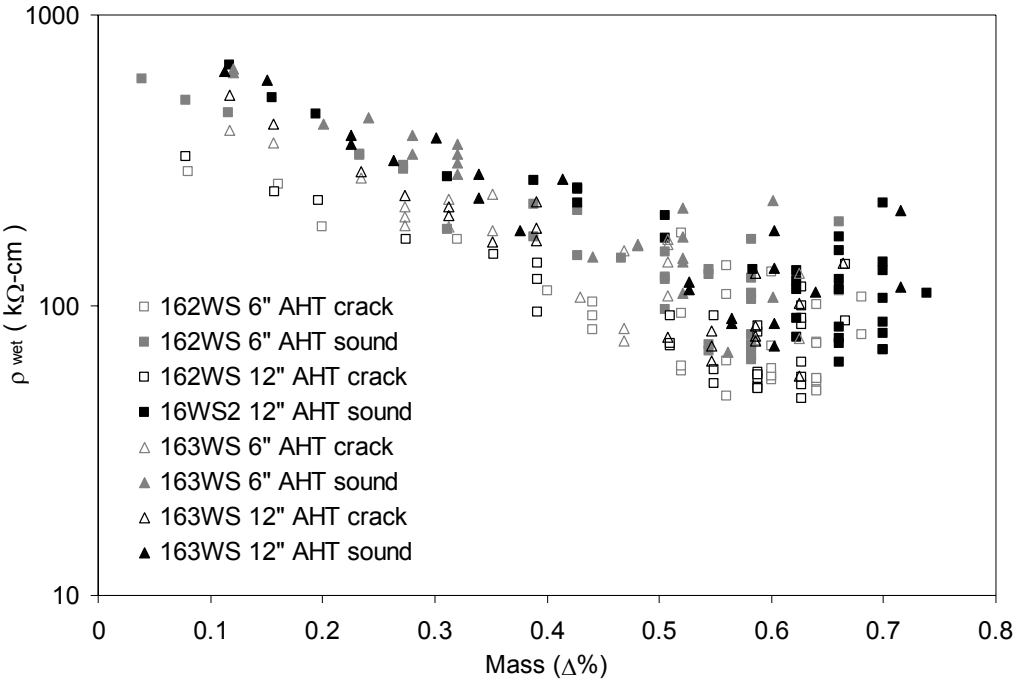

Figure 4.11 St. George Island Bridge core apparent wet resistivity as function of mass increase due to water absorption.

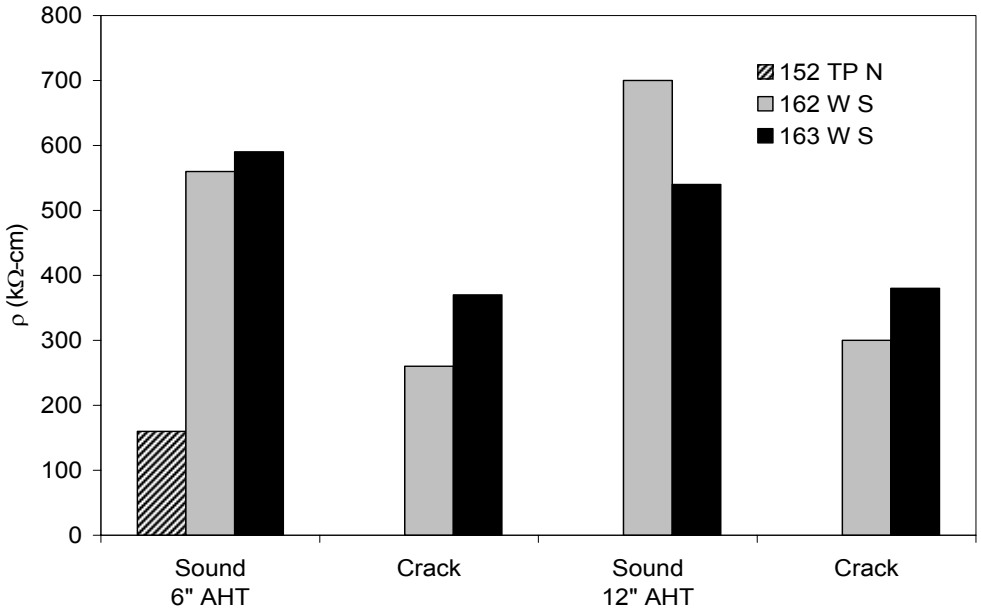

Figure 4.12 St. George Island concrete resistivity measurements on as-extracted cores.

The SGI Bridge cores from the two in-service piles evaluated showed the highest long term resistivity levels of the bridges in the study (~50 to ~200 kΩ-cm) and low mass gain (Figures 4.7- 4.11). These trends are to be expected from the concrete formulation that included pozzolanic additions intended to further reduce permeability. It is noted that resistivity tended to be higher in specimens for Pile 162 than in those of Pile 163. As it will be shown later the apparent chloride diffusivities for concrete cores from pile 162 were significantly lower than for those from Pile 163, which is as expected as wet resistivity and ion diffusivity are opposite indicators of concrete permeability [29]. Moisture-resistivity trends were as expected and seen for the other bridges (Figure 4.11).

For both piles the resistivity of the core drilled on a crack was noticeably smaller than that of the core on sound concrete (Figure 4.8, Figure 4.10). This behavior indicates enhanced ionic transport through the crack region. It should be noticed that similar enhanced transport may be present in cracks in cores from the other bridges.

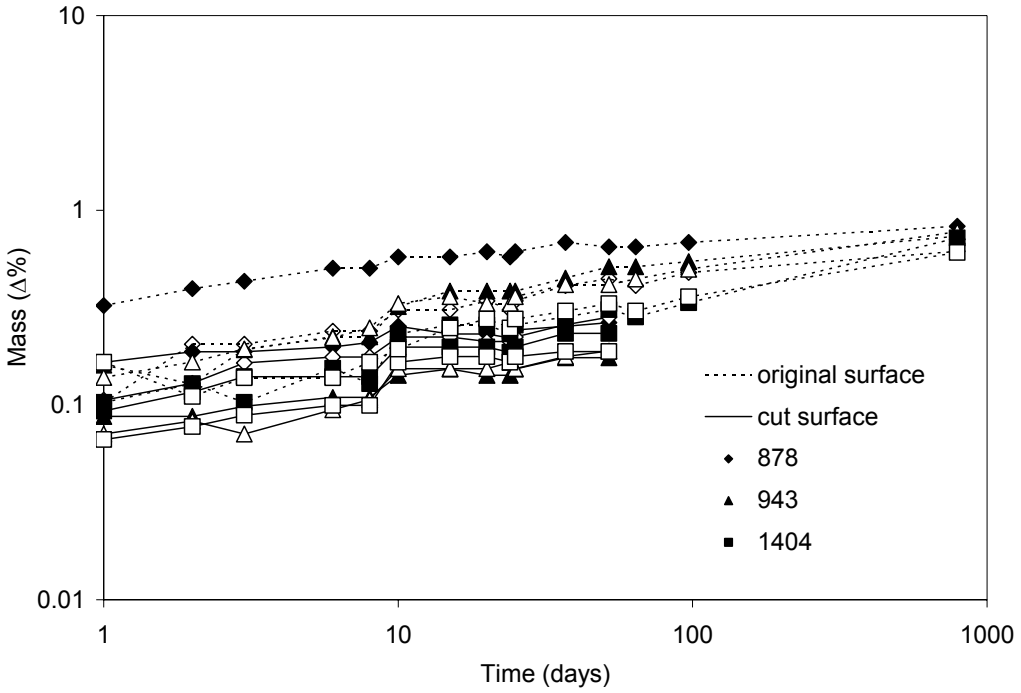

Figure 4.13 St. George Island Bridge pile cutoff mass change as function of exposure time to 100%RH.

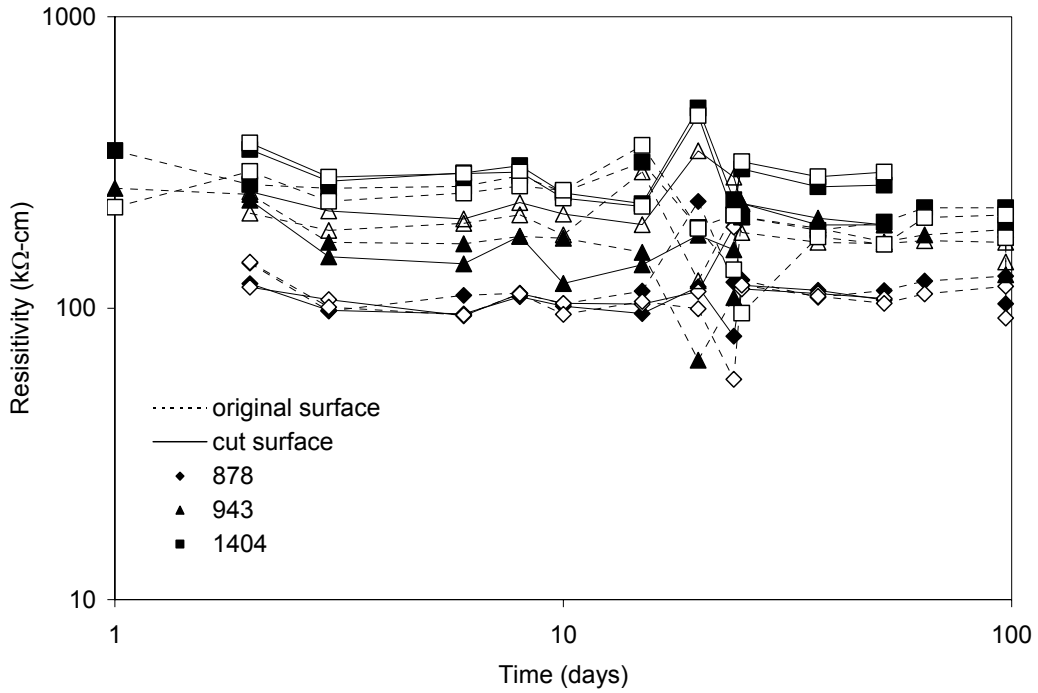

Figure 4.14 St. George Island Bridge pile cutoff wet resistivity measurements as function of exposure time to 100%RH.

The concrete samples from the SGI Bridge cutoff sections not in service were tested similar to the in-service cores. Three sets of concrete samples were monitored: 878, 943, and 1404. The designations were labels for concrete mixes used in construction of the SGI Bridge. Concrete sample 878 included river rock coarse aggregate. Concrete samples 943 and 1404 had as coarse aggregate primarily limestone, but with some river rock. The core samples extracted from the pile cutoffs were cut into two specimens; one (avg. length 4.8 cm) consisted of all cut edges and the other (avg. length 1.9 cm) retained the original outer surface of the core. The original outer surface may contain a surface layer in which water absorption [28] and ionic diffusion may be slower.

Upon testing, the uncut original concrete surface did not appear to have affected significantly water absorption or wet resistivity, but it should be noted that the perimeter and opposite face of the specimen were cut surfaces. Similar to other bridge core samples conditioned in high humidity, water absorption appears to continue upon extended exposure. Resistivity values were high, consistent with the expected high concrete quality, but as seen in figures 4.13 and 4.14 the 878 mix with river rock had not as high wet resistivity (~ 100 kΩ-cm) as the 943 and 1404 mixes (~ 200 kΩ-cm). The 878 mix also showed faster water absorption that compared to the other mixes.

4.2 Porosity

Volumetric porosity measurements generally following ASTM C642-97 were made for samples from the concrete cores extracted from SGI Bridge pile cutoffs. Concrete mix 943 and 1404 had similar results (~ 8 – 11%); concrete mix 878 showed high porosity in three out of four tests (~ 13%) as shown in Figure 4.15. As mentioned in Section 4.1, mix 878 (limestone-river rock mix) had markedly lower wet resistivity than mixes 943 and 1404 which would be in agreement with the observed higher porosity. It is noted that the effectiveness of soaking and boiling methods used in ASTM C-642 to saturate high quality concrete has been questioned in the literature [30]. One porosity test result for concrete mix 878 was significantly lower than those of replicate measurements. It is noted that the river rock was intended in the SGI Bridge for concrete mixes for pile sections to be placed below tidal zone.

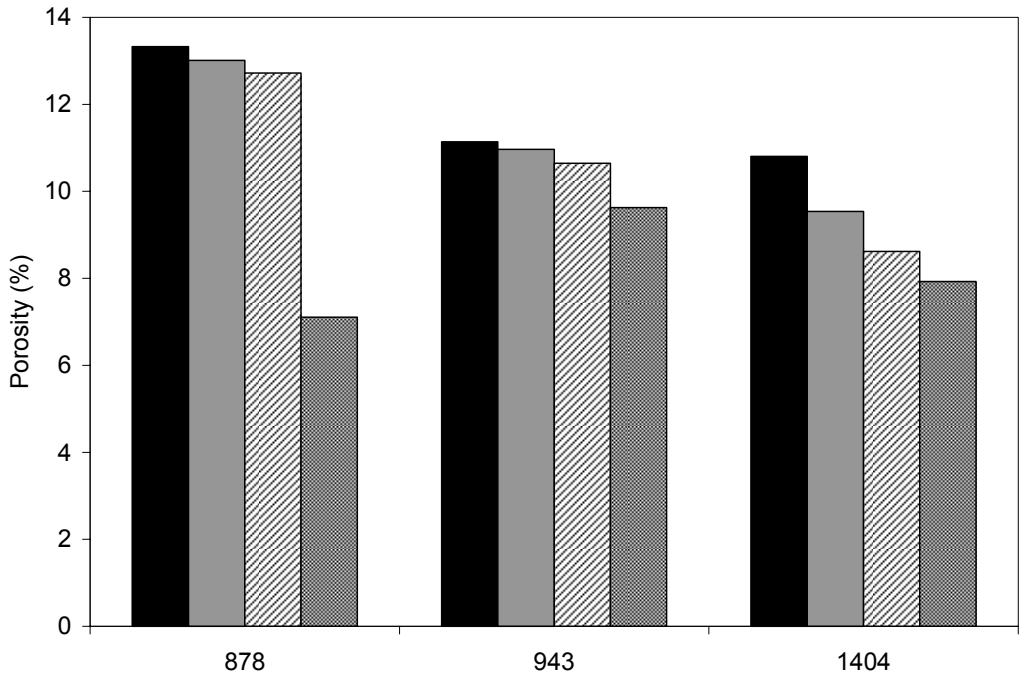

Figure 4.15 St.. George Island Bridge pile cutoff porosity. Four replicate measurements, as shown by the bars, were made for each sample: 878, 943, and 1404

4.3 Chloride Ion Penetration Profiles Observations and Diffusion Parameters

Chloride concentration data from potentiometric titrations of all powdered concrete samples are shown in Table A4 of Appendix III. The average chloride content of each concrete core slice as well as the idealized profile fit per Eq. (1) (whenever appropriate) of all tested specimens are shown in figures 4.16 to 4.19. Results from sound or cracked concrete locations as well as elevation regions (below high tide, splash and atmospheric) are so noted. Calculated apparent diffusion parameters are given in Tables A3 and A4 of Appendix II. In some instances the datum for the outermost concrete sample of the core was excluded for diffusion parameter calculations as being unrepresentative of bulk transport, or due to suspect analysis methodology; those cases are so identified in Table A4 of Appendix III. In all instances it was assumed that the native chloride ion concentration of the concrete (C_o in Eq. (1)) was 0.08 mg/g (~0.32 pcy (~0.2 kg/m^3) for typical concrete with unit weight of 4,000 pcy (2,400 kg/m^3). This value is a rounded off average of values measured at large depths in the SGI Bridge cores in service as well as from piles not in service, and it is also in the order of the average of the two lowest concentration measurements obtained in the Hathaway and Pensacola Bay bridges where several deep cores were extracted. The value is also in the order of typical native chloride values commonly observed in other FDOT investigations of marine substructure. As the cylinder piles are large in diameter and penetration depths very limited, a one-dimensional flat-wall approximation was used instead of a cylindrical geometry treatment in the diffusion models.

The most notable feature of the chloride concentration data from piles in service in all four bridges was the very low resulting values of the apparent chloride ion diffusion coefficient. Figure 4.24 shows cumulative distributions of the values obtained for each of the structures assessed as well as for the previous assessment of the Escambia Bay bridges. The overall median value for the four bridges was only ~1x10^{-13} m^2/s (~0.005 in^2/y), which is less than the median value recently obtained for the best performing structures built with modern FDOT class V concretes for aggressive marine service, ~ 4x10^{-13} m^2/s (0.02 in^2/y) [2]. The range of diffusivity values observed in this study are also in the same class as those obtained for cylinder piles at the Escambia Bay bridges [1], underscoring the overall low permeability of the concrete in these components.

Measurement and model uncertainty are inherent to the process of evaluation of the apparent diffusion parameters obtained here [31]. In addition, there is large actual variability of transport parameters with factors such as elevation, as shown below. Consequently, the differences in the diffusivity cumulative distribution curves (Figure 4.24) of the Escambia Bay, Pensacola and

Hathaway bridges may not be statistically meaningful and will not be discussed. The D values obtained for the Brooks bridge samples are on average ~3 times greater than for the other three bridges of similar age, but it should be noted that only 4 samples were evaluated, and all came from a single pile. Consequently, without additional samples from other locations in that bridge it cannot be ascertained whether the concrete used in those piles was indeed significantly more permeable than in the comparable bridges. Of more varied origins were the data for the new SGI Bridge, which include cores from two piles in service (Figure 4.19), to which have been added from laboratory ponding tests of cores extracted from unused pile sections (Figure 4.20). Chloride penetration was shallow as expected for the limited time of service in seawater. Nevertheless, the overall results tended to show values comparable to those obtained in the other, much older structures. It is recalled that concrete with pozzolanic additions tends to show a marked decreasing apparent diffusivity trend with time, typically described by $D=Do\ t^{-n}$, which n is in the order of 0.5 to 0.7 [32]. Such trend reflects the decreasing connectivity of the pore network as the pozzolanic reactions progress over long times. As a result, it is possible that the median apparent diffusivity of concrete in this structure at age 40 years (~ one order of magnitude greater than present age) may become several times smaller than at present. As pointed out earlier, SGI Bridge cores extracted from 162WS showed markedly deeper penetration than those from 163WS, even when both piles supposedly were made with the same type concrete with the same mixture proportions. It has been speculated that differences in pozzolanic content in the concrete of both piles may be responsible for the difference, and magnetic susceptibility measurements for determination of fly ash presence were made as discussed in Section 2.4.4. There may also be some segregation of aggregate during concrete pile casting which would also affect the permeability of the concrete at near surface layers. The concrete of the SGI Bridge pile segments above tide level typically comprise of limestone and some river rock. No dramatic differences in aggregate amount or spacing were visually noticeable between 162WS and 163WS; however, it should be noted that the small diameter of the cores precludes drawing definite conclusions when comparing only two samples. Thus, the causes for the observed differences in chloride penetration of both piles remain undetermined.

In agreement with a commonly observed trend in marine substructure [2], the apparent diffusivity tended to decrease with increasing elevation AHT. This behavior is visible in the example of Figure 4.16a where the profiles are significantly wider for cores extracted from below tide than for cores in the atmospheric exposure zone. The composite graph in Figure 4.22 shows diffusivity as function of elevation for all of the core locations in this survey as well as those from the Escambia Bay bridges. Although there is significant local scatter, there is a clearly decreasing trend in D as elevation increases. The decrease is expected as the water content of the concrete decreases with

increasing elevation, with consequent reduction in the ion transport ability through the concrete.

As shown in Table 2.1, the typical chloride ion concentration of the water traversed by the bridges in study is ~ 10,000 ppm; St. Andrews Bay traversed by the Hathaway Bridge has a moderately higher chloride concentration (~25,000 ppm). The chloride content of Escambia Bay was documented to be 5,640 ppm [1]. These values are characteristic of the chloride content of gulf and intracoastal water in the Florida Panhandle; St. Andrews Bay is comparable among the most aggressive chloride environments statewide.

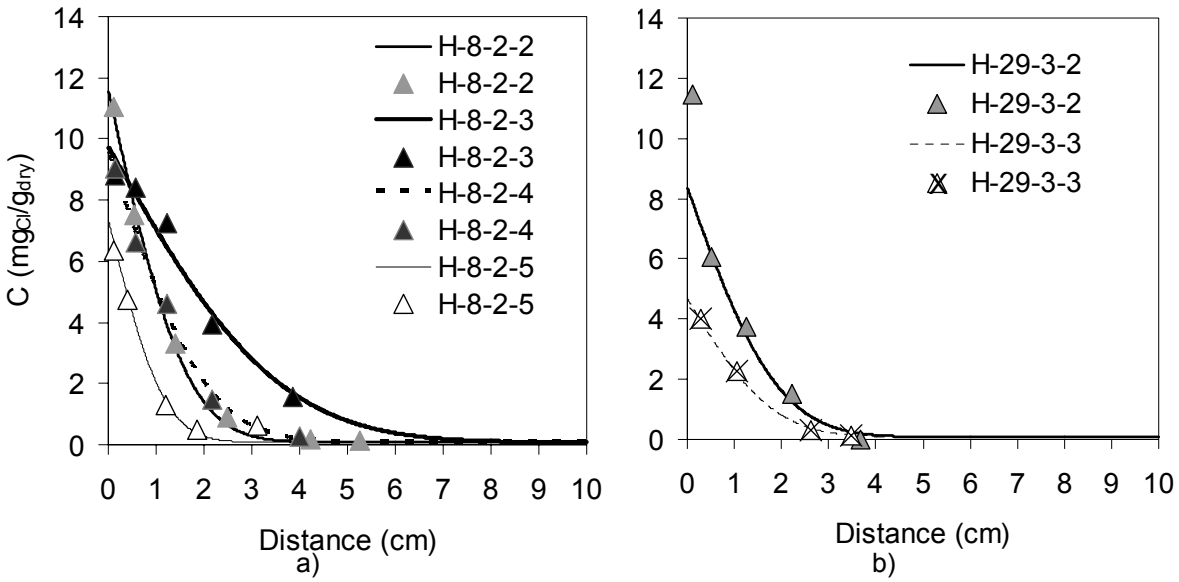

Figure 4.16 Hathaway Bridge chloride ion penetration profile. a) H-8-2. b) H-29-3. ■ Below high tide. ■ Splash/ tidal zone. □ Atmospheric exposure zone. X Cracked concrete. Lines represent chloride penetration profiles predicted by Eq. 1.

Figure 4.21 shows that the ranges of Cs values observed in the various bridges investigated generally overlap, roughly independent of the chloride content of the water in the span of salinity encountered. The similarly overlapping data from an additional statewide sampling of Florida bridge [2] substructures made with conventional concrete is also shown. This behavior has been noted elsewhere [34] and it reflects the development of nearly salt-saturation conditions (and hence approximately equal concentration independent of salinity of the source) on much of the surface of the concrete by evaporative concentration of marine or estuary water.

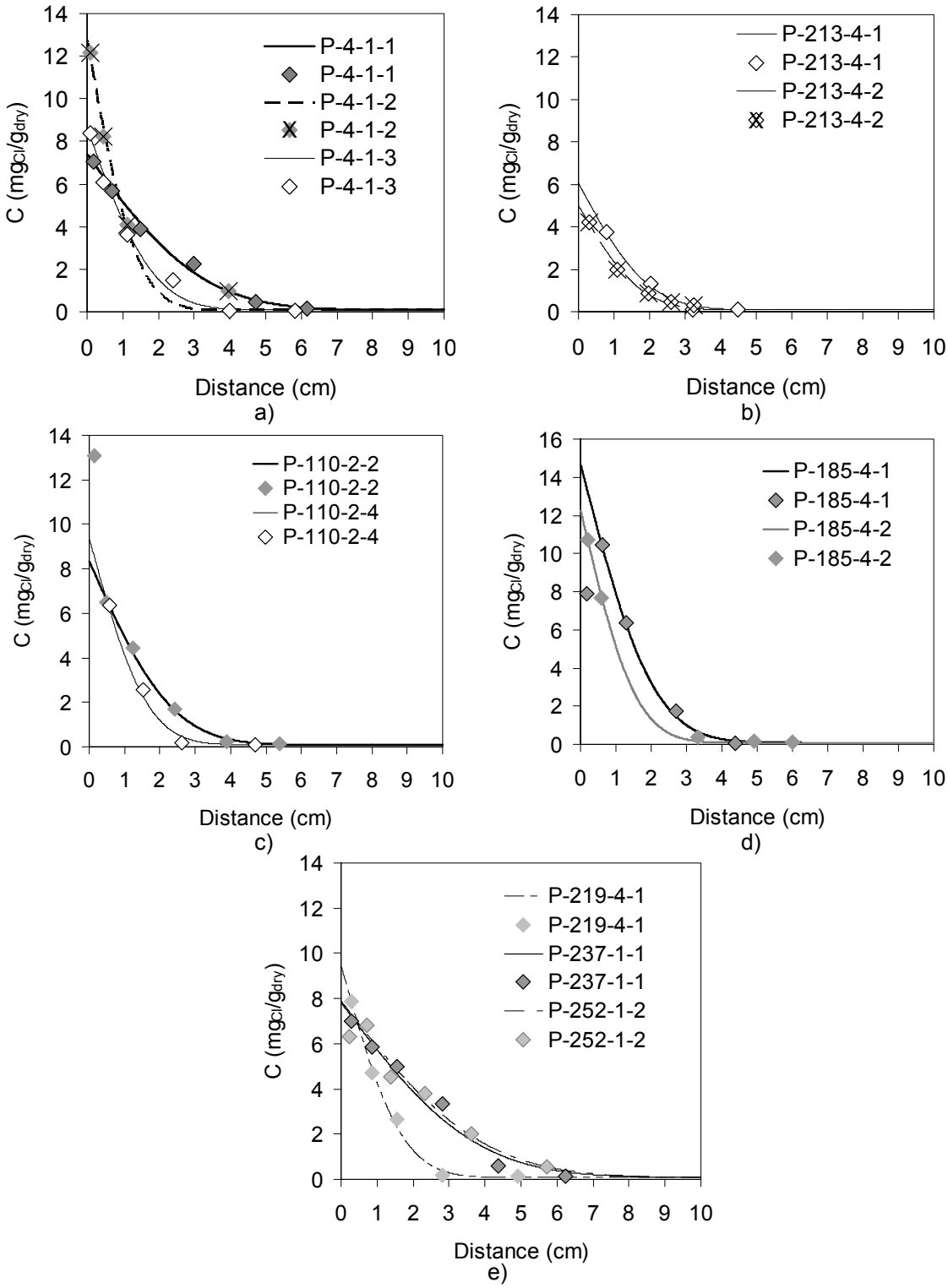

Figure 4.17 Pensacola Bay Bridge chloride ion penetration profile. a) P-4-1. b) P-213-4 c) P-110-2 d) P-185-4 e) P-219-4, P-237-1, and P-252-1 ■ Splash/ tidal zone. □ Atmospheric exposure zone. X Cracked concrete. Lines are chloride penetration profiles predicted by Eq. 1.

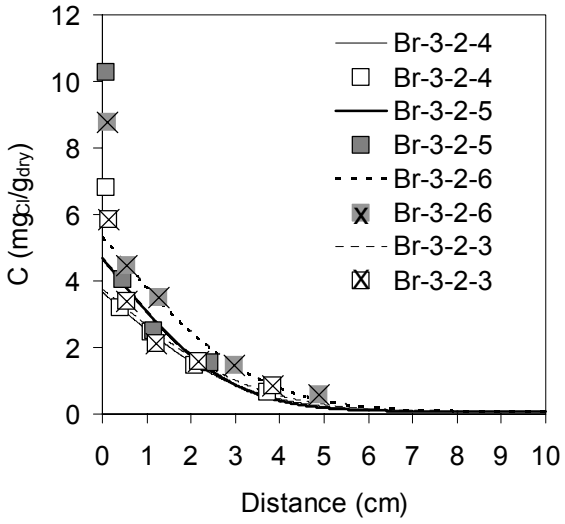

Figure 4.18 Brooks Bridge chloride ion penetration profile. ■ Splash/ tidal zone. □ Atmospheric exposure zone. X Cracked concrete. Lines represent chloride penetration profiles predicted by Eq. 1.

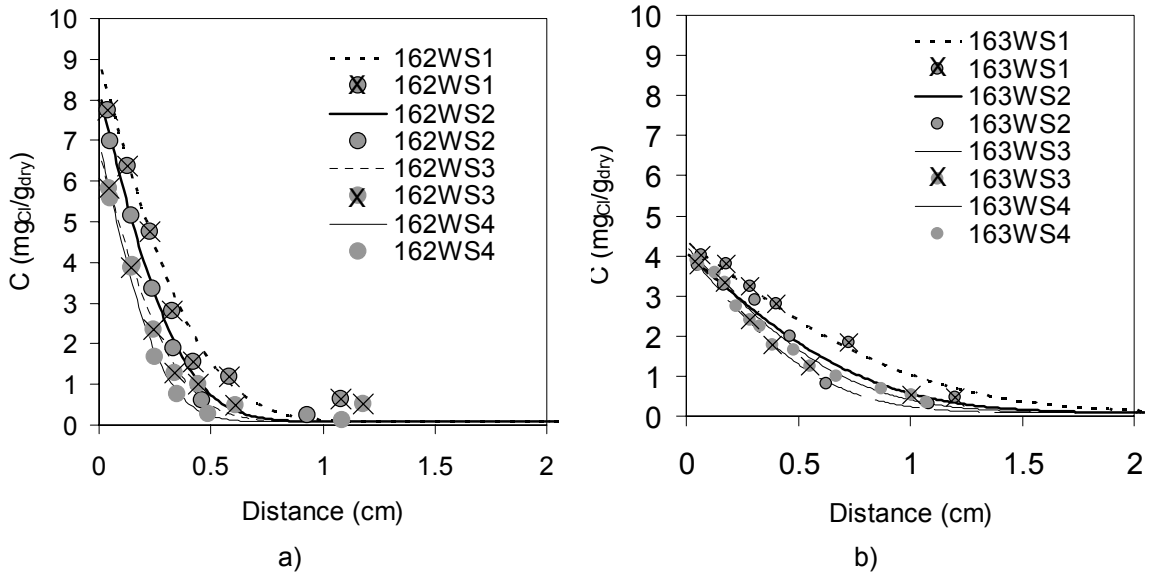

Figure 4.19 St. George Island Bridge chloride ion penetration profile. a) 162WS. b) 163WS. ■ Splash/ tidal zone. X Cracked concrete. Lines represent chloride penetration profiles predicted by Eq. 1.

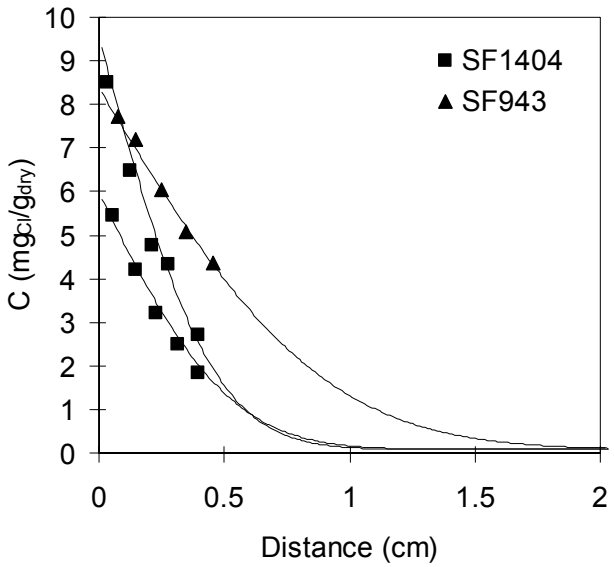

Figure 4.20 Salt-solution-ponded concrete chloride ion penetration profile. Nordtest Method NT Build 443. St. George Island Bridge pile cutoffs. Lines represent chloride penetration profiles predicted by Eq. 1.

The cylinder piles in the old structures, and especially those in the newer SGI Bridge, had many instances of fine (< 0.013 in at the surface) longitudinal cracks. The measured crack widths of the concrete are tabulated in Table A3 of Appendix III. The cracks often were observed to run along the entire depth of the cores drilled at crack locations, even at SGI Bridge where the concrete cover is thick. It is noted that the thickness of the cracks fluctuated along the core length, and also it is cautioned that the coring process may have disrupted the cracks and possibly created artifacts that alter the observed internal width. While the cracks likely originate from mechanical factors or other phenomena not related to corrosion, it is of much interest to determine whether preferential chloride ingress along the cracks (and consequent localized corrosion initiation) could become important. A recent investigation of FDOT marine substructures built with highly impermeable concrete [2], in marine environments similar in chloride content as the bridges in the current study as shown in Figure 4.21 (~10,000 to 20,000 ppm), showed much enhanced chloride penetration along cracks as narrow as those observed here. Chloride transport modeling for those cases suggested that enhanced transport could be important even in very narrow cracks [2], and other work suggest similar behavior [35]. Examination of the chloride profiles obtained in this investigation showed some limited indications of enhanced chloride penetration, for example the Pensacola Bay Bridge P-4-1-1 and P-4-1-2 cracked/sound concrete pair in Figure 4.17, and the shallow penetration (0.4 in (1 cm)) pair from the SGI Bridge, 162WS1-1 to 162WS1-4 (Figure 4.19). As mentioned earlier, there are indirect resistivity indications of increased ionic transport in cracked specimens in SGI Bridge. These cases however appeared to

be much less developed than the dramatic examples of enhanced chloride penetration documented elsewhere for conventional marine substructure [2]. In addition, the present steel corrosion survey failed to show any examples of clear association between prior presence of cracks and preferential corrosion initiation, even in the bridges that had been in service for 40 years. Consequently, there is no clear indication at present that fast chloride transport at thin cracks is a significant corrosion initiation factor in cylinder piles, at least those built with traditional relatively low external clear concrete cover. It is cautioned however that evidence from mechanically distressed piles at SGI Bridge, being investigated independently by FDOT, may require revisiting this issue in the future for the case of new cylinder pile construction using thicker concrete cover. It is noted also that surface rust observations did not appear to be associated with joints between pile segments.

As in most instances the presence of cracks did not appear to significantly alter the shape and depth of the chloride profile compared to that of companion sound cores, the apparent diffusion parameters calculated from both sources have been considered together in the rest of this report.

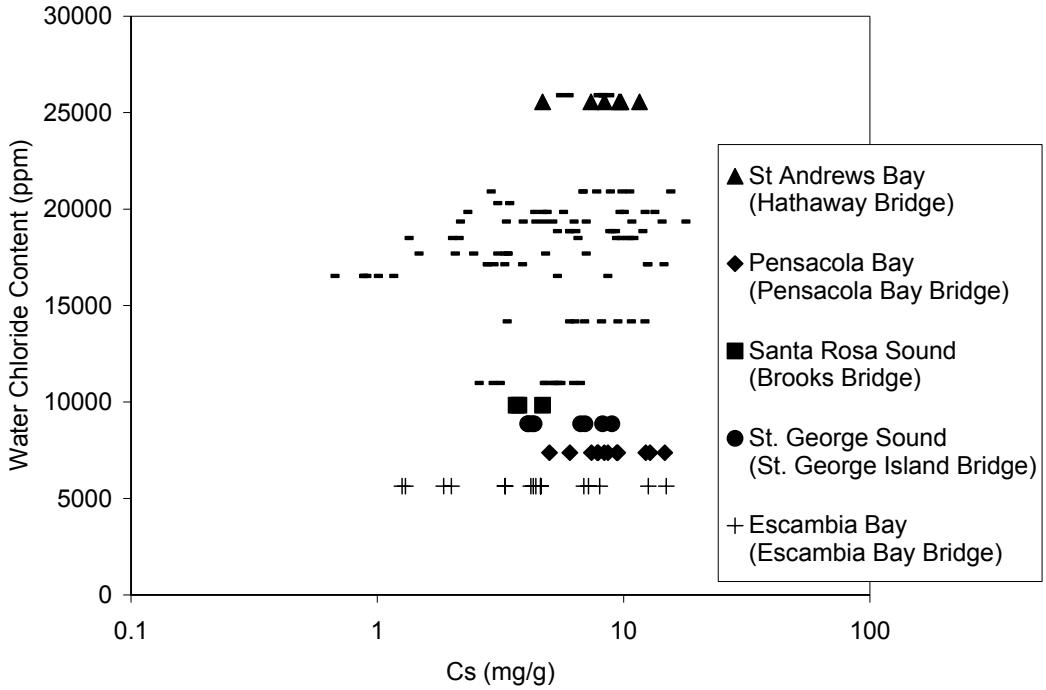

Figure 4.21 Comparison of water chloride content and concrete chloride surface concentration Cs at elevations -0.14 to 1.52 m AHT (-0.5 to 5 ft AHT). (-) data from [2] for various FDOT bridges built with conventional modern concrete.

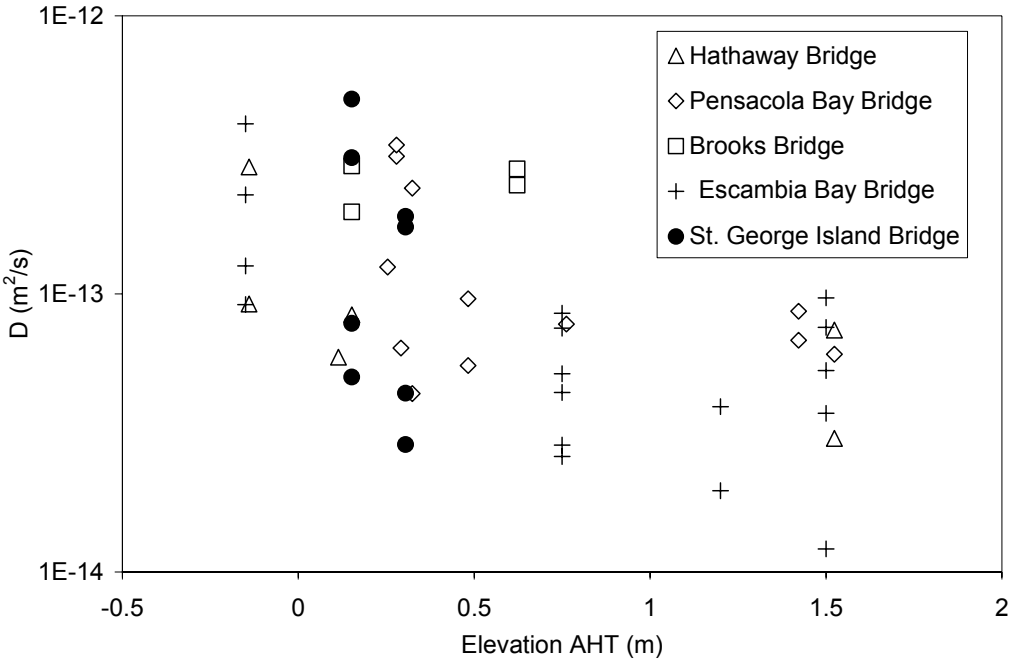

Figure 4.22 Apparent chloride ion diffusivity as function of pile elevation.

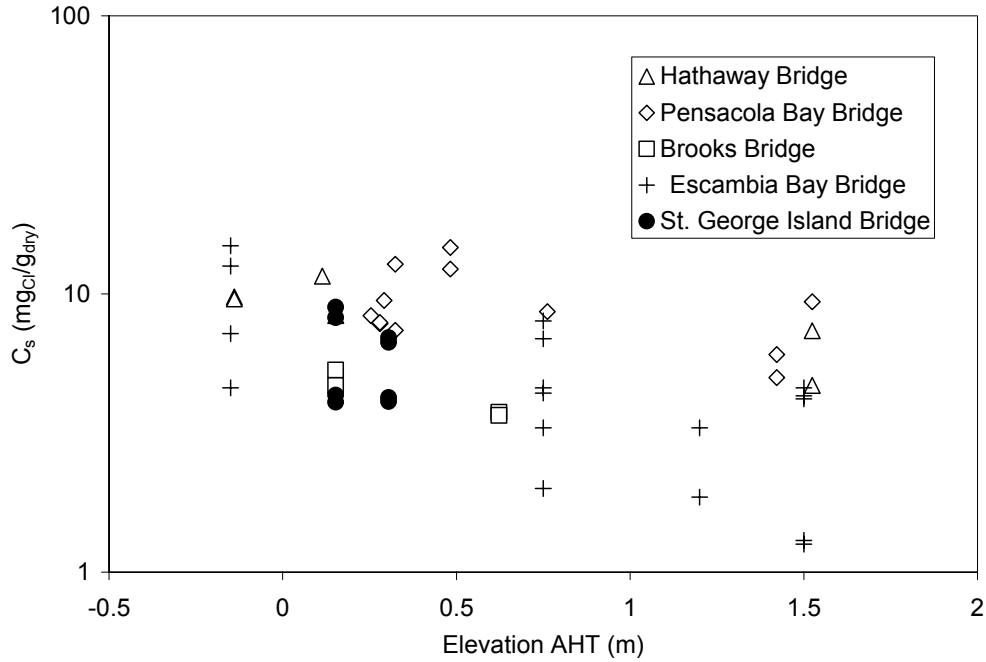

Figure 4.23 Chloride surface concentration as function of pile elevation.

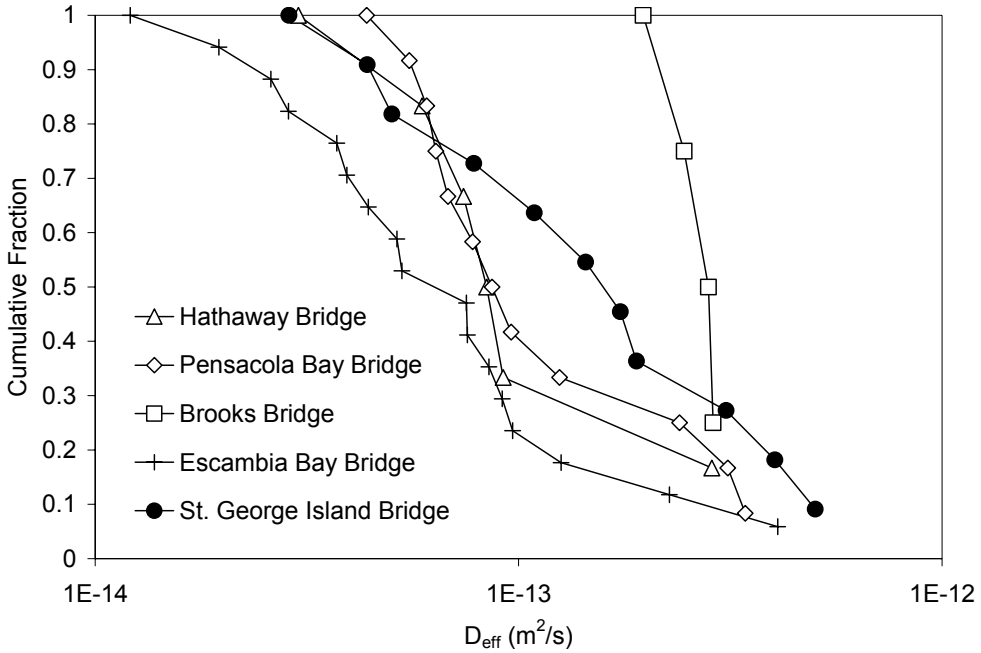

Figure 4.24 Cumulative Fraction of Deff values for cylinder piles in study and Escambia Bay Bridge study [1]

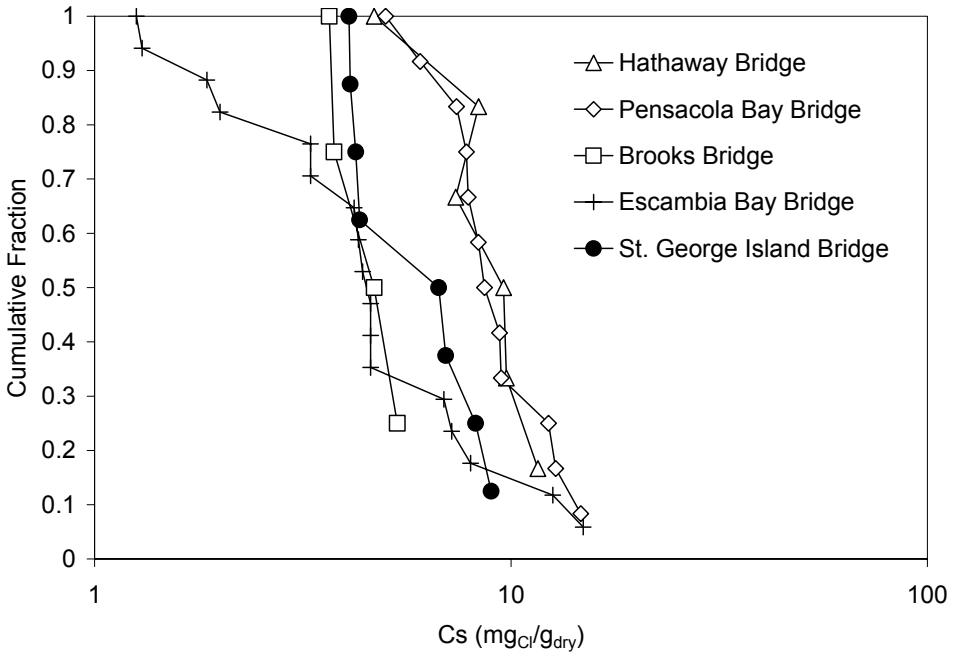

Figure 4.25 Cumulative Fraction of Cs values for cylinder piles in study and Escambia Bay Bridge study [1].

4.4 Concrete Pore Water pH

ISL measurements of pore water pH were made for samples of in-service piles from the Hathaway and Pensacola bridges, as well as samples from SGI Bridge piles cutoffs that were not in service. Results are shown in Figures 4.26 and 4.27. Terminal pH values for the SGI Bridge cutoffs ranged from 12.8 to 13.5. Those values are within the commonly observed range for present day concretes [36], so it appears that the pozzolanic additions used in the SGI Bridge concrete formulation did not result in a pronounced pore water pH drop. Some of the samples the older bridges had also terminal pH values of ~ 13, but most of the cores yielded values between 12 and 13 (and in one instance as low as ~ 11). Experimental artifacts, likely when using small cored specimens of highly impermeable concrete, may account for some of the lowest values observed. The overall modest pH values observed in the older bridge samples are nevertheless intriguing, considering that these older piles were expected to be made using unblended cement, and that pH lowering processes such as carbonation do not penetrate deeply in lower marine substructure elements [18]. It is possible however that the cements used in the older piles had lower alkali content than modern cements. Further assessment of this issue is recommended.

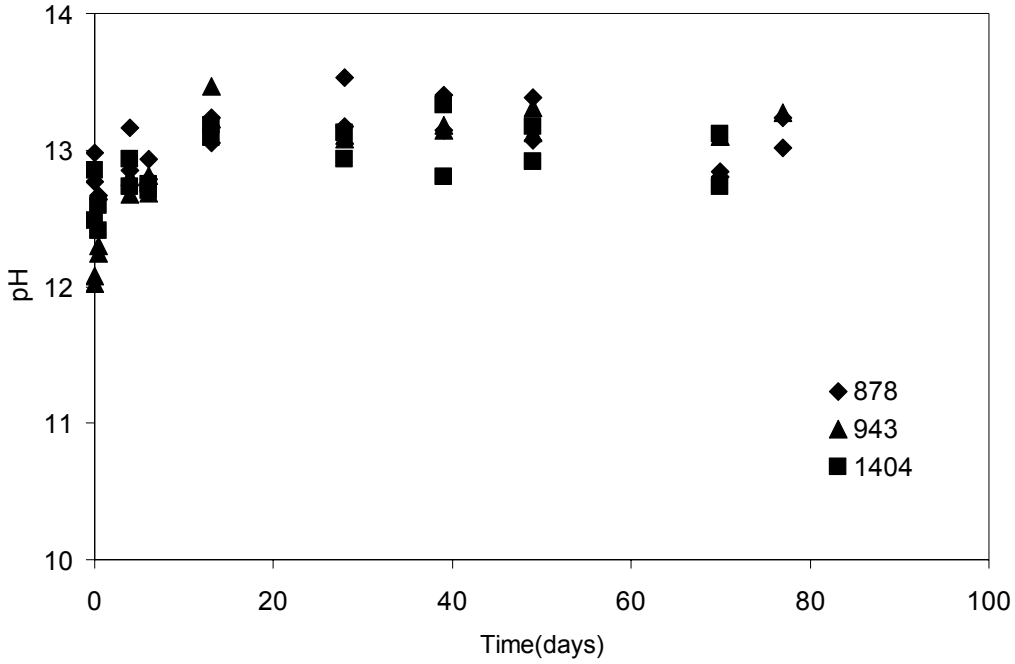

Figure 4.26 Pore water pH of St. George Island Bridge pile cutoffs by ISL technique.

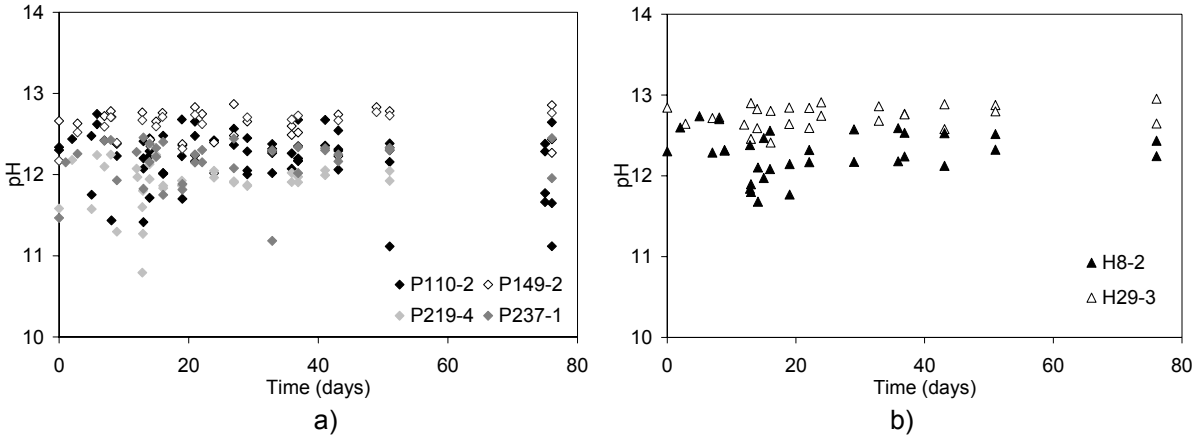

Figure 4.27 Pore water pH by ISL technique. a) Pensacola Bay Bridge. b) Hathaway Bridge

4.5 Magnetic Susceptibility Measurements

These tests were performed in the SGI Bridge samples as an indirect means to detect presence of fly ash as an admixture, and reveal possible pozzolanic addition shortage in the samples from P-162 which had shown relatively fast chloride penetration. Figure 4.28 shows that the magnetic susceptibility of all the SGI Bridge samples tested (with no clear trend differences between samples from both in-service piles) is of the same order or greater than the typical values encountered for other concretes known to have fly ash addition [2]. Therefore, all the SGI Bridge samples show a positive fly ash indication per this method. In Figure 4.28 the apparent diffusivity measured in the same or in the companion cores is used as a plotting parameter. Interestingly, for the SGI Bridge samples the apparent diffusivity tended to be smaller for the samples with the greatest magnetic susceptibility. However, susceptibility is only qualitatively representative of fly ash content and the observed trend may only be fortuitous.

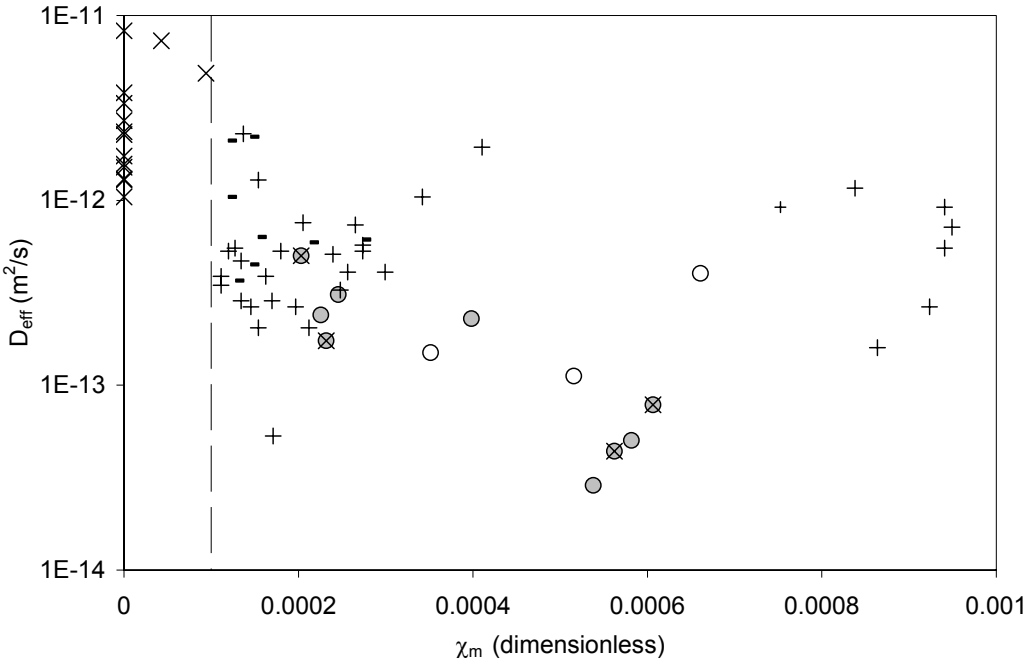

Figure 4.28 Magnetic susceptibility indication of fly ash presence and apparent chloride ion diffusivity. ● St. George Island Bridge samples. ○ Laboratory ponded samples. ⊠ Cracked concrete. + Concrete samples with known fly ash [2]. X Concrete samples without fly ash [2]. – Concrete samples with unknown presence of fly ash [2]. Vertical line represents susceptibility detection limit.

4.6 Laboratory IRH Measurements

Concrete cores from unused pile cutoffs from the SGI Bridge were used to measure internal relative humidity as indication of concrete permeability. A cylindrical cavity 1-in (2.5 cm) in diameter and 1.5-in (3.8 cm) in length was drilled centered into the flat surface of 3.75-in (9.5 cm) diameter, ~ 3-in (~7.6 cm) length, concrete cores for IRH measurements as described in Section 2.2. IRH measurements were initially made storing the core samples in ambient laboratory conditions where the room humidity and temperature was typically in the range of 60 to 75% RH and 20 to 25^{o}C, respectively for approximately 100 days. The concrete IRH reflected a similar range in humidity level during that time. Figure 4.29 shows the moisture pickup in the core samples from conditioning in a 100% RH chamber as measured by IRH. As indication of low concrete permeability, the concrete IRH only began to show signs of stabilization after approximately 100 to 200 days. It should be noted that the entire surface area of the concrete core was exposed to conditioning and the laboratory test results may not be representative of actual field conditions.

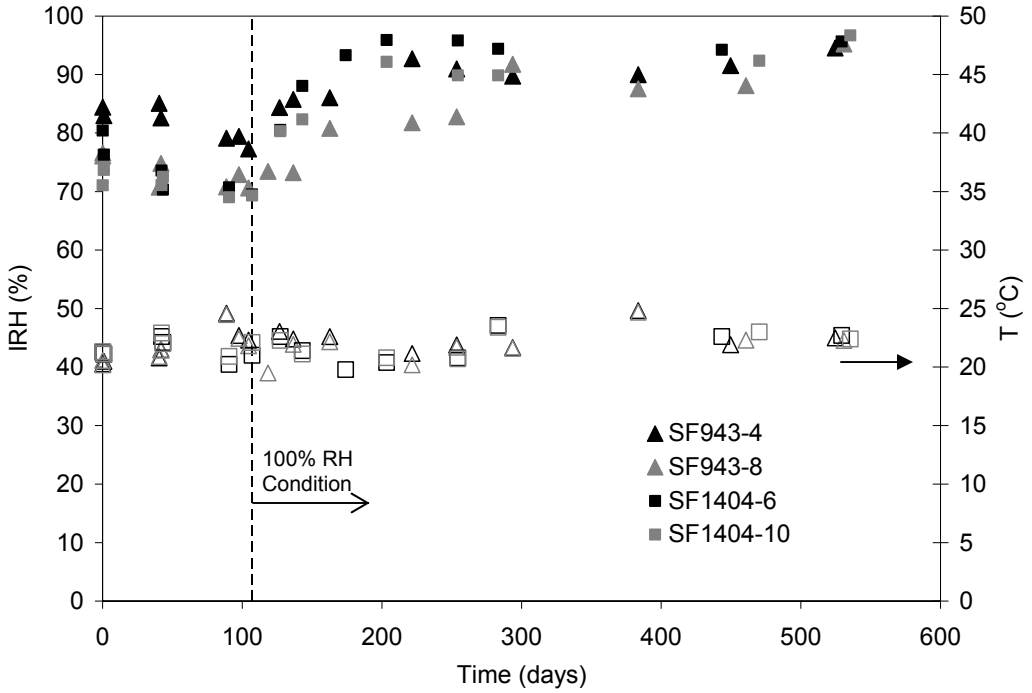

Figure 4.29 Concrete IRH and temperature as function of time conditioned in ambient conditions and 100% RH. The vertical line represents the time when the samples were placed in high humidity.

5 Durability and Pile Design

5.1 Performance of Cylinder Piles from Older Bridges

The field and laboratory findings are indicative of very good corrosion performance of older cylinder piles over service periods of several decades, confirming similar indications in the previous Escambia Bay bridges investigation[4]. Exceptions were locations such as the upper end of the pile by the pile cap, where mechanical distress during construction had exposed reinforcement that was not sufficiently covered afterwards. Early repair patches at the Pensacola Bridge appear to reflect similar local construction deficiencies. Those cases will not be considered further as they involve detailing control common to most pile types. Conspicuous rust stains at intermediate elevations, notably in the Pensacola Bay Bridge, appear in most cases to have resulted from corroding steel debris or other auxiliary components but not related to corroding reinforcement or strand. In the following, only the condition of the normally constructed and exposed portion of the piles will be addressed.

No telltale rust patterns on the surface of the piles, reflecting the position of spiral reinforcement or strand, were noticed upon examination. Extraction of cores focused on spots selected for showing unusually high rust staining, and yet only two cases of appreciable loss of steel due to corrosion were found in the three bridges investigated. All the other observations of steel corrosion (including some on the post tensioning strand) were of only minor rust or discoloration, some of which may have been present prior to embedment in concrete or grout. Steel potential measurements were equally indicative of a passive steel condition over much of the substructure region investigated. The general evidence of little or no corrosion is striking in view of the aggressiveness of the environment, the four-decade long service life of the structures investigated, and the thin clear steel concrete cover existing (especially in the Pensacola Bay bridge, with <1 in (2.54 cm) cover on average).

[4] A caveat applies in that only the tidal and higher elevation portion of the substructure was surveyed in these bridges. Evidence from other FDOT concrete substructures indicates that most corrosion related damage manifests itself first above water, as evaporative chloride accumulation and oxygen availability is greater there. That trend is assumed to apply here as well but deterioration below the waterline cannot be discounted without direct evidence. Autopsy of the submerged portion of cylinder piles removed from service in the future is recommenced to confirm absence of severe damage there.

The observed high corrosion resistance of these older piles appears to stem from a combination of very slow chloride ion penetration rates through the concrete with either or both of the following: a substantial critical chloride concentration threshold for steel corrosion initiation, and low corrosion propagation rates if the threshold was exceeded. These factors are considered next.

5.1.1 Chloride penetration

As shown in Figure 4.21, the range of surface chloride concentrations observed in the cylinder pile surfaces were similar to those encountered in other marine and estuarial Florida bridges built with conventional concrete. Thus the driving force for chloride penetration in the older cylinder piles was not unusually high or low. The observed chloride diffusivities were however extremely small (typically about 10^{-13} m^2/s) which caused chloride penetration to be greatly retarded in the bulk of the concrete. Furthermore, in contrast to observations in conventional FDOT substructures [2], rapid chloride transport through thin cracks was not strongly apparent in the older cylinder piles. Thus, even though thin cracks were frequently observed, inward chloride ion penetration appeared to be ruled mostly by bulk parameters.

Low bulk chloride diffusivity was expected in high quality concrete with high cement content, low w/c ratio and good compaction, as used in the cylinder piles. Both the low bulk diffusivity and the lesser importance of thin cracks may have been promoted by low internal concrete moisture as indicated by the low internal RH levels measured in the field. Low internal moisture can exist even under wet external conditions if the concrete is dense and the low w/c induces self-desiccation upon long term hydration of the cement [37]. Under those conditions ionic transport in the bulk, already slow due to a tight pore network, is made slower by fewer liquid paths within the pores. Transport through thin cracks is lowered as well, since the presence of liquid along the crack line is equally diminished. This condition is manifested, for example, by the lesser importance of crack transport even in conventional substructure, when cores containing cracks are extracted at higher elevations where the concrete is drier [2].

5.1.2 Critical chloride threshold

Because most corrosion observations involved LC cases, it is uncertain whether sustained active corrosion was actually in progress. Indeed, in some instances the assignment of an LC rating was accompanied by steel potential readings indicative of passive conditions. A highly conservative chloride threshold estimate can be made nevertheless by assuming that LC ratings represent active corrosion in progress, and calculating the value of the chloride concentration at the corresponding steel depth. To that end, the data on the condition of the steel and chloride concentration at the recorded steel depth in Table A3, Appendix III were used to construct the composite cumulative distribution in Figure 5.1. The chloride concentration at the time of the survey (although for the two SC instances corrosion initiation probably took place much earlier) at the steel depth was calculated from the diffusion parameters determined by the core that exposed the steel. For cases where no chloride data or cover was available for that core, estimates were made as detailed in Table A3, Appendix III. Only data for spiral steel and spacing rebar were used for this graph; conditions of the deeper, grout-surrounded strand are considered separately.

The trend in Figure 5.1 (although affected by large uncertainty from the many assumptions made) suggests that no corrosion initiation took place at concentrations below ~ 0.5 mg/g (or ~ 2 pcy (~ 1.2 kg/m^3) for typical 4000 pcy (2400 kg/m^3) concrete), and that in many instances the chloride content was higher and not even incipient signs of corrosion took place. Thus a value of 0.5 mg/g may be suggested as a conservative lower bound for the critical chloride threshold of reinforcing steel in these piles, recognizing that the actual effective threshold value (or range of values[5]) is likely to be significantly greater. It is worthwhile noting that corrosion thresholds reported in the literature for steel in conventional concrete but with high cement content similar to that present in the circular piles are in the order of ~1 mg/g [40]. Factors such as better concrete compaction in the cylinder piles may result in higher threshold values compared with that in conventional cast concrete.

The trend in Figure 5.1 suggests that corrosion initiation was just beginning to affect a small fraction of the pile inventory in these bridges at the

[5] Corrosion initiation in concrete, even under controlled conditions, is of a stochastic nature [38]. In addition, corrosion initiation at a given place on a steel assembly may be significantly retarded if the local potential of the passive steel has been driven to more negative values by ongoing corrosion in nearby regions of the same assembly, or by low oxygen availability [39]. Those phenomena may have been responsible for the absence of corrosion in some of the higher chloride concentration regimes.

time of the survey. This is consistent with a combination of normal chloride surface concentrations, very low diffusivities and considerable threshold levels. By application of Eq. (1) this combination results in long projected times to corrosion initiation, even though the observed clear concrete covers were so thin. For example, one may assume values representative of the present findings: Cs=10 mg/g, near zero native chloride, $D=10^{-13}$ m^2/sec and x_C=2.5 cm, together with C_T=1 mg/g. Eq.(1) then projects a time to corrosion initiation of 37 years. A higher threshold value would extend the projected time to initiation accordingly.

The above discussion applies to spiral or rebar steel. Little can be said from the present findings about the effective threshold for strand steel as in most cases the projected chloride penetration to the strand depth was very small, and the few instances of rust on strand wires are not clearly related to ongoing corrosion. In the absence of other information, it will be assumed that the corrosion threshold for properly grouted strand is comparable to that of the other steel in these structures, with consequent expectation of much longer times to corrosion initiation due to the deeper clear cover of the strand. A potential concern is the observation of two cases of clearly visible grout voids (core P237-1-2 and P252-1-1), which may locally lower the corrosion threshold. Control of grouting quality is essential.

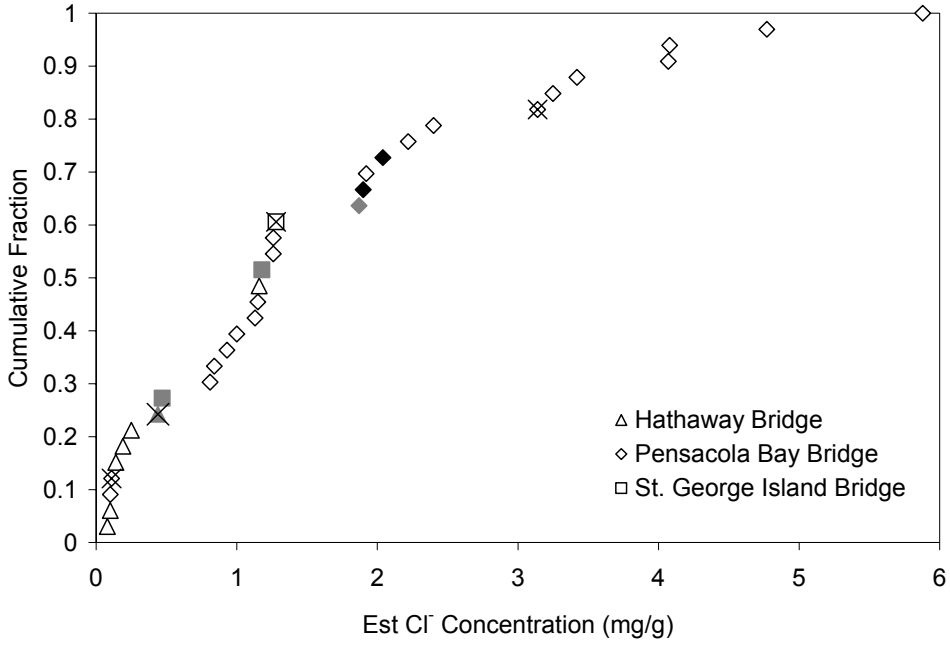

Figure 5.1 Cumulative fraction of estimated chloride concentration at steel depth determined for locations where spiral or spacing bar steel was exposed by coring in the Hathaway, Pensacola, and Brooks bridges. See Table A3, Appendix III for details and assumptions. Solid symbols- SC. Grey symbols- LC. Open symbols- NC. X- core drilled on crack.

5.1.3 Corrosion propagation rates

From the previous section and the generally low external manifestations of corrosion, it can be said that corrosion propagation (topical extraneous damage excluded) has either not commenced in most of the piles, or is proceeding at a very low rate. The steel exposed by coring that most commonly showed some signs of corrosion (LC condition) had very small average corrosion penetration, perhaps only a few micrometers. If that corrosion actually occurred in service, the previous discussion suggests that initiation took place relatively recently, so typical corrosion propagation rates should be in the micrometer per year range (barely above usual estimates of passive corrosion rates [41]). This modest range estimate is not surprising considering that the concrete in the piles, even when wet, had high resistivity (reflecting low pore connectivity and often moderate internal humidity), of a level commonly associated with very low or outright insignificant corrosion rates [27].

The corresponding time necessary for a corrosion-induced crack to occur may be evaluated using the expression by Torres-Acosta [42].

$$\frac{X_{CRIT}}{mm} \sim 0.011 \left(\frac{Xc}{\Phi}\right)\left(\frac{Xc}{L} + 1\right)^2 \qquad (2)$$

where x_{CRIT} is the steel corrosion penetration necessary to cause a crack in the concrete, Xc is the concrete cover thickness, Φ is the steel bar diameter, and L is the corroding length. Assuming conservatively that L is large compared to Xc, and taking representative dimensions for the spiral wire in the old bridges (Φ = 6 mm, Xc = 30 mm) the result is x_{CRIT} ~ 0.055 mm. Corrosion is likely to be more localized during the early initiation events. In such case if e.g L ~ Xc, then x_{CRIT} would be twice as large. With corrosion rates in the micrometer per year range, the typical time required to develop a corrosion induced crack after the initiation event could then easily stretch into two or more decades.

After the first corrosion induced cracks take place the corrosion rate is likely to increase so subsequent deterioration would be faster and concrete delamination would quickly ensue. The two recorded incidents of severe wire corrosion may reflect such occurrence. In one of those cases the estimated clear cover was only 1.4 cm, and corrosion propagation may have been in progress for many years already. It is noted that even in those cases, the actual metal loss was quite localized and much of each wire segment extracted retained the initial dimensions.

The longitudinal steel strands in these structures are placed about 1/3 to 1/2 deeper than the spiral wires or spacing bars. All other factors being equal, the

time necessary to reach threshold chloride levels at reinforcement depth is approximately proportional to the square of the cover (Eq.1). Corrosion of the strand is then expected to start much later in the life of the structure. Thus, any future corrosion-related severe damage to the concrete, and related repair needs, are likely to result first from the corrosion of the spiral reinforcement.

5.1.4 Corrosion-related durability prognosis

A small fraction of piles have already shown indications of corrosion damage. The factors considered above indicate that incipient indications of concrete damage from corroding reinforcement beyond those observed may already exist in a small fraction of the piles, and might become apparent upon extensive re-examination of the structures. However, threshold values may span a wide range above the value tentatively identified above, and evolution of the corrosion propagation stage is expected to be slow. Thus, development of corrosion damage serious enough to require repair or rehabilitation appears to be several decades into the future. There is then a good chance that, despite their low concrete clear cover, the cylinder piles bridges built in the 1960's and still commissioned will perform with little corrosion-related maintenance needs well into a 75-year service life span. The quantitative durability treatment developed earlier for the Escambia Bay bridges [2] reached similar conclusions using assumptions for the initiation and propagation stage that were approximately equivalent to considering the findings from the present program, so reference is made to that work.

5.2 Performance of Cylinder Piles Built Under Current FDOT Guidelines

The very early information developed to date for the piles at the SGI Bridge indicates, on average, excellent bulk concrete properties to slow down chloride ingress. Attention is called to the somewhat higher (but still quite small in absolute terms) diffusivity encountered in one of the piles tested; its chloride penetration behavior should be mentioned in the future and testing extended to other piles to assess any possible systematic deficiency. Nevertheless, because of the high pozzolanic content of the concrete, bulk chloride transport is expected to become even slower in the future. Surface chloride concentration levels were indicative of no unusual driving force for chloride penetration.

The cylinder piles in the SGI Bridge section investigated showed frequent thin cracks (not caused by corrosion), in some instances propagating deep into the reinforcement level. It is too early to assess the effect of those cracks on

chloride transport, except to note that preferential chloride ingress was observed in two instances in the shallow range (~1/2 in (~1 cm)) where chloride profiles were measurable. It is possible however that the same conditions that seem responsible for mitigating chloride crack transport in the older bridge piles will be active here as well. Future evaluation as the structure ages is important to better assess this issue.

Chloride threshold cannot be directly evaluated at present, as no reinforcement corrosion cases were documented (rust spots seen on the surface of some SGI Bridge piles appear to be related to steel debris or other extraneous sources). However, the pore water assessment indicated a high pH in spite of the high pozzolanic content. Thus, it appears likely that normal chloride threshold values may apply. Corrosion propagation would be expected to be limited in these piles by the same factors prevalent in the older bridges, except that the thicker concrete cover may further extend the time to corrosion induced cracking if the cover to steel diameter is greater. As in the older bridges, most of the corrosion-induced damage to the concrete is expected to originate from the spiral reinforcement before any strand corrosion becomes important.

5.3 Concrete Cover and Cylinder Pile Corrosion Performance

If bulk transport of chlorides were the only relevant factor, the corrosion limited durability of the modern cylinder piles would be expected to be exceedingly long. As indicated earlier, projected corrosion initiation times per Eq. (1) are proportional to the square of the clear cover. The average of the cover from the three older bridges (Table A2) is 1.17 in (2.96 cm), while that of the SGI bridge is 3.18 in (8.1 cm). Thus, if as suggested by the present findings the chloride diffusivity and corrosion threshold are comparable, the length of the corrosion initiation stage in the newer piles would be in the order of $(3.18/\ 1.17)^2$ ~ 7 times greater than for those in the older bridges. Nominal durability far in excess of 100 years would be then projected.

The above simplistic analysis does not take into consideration the potential for localized chloride ingress paths, notably preexisting cracks as those noted earlier. Because of the much thicker clear cover, both the propensity for any cracks and the width of the cracks may be significantly greater than in the older cylinder pile design[6]. The use of microsilica in newer piles may also increase the chances of cracking due to less tolerance to curing anomalies [43]. As indicated in Section 5.2, the extent of enhanced chloride penetration can not

[6] It is noted however that cracking at the piles in the investigated portion of SGI is generally related to other construction issues, examined separately by FDOT.

be assessed well at this early pile age. Thus, the possibility of severe chloride penetration through preexisting cracks, as noted in other FDOT structures with otherwise highly impermeable concrete, cannot be disregarded and continuing monitoring of those locations is needed.

The above findings suggest that, from a bulk chloride penetration standpoint, cylinder piles constructed with the materials examined here could have clear cover levels significantly less than the currently specified 3 in (7.5 cm) and still result in times to corrosion initiation amply consistent with a 75-year durability goal. In addition to lowered material requirements and fewer fabrication constraints, a smaller cover might reduce the propensity for incidence of cracks. Improved reliability may result as well as fabrication methods would approach established practice that has resulted in the good corrosion performance documented here for the older piles.

Present FDOT Structure Design Guidelines (Section 4.5, Post Tensioning) establish multiple levels of protection for critical bridge components which may be extended to cylinder piles as well. Of special interest is the condition of the tendons at the joint between pile segments. At present protection to the strand there is provided by two consecutive elements: the grout around the strand, and the parallel combination of the concrete at both sides of the joint and the epoxy or similar filler material placed between the two joined segment faces. A reduction in design cover as considered above would also reduce the length of the thin polymer-filled region between the segment faces possibly facilitating chloride ingress at the joint. Special provision for added quality control or supplemental protection there, as well as dimensioning piles to avoid joint placement in the tidal or splash zones, may merit consideration. A possible enhancement being considered by FDOT is the installation of a consecutive protection element provided by a corrugated polymeric duct cast in the grout channel. The mechanical consequences of such addition need examination for possible disadvantages; placement of similar ducts only near the segment ends may be a desirable alternative with fewer potential drawbacks if consistent with practical implementation. It is noted that no particular association between pile joints (where the joint cover is, as elsewhere, very thin) and evidence of corrosion was noted in the survey of the three older bridges.

Based on the above findings and discussion, it is recommended that alternative compromise minimum cover thickness levels of 2 in (51 mm) and 2.4 in (61 mm) be considered for possible implementation of a special cover guideline for cylinder piles to replace the present 3-in (76 mm) value. Those values are approximately $3^{1/2}$ = 1.73 times and $4^{1/2}$ = 2 times respectively greater than the average 1.17 in (2.96 cm) cover of the three older bridges surveyed. All other things being equal, the proposed cover values would result in nominal increases in time to corrosion initiation by a factor of 3 and 4 respectively over

the older implementation, depending on the level of conservatism desired. Based on the findings of the evaluation of the older bridges, the resulting piles under either alternative (with strict control of minimum values) would have an excellent prognosis for good corrosion control over a 75 year service span, while incurring less risk of crack development and approaching successful experience with previous production practices. The fabricability and quality assurance aspects of both alternatives should be examined in cooperation with pile manufacturers.

6 Conclusions

1. Examination of three 40 year old cylinder pile bridges (Hathaway, Pensacola Bay, and Brooks) indicated in general minor or no corrosion distress of the spiral reinforcement or strand in the piles, in spite of small clear concrete cover values of ~ 0.4 to 1.5 in (10 to 39 mm). Some corrosion noted near pile caps as well, or the presence of topical patches, appear to reflect early mechanical damage unrelated to normal exposure. Similar good corrosion performance was found in a previous FDOT examination of the Escambia Bay bridges, also built with cylinder piles.

2. The rate of chloride ion penetration in the 40-year old bridges, as indicated by the apparent diffusion coefficient, had a median value of only ~0.005 in^2/y (~$1x10^{-13}$ m^2/s), lower than that of the best performing modern FDOT class V concretes specified for aggressive marine service. High electrical resistivity and moderate internal humidity of the concrete were consistent with the slow chloride transport observed. These properties appear to have resulted from high cement content, low water to cement ratio, and good compaction inherent to the pile fabrication process.

3. Thin (< 0.013 in (<0.3 mm)) concrete cracks were observed in some of the piles in the 40-year old bridges. However, unlike behavior recently noted in other FDOT bridges with conventional concrete substructure, preferential chloride penetration along the crack was less pronounced.

4. Tests of the early performance (~2 years) of new cylinder piles built to current FDOT guidelines (thicker cover, pozzolanic admixtures) for the recently constructed Saint George Island bridge show also excellent average resistance to chloride penetration. No reinforcement corrosion was identified at this early bridge age. Thin cracks were observed here as well, together with evidence of enhanced chloride penetration at shallow depths, so continuing monitoring as the bridge ages is recommended.

5. The survey information from the older bridges was used to estimate a lower bound value for the chloride threshold for corrosion initiation in the order of ~2 pcy (1.2 kg/m^3). This bound is consistent with the reported high cement content of the concrete and the observation of pH values in extracted cores approaching normally expected values. Effective threshold values could be significantly higher. The concrete in the new bridge piles had a desirably high pore water pH

despite its high pozzolanic content, suggesting that chloride threshold values in the new material will be in the normal range.

6. Simplified corrosion damage forecasts for the older and new piles suggest that very long service lives with minimum corrosion-related maintenance are possible. The projections suggest also that if concrete quality could be sufficiently assured, moderate relaxation of absolute minimum cover requirements for new construction (for example from 3 in (7.5 cm) to ~2 in (5 cm)) could be made without severely compromising the requirements for minimum corrosion damage within a 75-year service life goal. Recommendations of alternative cover guidelines are presented for consideration of manufacturing and quality control factors.

7 References

1. Sagüés, A.A., W. Scannel and F.W. Soh. "Development of a Deterioration Model to Project Future Concrete Reinforcement Corrosion in a Dual Marine Bridge" in *Proc. International Conference on Corrosion and Rehabilitation of Reinforced Concrete Structures*, Orlando, FL, Dec. 7-11, 1998, CD ROM Publication No. FHWA-SA-99-014, Federal Highway Administration, 1998.

2. Sagüés, A.A. and S.C. Kranc. "Corrosion Forecasting for 75-Year Durability Design of Reinforced Concrete." Final Report to Florida D.O.T. WPI 0510805, Contract No. BA-502. December, 2001.

3. FDOT Structures Design Guidelines, Topic No. 625-020-150c, Chapter 2: Site and Material Durability Criteria, Effective: July 1, 1998, Revised: January 1, 1999.

4. Graves, A.S., and W.F. Knight letter to T. Malerk, FDOT, September 21, 1999.

5. Buslov, V. B., Gould, J. P & Koch, R.C. "The Precast Pier." *Civil Engineering.* 1988.

6. Cook, J.R. "Severe Foundation Problem Solved Using Long Precast Prestressed Concrete Piles." *PCI Journal*. 1974.

7. *Bayshore Concrete Products*, Bayshore Concrete Products Private Publication.

8. Fuller, F.M. *Raymond Cylinder Piles Meet The Challenge of High-Load Tests*, Foundation Facts, Houston, TX: Raymond International Builders, Inc. 1979.

9. Snow, R. K. *Performance of the Raymond Cylinder Pile*, Foundation Facts. 1983.

10. Brown, D.D. *Elba Island Bridge Construction*, Foundation Facts. 1974.

11. LeMieux, G.F. "Underwater Inspection of the World's Longest Overall Bridges, Part I." *Concrete International*. 1998.

12. Avent, R.R. and Mukal, D. J. “Investigation of Cracks in Cylindrical Spun-Cast Concrete Piles in a Marine Environment.” Final Report for Louisiana Transportation Research Center. 1998.

13. Garder, D. R. “Inspection of Substructure of the Chesapeake Bay Bridge-Tunnel above and below the Waterline.” *Transportation Research Record.*

14. Gerwick, B.C. “International Experience in the Performance of Marine Concrete.” *Concrete International*. 1990.

15. Florida Department of Transportation. Bridge Management System. Comprehensive Inventory Data Report. Bridge No. 460012. 2001.

16. Florida Department of Transportation. Bridge Management System. Comprehensive Inventory Data Report. Bridge No. 48035. 2000.

17. Florida Department of Transportation. Bridge Management System. Comprehensive Inventory Data Report. Bridge No. 570034. 2001.

18. Sagüés, A.A., et al. “Carbonation in Concrete and Effect on Steel Corrosion.” Final Report to Florida D.O.T. WPI. No. 0510685. June 1997.

19. Carlsin, J.E. “Chloride profile based on sampling of dust by hand drill with vacuum attachment.” in *Proc. of the Nordic Seminar in Lund*. February 1-2, 1995.

20. Concrete, Hardened: Accelerated Chloride Penetration. Nortest Method NT Build 443, (1995).

21. Florida Method of Test for Determining Low-Levels of Chloride in Concrete and Raw Materials. FM-5-516 (2000).

22. Berke, N.S. and M.C. Hicks. “Predicting Chloride Profiles in Concrete.” *Corrosion*. Vol.50, no. 3. Pp. 234-239. 1994.

23. Morris, W., E.I. Moreno, and A.A. Sagüés. “Practical Evaluation of Resistivity of Concrete in Test Cylinders Using a Wenner Array Probe.” *Cement and Concrete Research*. Vol.26, no.12. p.1779-87. 1996.

24. Standard Test Method for Density, Absorption, and Voids in Hardened Concrete. ASTM C642 (1997).

25. Sagüés, A.A., Moreno, E.I. and. Andrade, C. “Evolution of pH During In-Situ Leaching in Small Concrete Cavities”, *Cement and Concrete Research*, Vol. 27, p.1747, 1997.

26. Half-Cell Potentials of Uncoated Reinforcing Steel in Concrete. ASTM C876. (1991).

27. Carino, Nicholas J. “Nondestructive Techniques to Investigate Corrosion Status in Concrete Structures.” *Journal of Performance of Constructed Facilities.* Vol.13, no.3. p.96-106. 1999.

28. Emerson, M. “Mechanisms of Water Absorbtion by Concrete.” In Protection of Concrete. London: E&F.N. Spon, 1990. p.689-700

29. Berke, N.S. and M.C. Hicks. The life cycle of reinforced concrete decks and marine piles using laboratory diffusion and corrosion data. In *Corrosion Forms and Control for Infrastructure*, ed. V. Chaker. ASTM STP1137, American Society for Testing and Materials, Philadelphia, 1992.

30. Safiuddin, Md., Nataliya Hearn. “Comparison of ASTM saturation techniques for measuring permeable porosity of concrete.” *Cement and Concrete Research.* 2004.

31. Sagüés, A.A., S.C. Kranc. “Advanced Analysis of Chloride Ion Penetration Profiles in Marine Substructure.” Final Repot to Florida D.O.T., Contract No. BB-880, January 2003.

32. Bamforth, P. “Improving the durability of concrete by the use of mineral additives.” Paper presented at Concrete Durability in the Arabian Gulf, Bahrain Society of Engineers, March 19-21, 1995.

33. Sagüés, A.A. “Corrosion of Epoxy Coated Rebar in Florida Bridge.” Final Report to Florida D.O.T., WPI No. 0510603. May, 1994.

34. Sagüés, A.A. et al. “Corrosion Resistance and Service Life of Drainage Culverts.” Final Report to Florida D.O.T., WPI NO. 0510756. August 2001.

35. Rodriguez, O. and R. Hooton. “Influence of cracks on chloride ingress into concrete.” *ACI Materials Journal*. Vol.100, no.2. p.120-6. 2003.

36. Caseres, Leonardo. “In-Situ Leaching for Determination of Chloride and pH in Concrete and Mortar Pore Water.” Master Thesis. University of South Florida. 2002.

37. Nilsson, L.O., “Moisture in Marine Concrete Structures.” In *Durability of Concrete in Saline Environment*. Lund: Cementa AB, 1996.

38. Li, Lianfang. “Chloride Corrosion Threshold of Reinforcing Steel in Alkaline Solutions- Cyclic Polarization Behavior.” *Corrosion*, Vol. 58, p.305. 2002.

39. Presuel-Moreno, F.J., A.A. Sagüés, and S.C. Kranc. “Steel Activation in Concrete Following Interruption of Long Term Cathodic Polarization.” *Corrosion*. Vol. 61, p. 428-436. 2005.

40. Li, Lianfang. “Chloride Corrosion Threshold of Reinforcing Steel in Alkaline Solutions - Open-circuit Immersion Tests." *Corrosion.* Vol. 57, p.19, 2001.

41. Sagüés A.A., Pech-Canul M.A. and Shahid Al-Mansur. “Corrosion Macrocell Behavior of Reinforcing Steel in Partially Submerged Concrete Columns”, *Corrosion Science*, Vol.45, p.7. 2003.

42. Torres-Acosta, A.A. and A.A. Sagüés. “Concrete Cracking by Localized Steel Corrosion- Geometric Effects.” *ACI Materials Journal*. Vol. 101, no.6. p.501-507. 2004.

43. Diamond, Sidney, S. Sahu, and N. Thaulow. “Reaction products of densified silica fume agglomerates in concrete.” *Cement and Concrete Research*. Vol.34, .1625-32. 2004.

Appendix I Bridge Inspection Survey

Table A1a Hathaway Bridge Survey 12/17/02

Bent	General Remarks	Inspection Notes	Potential	Resistivity	Continuity	IRH	Core Extraction
1	Abutment. Begin bridge.						
2	Begin pile bent. Four 54" cylinder piles.						
3	H-3-2 rust stain near top of pile.						
5	H-5-3 rust stain near top of pile. H-5-4 repair patch near top of pile.						
6	H-6-2 rust stain at top of pile. H-6-3 rust stain.						
7	H-7-2 minor rust stain near top of pile. H-7-4 rust stain near top of pile.						
8	H-8-2 rust stain in splash zone.	H-8-2 rust stain on east side of pile in splash zone. Removed delaminated concrete, but hoop wire was not observed.	H-8-2	H-8-2	H-8-2	H-8-2	H-8-2
9	H-9-1 crack near top of pile. H-9-4 rust stain at intermediate elevation.						
11	H-11-1 delaminated concrete.						
13	H-13-4 rust stain near top of pile.						
14	H-14-1 repair patch near top of pile.						
15-28	column piers	H-16 rust stain on footer. H-27 rust stain on footer. H-28 severe rust staining on footer.					
29	Pile bent. Four 54" cylinder piles. H-29-3 crack.	H-29-3 crack 0.3mm width.	H-29-3	H-29-3	H-29-3	H-29-3	H-29-3
30	H-30-3 crack. H-30-4 rust stain in splash zone.						
31	H-31-2 spall in tidal zone. H-31-3 spall at intermediate elevation.						
32	H-32-2 rust stain at intermediate elevation.						
33	H-33-1 crack repair. H-33-3 rust stain in splash zone. H-33-4 rust stain in splash zone.						

Table A1b Pensacola Bay Bridge Survey 3/10/03–3/11/03

	General remarks	Inspection Notes	Potential	Resistivity	Continuity	IRH	Core Extraction
1	Abutment. Begin Bridge.						
2	Begin pile bent. Four 54" piles. P-2-2 rust stain on west face. P-2-3 crack below pile cap.						
3	P-3-1 crack below pile cap. P-3-2 rust stain on east face above tidal zone.						
4	P-4-1 crack. P-4-3 crack below pile cap.	P-4-1 vertical thin crack 0.3mm width.	P-4-1		P-4-1		P-4-1
5	P-5-1 rust stain on north face above tidal zone. P-5-3 rust stain on east face at tidal zone.	P-5-3 large delaminated area ~63in^2.					
6	P-6-1 rust stain on west face. P-6-3 rust stain on north face. P-6-4 rust stain on north face at tidal zone.						
8	P-8-1 rust stain on northeast face. P-8-3 rust stain on north face. P-8-4 rust stain on west face at tidal zone.						
9	P-9-1 crack on north face. P-9-4 rust stain on south face.						
10	P-10-1 rust stain on south face						
12	P-12-2 rust stain on west and east face.						
13	P-13-2 crack on south face.						
14	P-14-3 rust stain on south face. P-14-4 rust stain on east face.						
15	P-15-2 rust stain on south face.						
16	Tower bent. Six 54" piles. P-16-2 rust stain on south face. P-16-3 rust stain on west face. P-16-6						
18	P-18-1 rust stain on west face. P-18-2 rust stain on west face.						
19	P-19-2 rust stain on south face. P-19-3 rust stain on west face. P-19-4 rust stain on north face.						

Table A1 b (continued)

Bent	General Remarks	Inspection Notes	Potential	Resistivity	Continuity	IRH	Core Extraction
21	P-21-1 possibly crack. P-21-3 rust stain on west face.						
23	P-23-1 rust stain on east face.						
24	P-24-1 rust stain on northeast and southeast face.	P-24-1 delaminated concrete removed ~4in^2.					
25	P-25-3 rust stain on south face. P-25-4 rust stain on north face.						
26	P-26-1 rust stain on north face.						
27	P-27-3 rust stain on east face. P-27-4 rust stain on west face.						
29	P-29-2 rust stain on east face.						
30	P-30-3 crack near pile cap. P-30-4 rust stain on west face						
31	Tower bent.						
32	P-32-1 rust stain on south face.						
33	P-33-3 rust stain on west face.						
34	P-34-4 rust stain on south face below pile cap.						
35	P-35-1 rust stain on east face.						
37	P-37-1 rust stain on south face.						
38	P-38-2 rust stain on north face.						
40	P-40-1 rust stain on west face.						
42	P-42-1 rust stain on west face.						
43	P-43-1 rust stain on east face.						
46	Tower bent. P-46-1 rust stain on east and west face.						
48	P-48-4 rust stain on south face.						
50	P-50-3 rust stain on W face.						
51	P-51-1 rust stain on east face. P-51-2 rust stain on NE face at tidal zone.						
52	P-52-2 rust stain on N face at tidal zone.						

Table A1 b (continued)

Bent	General remarks	Inspection Notes	Potential	Resistivity	Continuity	IRH	Core Extraction
53	P-53-1 rust stain on NE and S faces.						
55	P-55-2 rust stain on W face at tidal zone. P-55-4 rust stain on W face.						
56	P-56-1 rust stain on E and W face.						
57	P-57-4 rust stain on S face.						
58	P-58-1 rust stain on S face.						
59	P-59-3 rust stain on S face. P-59-4 rust stain on W face.						
60	P-60-2 rust stain on west face.						
61	Tower bent.						
63	P-63-1 rust stain on E face near top.						
64	P-64-2 crack near pile top.						
65	P-65-1 rust stain on E face.						
66	P-66-1 rust stain on E face.						
67	P-67-2 crack near pile top.						
69	P-69-3 rust stain on NW face.						
71	P-70-3 rust stain on NE face,						
74	P-74-4 crack.						
76	Tower bent. P-76-4 rust stain on N face.						
77	P-77-1 rust stain on E face.						
79	P-79-1 severe rusting on E face.	P-79-1 rust stain near pile cap. No indication of delamination.					
80	P-80-4 pop-out on E face.						
81	P-81-4 rust stain on E face at tidal zone.						
83	P-83-1 rust stain on E face near pile top.						
84	P-84-1 rust stain on N face. P-84-3 rust stain on W face. P-84-4 rust stain W face.						
86	P-86-4 rust stain on W face near top.						
87	P-87-4 pop-out on E face.						

Table A1 b (continued)

Bent	General Remarks	Inspection Notes	Potential	Resistivity	Continuity	IRH	Core Extraction
88	P-88-3 rust stain on W face.						
91	Tower bent.						
94	P-94-2 popout. P-94-4 crack.						
96	P-96-2 rust stain on N face.						
98	P-98-3 rust stain on W face near top.						
99	P-99-1 rust stain on E face near top. P-99-3 rust stain on W face near top.						
100	P-100-1 popout on S face.						
101	P-101-1 rust stain on E face near top. P-101-2 rust stain on SE face near top.						
102	P-102-2 rust stain on S face near top.						
103	P-103-1 rust stin on E face near top.						
104	P-104-1 rust stain on E face near top.						
106	Tower bent. P-106-4 rust stain on SW face near top.						
107	P-107-1 rust stain on east face. P-107-2 rust stain on S face. P-107-3 rust stain on N face.						
108	P-108-2 crack near top of pile.						
109	P-109-1 rust stain on E face. P-109-4 rust stain on N and W face.						
110	P-110-2 rust stain on E face.	P-110-2 spiral wire corroded in rust stain 14”AHT	P110-2			P110-2	P110-2
112-145	Column piers.						
146	P-146-4 rust stain at W face in tidal zone						
147	P-147-2 rust stain on W face near top.						
148	P-148-1 rust stain on E face in tidal zone. P-148-3 repair patch on W face.						
149	P-149-1 rust stain on E and S face. P-149-2 rust stain on S face. P-149-3 rust stain on S face.	P-149-2 two large delaminations, ~30 and 42 in^2. Wire appears corroded.	P149-2				P149-2

Table A1 b (continued)

Bent	General Remarks	Inspection Notes	Potential	Resistivity	Continuity	IRH	Core Extraction
150	P-150-1 rust stain on E face in intermed. Elevation. P-150-3 rust stain in W face.						
151	Tower bent. P-152-1 rust stain on W face. P-152-6 rust stain on S face.						
152	P-152-1 rust stain on W face. P-152-2 repair patch on SW face.						
153	P-153-2 repair patch on N face, rust stain on W face.						
154	P-154-1 repair patch on E face. P-154-2 repair patch on E face. P-154-4 repair patch on W face.						
155	P-155-1 repair patch on E face.						
156	P-156-1 repair patch on E face intermediate elevation, rust stain on S face near pile top. P-156-2 rust stain on N face.						
157	P-157-1 rust stain on N and W face. P-157-3 repair patch on S face.						
158	P-158-1 rust stain on N face. Delaminated concrete removed ~12in^2.						
160	P-160-1 rust stain on E face. P-160-2 rust stain on W face. P-160-4 repair patch on W face.						
161	P-161-1 rust stain on S face at tidal zone. P-161-3 rust stain on S face near top.						
162	P-162-3 repair patch. P-162-4 repair patch on W face.						
163	P-163-1 repair patch on E face near top. P-163-3 repair patch. P-163-4 crack.						
164	P-164-1 repair patch on N face, rust stain on E face. P-164-2 rust stain on S face. P-164-4 repair patch on N face.						
165	P-165-1 repair patch on SE face near top. P-165-4 repair patch on W face.						
166	Tower bent. P-166-4 rust stain on N and E face.						

Table A1 b (continued)

Bent	General Remarks	Inspection Notes	Potential	Resistivity	Continuity	IRH	Core Extraction
167	P-167-1 rust stain on N E and S face. P-167-4 rust stain on W face close to patch.	P-167-1 hammer sounding does not indicate delamination on N face					
168	P-168-3 rust stain on E face. P-168-4 rust stain on E and W face.						
169	P-169-2 rust stain on N face. P-169-3 rust stain on N face. P-169-4 rust stain on NE face.						
170	P-170-1 rust stain on S face near top.						
171	P-171-1 rust stain on N face. P-171-3 rust stain on S face. P-171-4 rust stain on NE face.						
172	P-172-1 rust stain on E and N face. P-172-4 rust stain on north face under patch.						
173	P-173-2 rust stain on E face under patch. P-173-3 rust stain on N face. P-173-4 rust stain on W face under patch.						
174	P-174-1 rust stain on S face. P-174-2 rust stain on S face. P-174-3 repair patch on E face. P-174-4 repair patch on E face.						
175	P-175-1 rust stain on E face a intermed. Elev, rust stain on W face. P-175-3 rust stain on E face. P-175-4 rust stain on N face.						
176	P-176-2 rust stain on E and W face. P-174-4 rust stain on W face.						
177	P-177-1 rust stain on E and S face. P-177-3 rust stain on N and E face near top. P-177-4 rust stain on W face under patch.						
178	p-178-2 repair patch in intermed. Zone. P-178-4 rust between patches.						
180	P-180-1 rust stain on E face. P-180-3 rust stain on E and W face.						
181	Tower bent. P-181-1 repair patch on E face at intermed level.						
182	P-182-2 repair patch. P-182-4 repair patch W face intermed. Level.						

Table A1 b (continued)

Bent	General Remarks	Inspection Notes	Potential	Resistivity	Continuity	IRH	Core Extraction
183	P-183-3 repair patch on N face. P-184-4 rust stain on N face under patch. P-183-4 rust stain on N face.						
184	P-184-1 rust stain on E face under patch. P-184-2 rust stain on W face. P-184-3 rust stain on N face under patch. P-184-4 rust stain on N face under patch.						
185	P-185-2 rust stain on E face under patch. P-185-4 rust stain on N and W face.	P185-4 W face spall ~32"AHT, exposed wire corroded. P185-4 N face delaminated ~6in^2.	P185-4				P185-4
186	P-186-1 rust stain on E face. P-186-4 rust stain on S face.						
187	P-187-1 repair patch on E face. P-187-2 crack on repair patch. P-187-4 rust stain on N W and S face.						
188	P-188-1 patch on SE face. P-188-4 rust stain on W face.						
189	P-189-1 rust stain on SE face. P-189-3 patch on N face. P-189-5 rust stain on WS face under patch.						
190	P-190-1 patch on S face.						
191	P-191-1 severe rust stain on NE face.						
192	P-192-1 rust stain. P-192-3 rust stain on E face.	P-192-1 NE face hammer sounding does not indicate delamination.					
193	P-193-1 rust stain on E face. P-193-2 repaired crack.						
194	P-194-1 rust stain on SW face. P-194-2 rust stain on E face at low elev.						
195	P-195-2 rust stain on E face at intermed. Elev.						
196	Tower bent. P196-1 severe rust stain on E face. P196-2 rust stain on N face, rust stain on W face under patch. P196-6 rust stain on E face.	P196-1 E face hammer sounding does not indicate delamination. Exposed reinforcement rust-free.					P196-1
197	P-197-4 rust stain on W face.						
198	P-198-1 rust on N W S faces. P-198-3 patch on N face. P-198-4 rust stain betw. patches.						

Table A1 b (continued)

Bent	General Remarks	Inspection Notes	Potential	Resistivity	Continuity	IRH	Core Extraction
199	P-199-1 rust stain on E face, patch. P-199-2 rust stain on N face. P-199-3 patch on W face.						
200	P-200-1 rust stain on E face. P-200-4 patch on E face						
201	P-201-3 rust stain on N face. P-201-4 rust stain on N face.						
202	P-202-1 patch on E face. P-202-4 rust stain on E face below patch.						
204	P-204-1 rust stain on S face.						
205	P-205-4 patch on NE face.						
206	P-206-1 patch on top of E face.						
207	P-207-1 rust stain on WS face. P-207-3 patch on NE face.						
209	P-209-2 patch on E face.						
210	P-210-1 rust stain on E face. P-210-4 rust stain on W face.						
211	Tower bent. P-211-2 rust stain on NE face. P-211-3 crack in N face.						
212	P-212-2 patch on E face.						
213	P-213-2 rust stain on E face. P-213-4 crack on W face.	P-213-4 crack length ~4', crack width ~0.3mm.	P213-4				P213-4
214	P-214-1 rust stain on NE face in tidal zone. P-214-2 patch south face.						
215	P-215-1 rust stain on E face at interm. Elev. P-215-4 rust stain on W and S face at tidal zone.						
216	P-216-1 patch on NE face. P-216-4 rust stain on W face.						
217	P-217-1 rust stain on E face. P-217-2 repaired crack. P-217-4 rust stain on north face.						
218	P-218-3 rust stain on N face at tidal elev.						
219	P-219-1 rust stain on S and W face in tidal zone. P-219-4 severe rust stain on west face.	P-219-1 rust stain on W face severely delaminated. Delaminated concrete removed. Exposed reinforcement rust-free.	P219-4				P219-4

Table A1 b (continued)

Bent	General Remarks	Inspection Notes	Potential	Resistivity	Continuity	IRH	Core extraction
220	P-220-1 rust stain on E face. P-220-4 patch on W face.						
221	P-221-1 rust stain on N face at tidal elev. P-221-2 patch on N face. P-221-4 rust stain on W face.						
222	P-222-4 severe rust stain on S W face.						
223	P-223-1 rust stain on N face. P-223-2 patch on N face.						
224	P-224-1 patch on E face. P-224-3 rust stain on E face. P-224-4 rust stain on N face.						
225	P-225-1 patch on E face, rust stain on N S face. P-225-4 rust stain on top of S face.						
226	Tower bent.						
227	P-227-1 rust stain on E face. P-227-4 rust stain on S face.						
228	P-228-4 rust stain on N face.						
229	P-229-1 rust stain on W face. P-229-3 rust stain on N face.						
230	P-230-4 rust stain on S face.						
231	P-231-1 rust on west face. P-231-3 rust on N face. P-231-4 rust on S face.						
232	P-232-2 rust on N E face.						
233	P-233-2 rust on W and S face.						
234	P-234-3 rust on N face.						
235	P-235-1 patch on E face. P-235-2 patch on E face, severe rusting. P-235-4 rust stain on NW face below patch.						
236	P-236-1 rust on E face, patch on W face. P-236-3 patch on W face.						
237	P-237-1 severe rust stain on E face intermed. Elevation. P-237-2 rust stain on E face	P237-1 delamination in bottom portion of rust stains ~20in^2. Exposed reinforcement rust-free.	P237-1				P237-1

Table A1 b (continued)

Bent	General Remarks	Inspection Notes	Potential	Resistivity	Continuity	IRH	Core Extraction
238	P-238-1 patch on E face. P-238-4 rust stain on N W face near patch.						
239	P-239-1 patch on E face. P-239-4 rust on W face, patch on W face.						
240	P-240-2 patch on E face. P-240-3 rust on E face. P-240-4 rust on N face.						
241	Tower bent. P-241-1 patch on E face. P-241-2 patch on E and W face. P-241-3 patch on E face. P-241-4 on W face.						
242	P-242-2 patch on E face. P-242-4 patch on W face.						
243	P-243-2 patch on N face. P-243-3 patch on N face. P-243-4 rust on N W face.						
244	P-244-1 patch on E face.						
245	P-245-1 rust on N face. P-245-2 rust on N face near patch.						
246	P-246-3 rust on E and S face.						
247	P-247-1 patch on E face. P-247-2 rust on W face. P-247-3 rust on W face.						
248	P-248-2 patch on N face. P-248-4 spall on W face.						
249	P-249-3 rust stain on E face intermed. Elev, rust stain on W face high elevation.	P249-4 Spall ~4in^2.					
250	P-250-1 patch on W face. P-250-2 rust on S face. P-250-4 rust on N face under patch.						
251	P-251-2 patch on E face. P-251-3 patch on N W face.						
252	P-252-1 rust stain on E face intermed. Elev. P-252-2 rust stain on W face high elev. P-252-4 repair patch on E face.	P-252-1 severe delamination 3'AHT. Area ~36in^2.	P252-1				P252-1
253	P-253-1 rust stain on N face. P-231-4 patch on E face.						
254	P-254-2 rust stain on W face.						
255	P-255-1 rust stain on N face at intermed. Elev. P-255-2 rust stain on E face at intermed. Elev.						

Table A1c Brooks Bridge Survey 3/13/03

Bent	General Remarks	Inspection Notes	Potential	Resistivity	Continuity	IRH	Core Extraction
1	End Abutment						
2	Ten 36” dimameter cylinder piles. Piles on shore						
3	Piles in shallow water. Br-3-2 fine cracks 0.2mm.	Br-3-2 Crack progated from top of pile section. Core extraction upon cracks. Br-3-7, 8, and 9 cracks. Br-3-4 and 8 rust stain. Br-3-2-5 exposed wire shows rust.	Br-3-2				Br-3-2
4	Br-4-1 rust stain on E face. Br-4-6 fine crack. Br-4-9 concrete spall.	Br-4-1 no indication of delamination. Br-4-5, 7, and 8 fine crack. Br-4-9 crack ~0.3mm.					
5	Column piers.						
6	Column piers.						
7	Column piers.						
8	Column piers.						
9	Br-9-1 concrete spall. Br-9-6 concrete spall.	Br-9-5, 6, and 9 cracks. Br-9-10 small rust stain.					
10	Piles onshore.						
11	Piles on shore.						
12	Piles on shore.						
13	Piles onshore.						
14	End Abutment.						

Table A1d St George Island Survey 3/2/04

Bent	General Remarks	Inspection Notes	Potential	Resistivity	Continuity	IRH	Core Extraction
73	73EN superficial rust stain. 73ES rust stain. 73CS longitudinal cracking.						
133	133ES rust stain and longitudinal crack.						
139	139EN longitudinal crack. 139ES longitudinal cracking. 139CS rust stain.						
145	145ES rust stain and longitudinal crack. 145CS longitudinal crack. 145WS longitudinal crack.						
146	146ES longitudinal crack. 146CN longitudinal crack.						
152	Test pile on west side of pile bent.		152-TP-N	152-TP-N			152-TP-N
162	162WS longitudinal crack. 4th bent from Eastpoint approach.		162WS		162WS		162WS
163	163WS longitudinal crack. 3rd bent from Eastpoint approach.		163WS		163WS		163WS

Appendix II Bridge Survey Diagrams

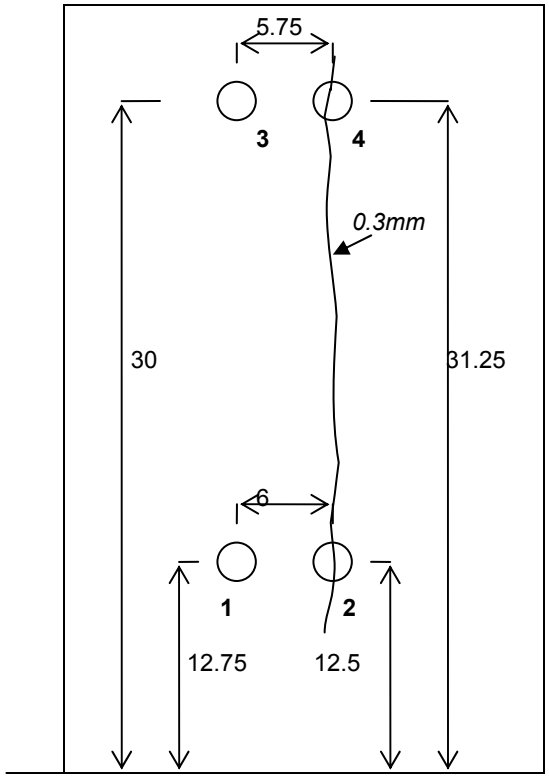

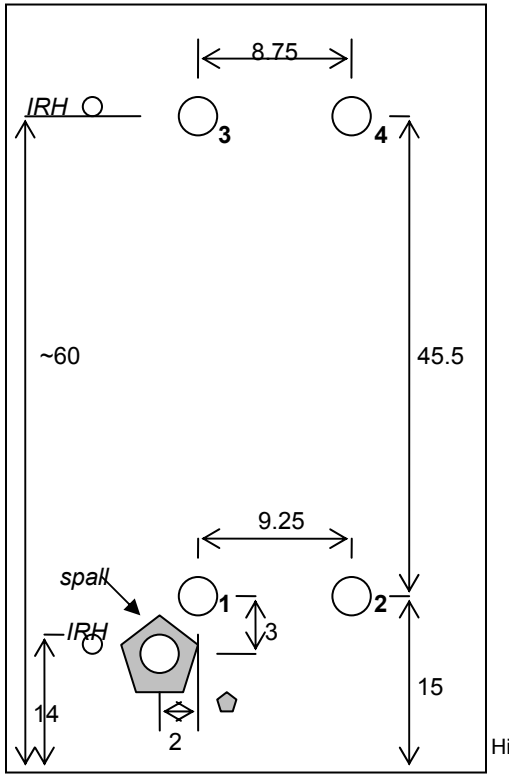

High Tide

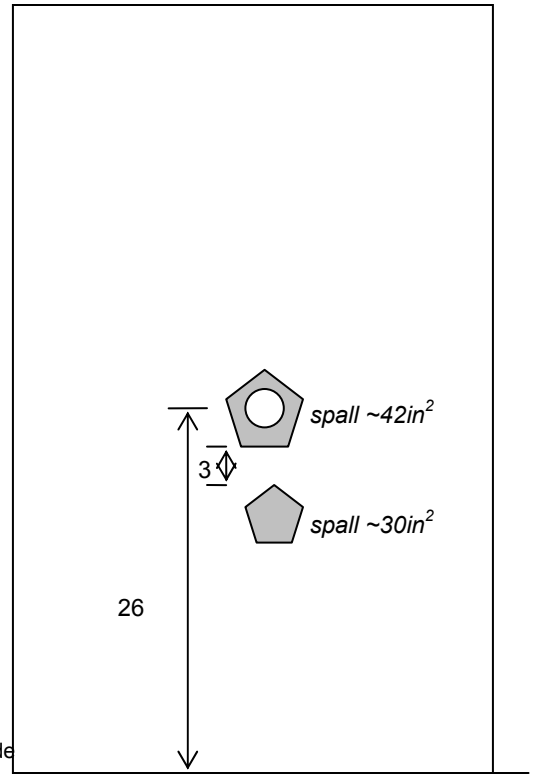

Figure A1 Core Extraction Diagrams (Not to scale. Units in inches unless otherwise noted).

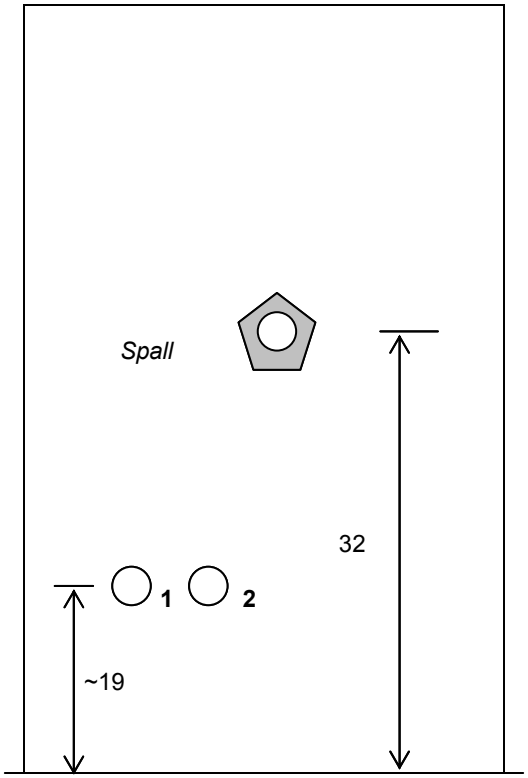

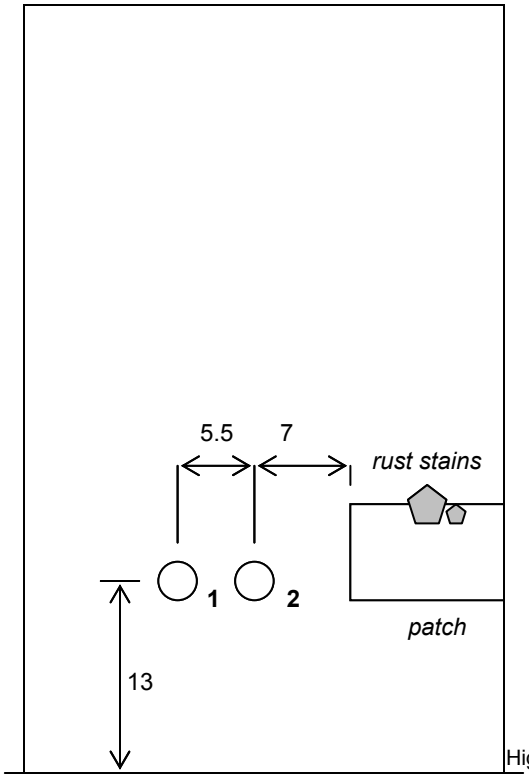

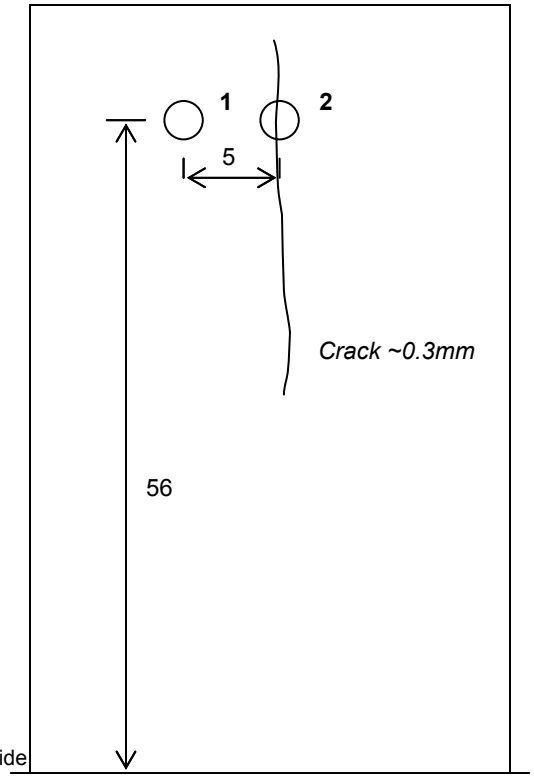

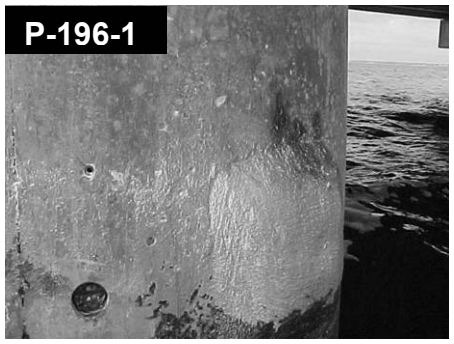

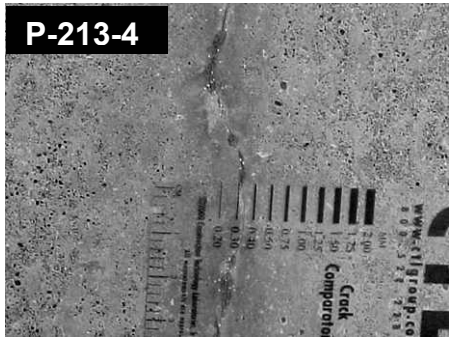

Figure A1 (continued)

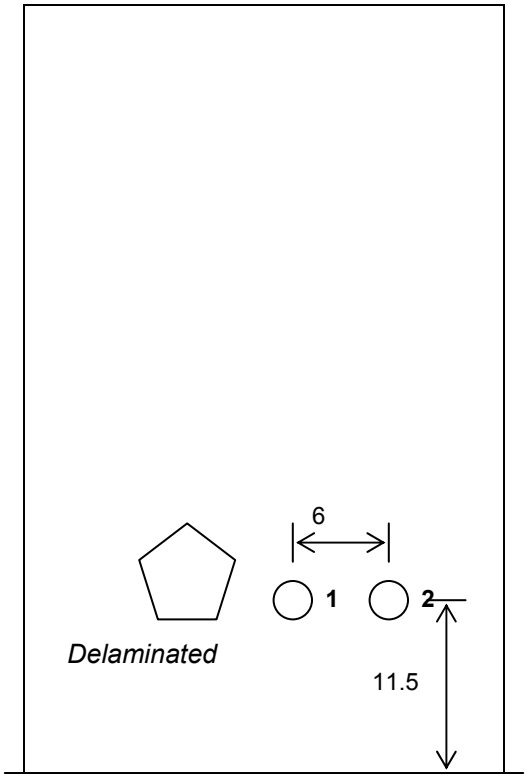

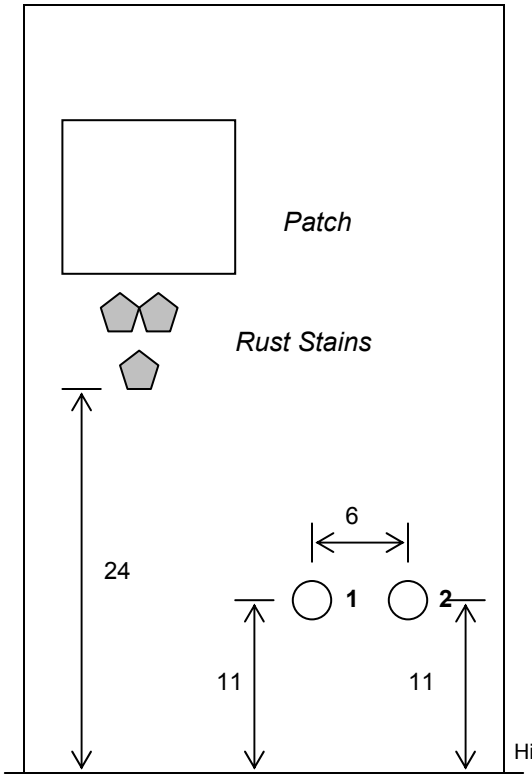

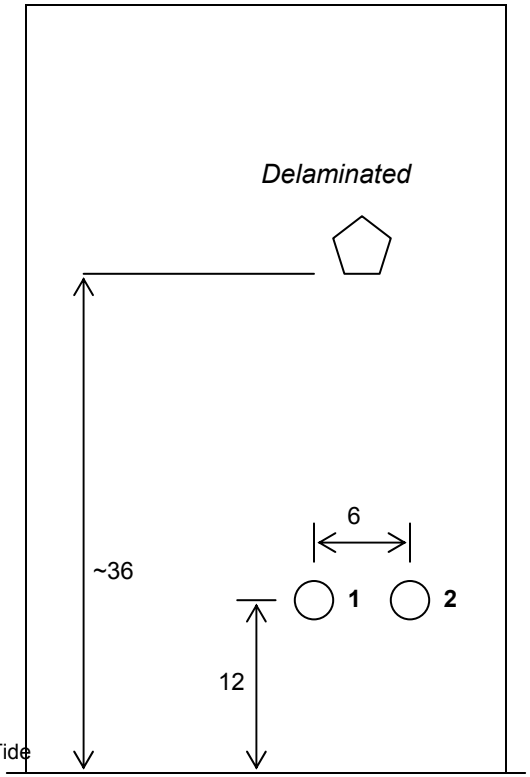

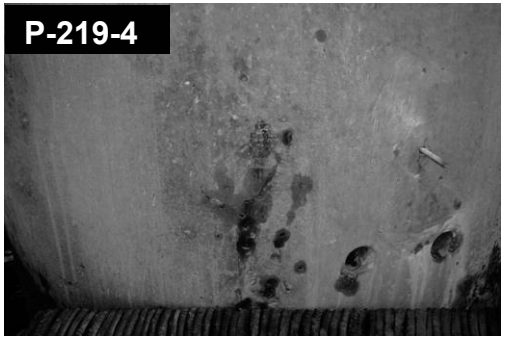

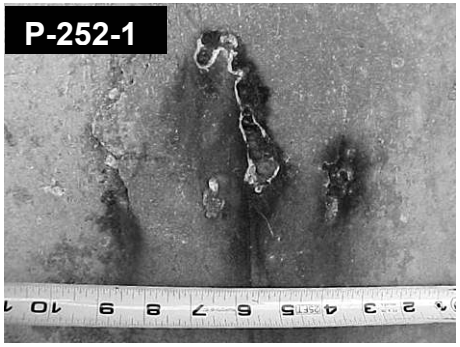

Figure A1 (continued)

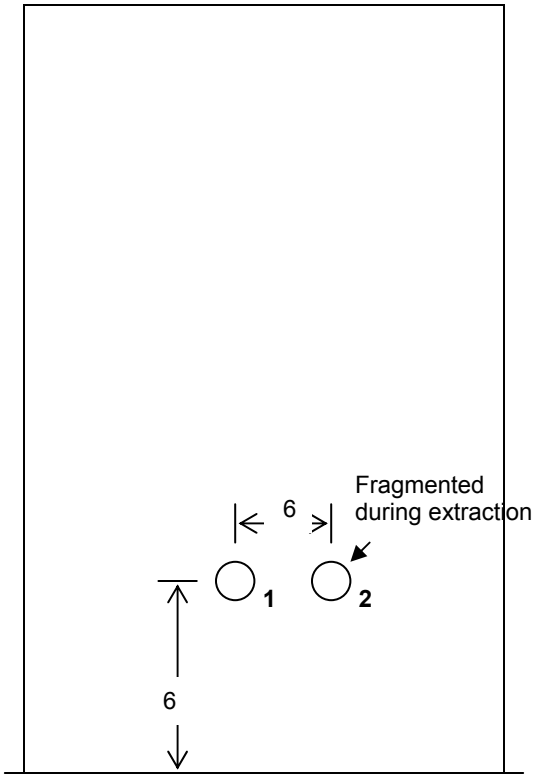

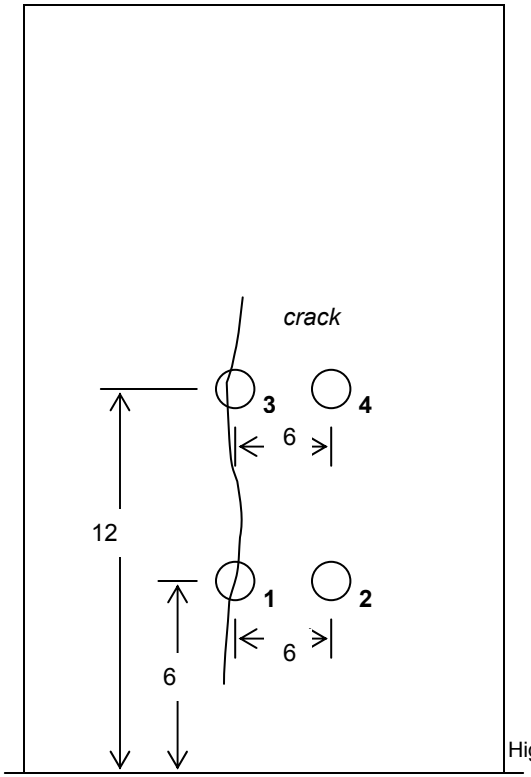

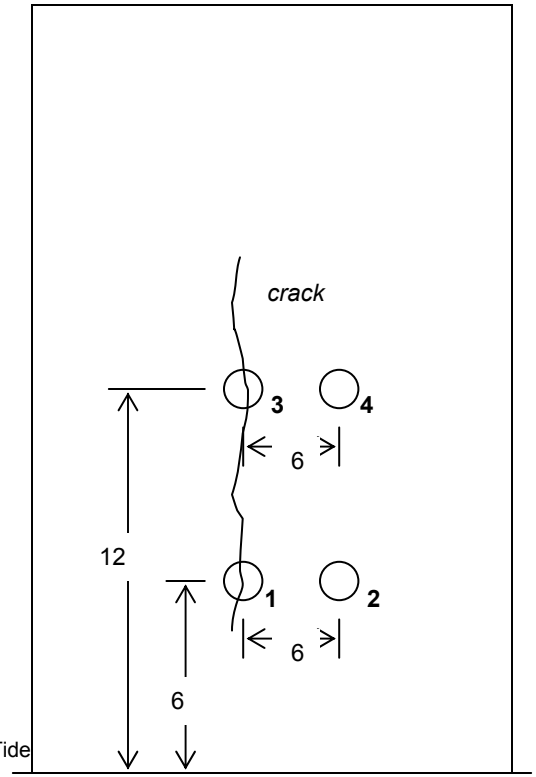

High Tide

152TPN

162WS

163WS

Figure A1 (continued)

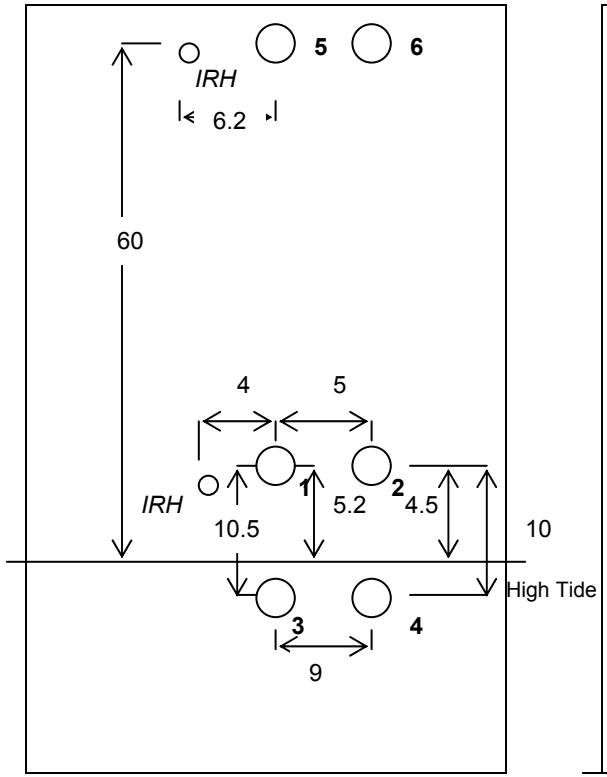

H-8-2

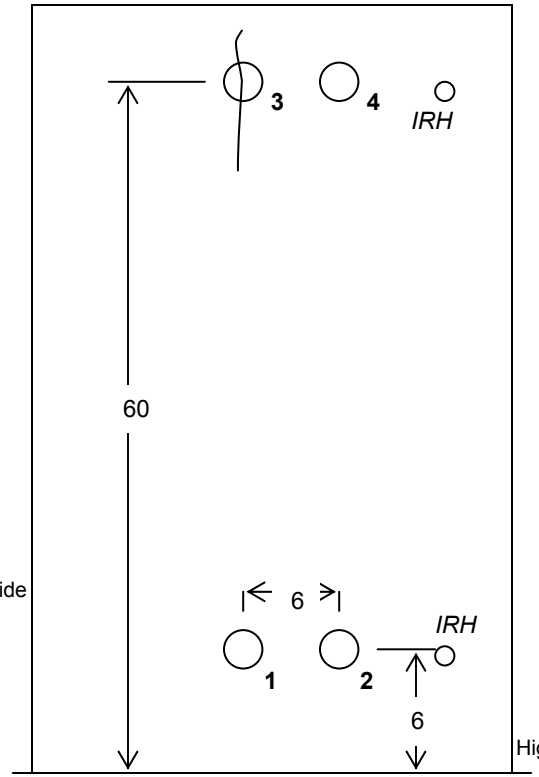

H-29-3

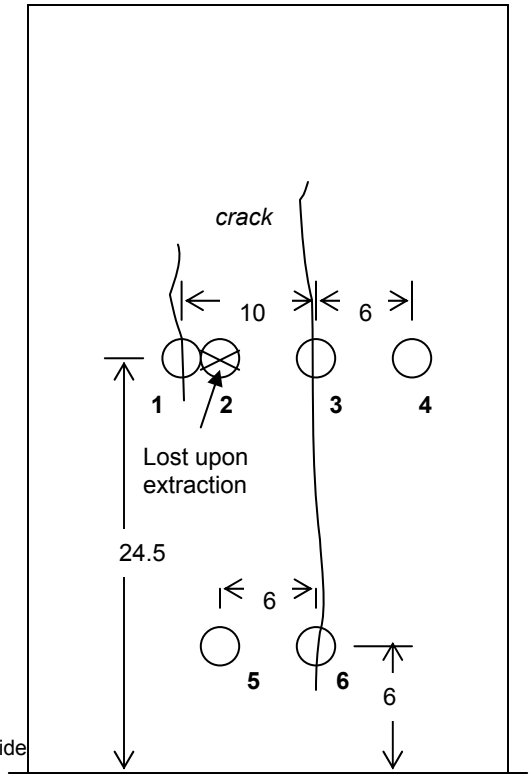

Br-3-2

Figure A1 (continued)

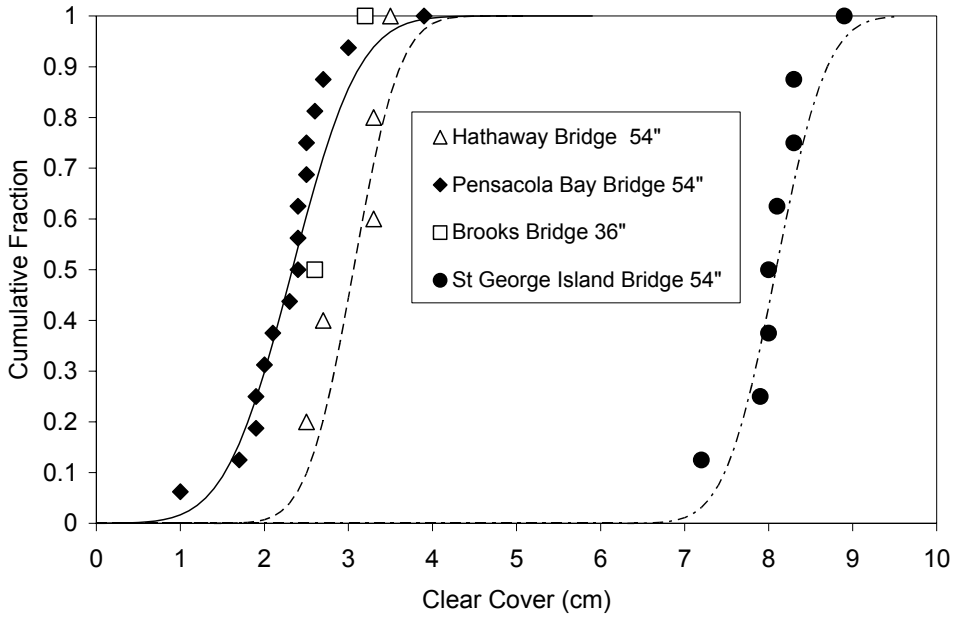

Figure A2 Cumulative fraction of clear cover.

Table A2. Direct clear cover measurements. (cm / *in*)

Bridge	Pile diameter (in.)	Steel Type								
		Spiral Wire			Spacing Bar			Strand		
		Min.	Avg.	Max.	Min.	Avg.	Max.	Min.	Avg.	Max.
Hathaway	54	2.5 *0.98*	3.06 *1.20*	3.5 *1.38*	2.5 *0.98*	2.5 *0.98*	2.5 *0.98*	4.4 *1.73*	4.7 *1.85*	5.0 *1.97*
Pensacola Bay	54	1.0 *0.39*	2.33 *0.92*	3.9 *1.54*	1.6 *0.63*	2.7 *1.06*	3.8 *1.50*	4.7 *1.85*	5.48 *2.16*	6.4 *2.52*
Brooks	36	2.6 *1.02*	2.9 *1.14*	3.2 *1.26*	3.8 *1.50*	3.8 *1.50*	3.8 *1.50*	N.A.		
Escambia Bay [1]	54	1.9 *0.75*	2.64 *1.04*	3.17 *1.25*	N.A.			1.27 *0.5*	3.51 *1.38*	5.08 *2.0*
	36	1.9 *0.75*	2.84 *1.12*	5.08 *2.0*				2.54 *1.0*	4.04 *1.59*	5.71 *2.25*
SGI	54	7.2 *2.83*	8.08 *3.18*	8.9 *3.50*				N.A.		

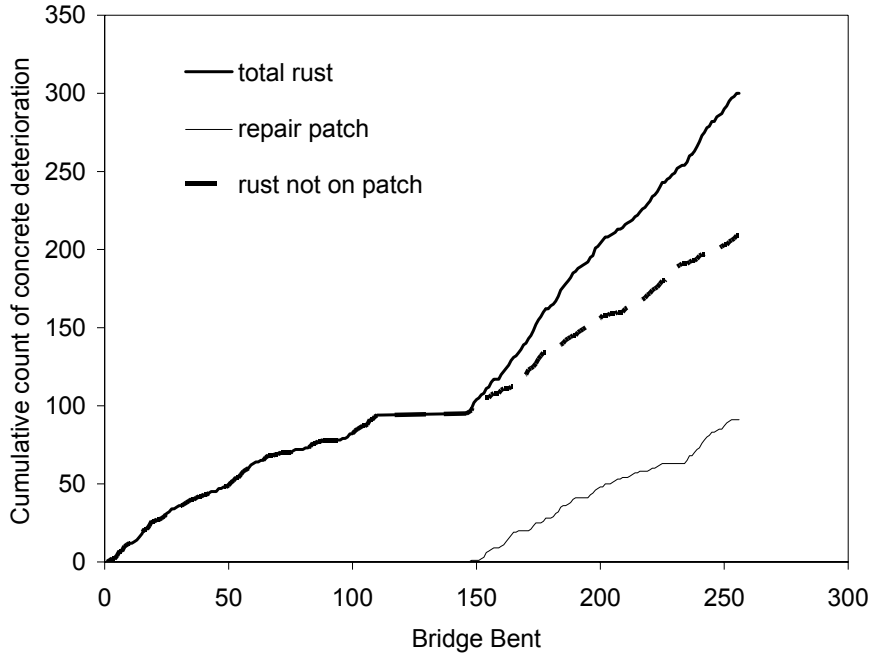

a)

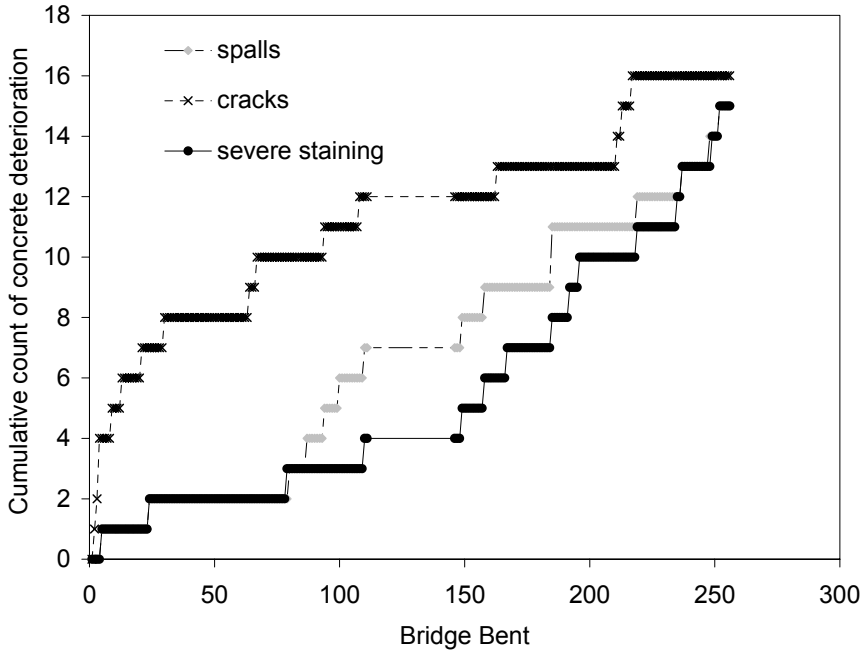

b)

Figure A3 Pensacola Bay Bridge cumulative count of concrete deterioration features. a) rust stain cumulative count. b) spalls, cracks, and severe staining cumulative count.

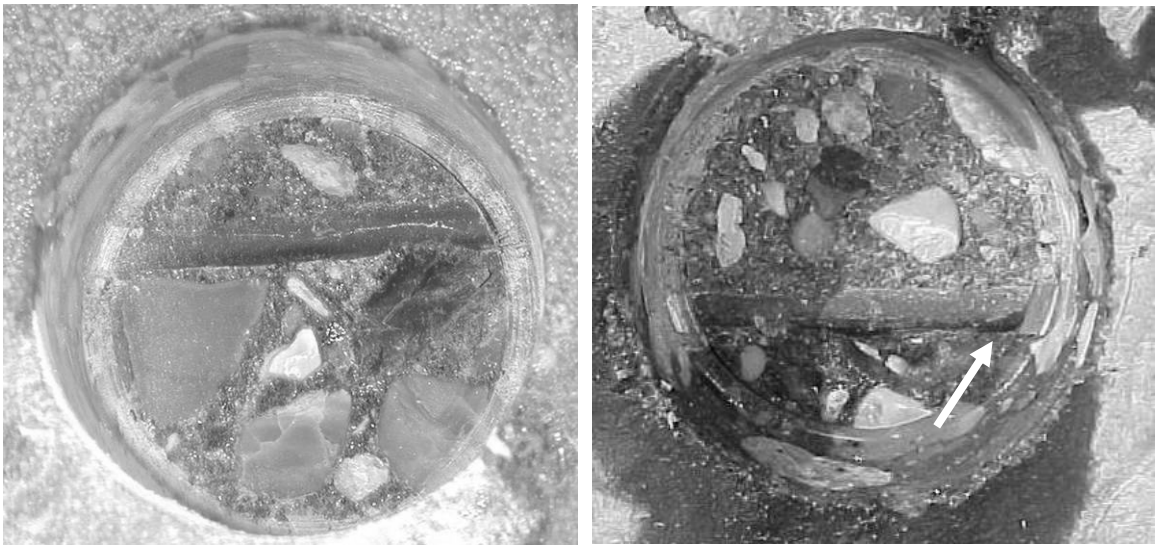

a) b)

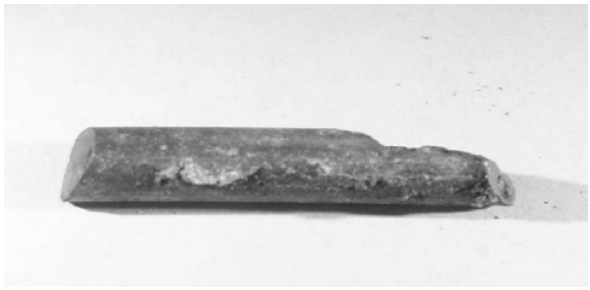

c)

Figure A4 Examples of corrosion ratings. a) Example of spiral wire with No Corrosion (NC) rating. Hathaway Bridge, bottom of core hole, Pile H29-3. b) Example of spiral wire with Light Corrosion (LC) rating. Arrow indicates spot showing minor rust discoloration. Pensacola Bay Bridge, bottom of core hole, Pile P110-2. c) Example of severe corrosion (SC) of ¼ in (0.64 cm) diameter spiral wire from Pensacola Bay Bridge (P149-2) showing appreciable localized loss of cross section at the right end of the wire segment cut out by coring.

.

Appendix III Data Tables

Table A3 Core Properties, Chloride Diffusion Parameters, Projected Chloride Concentration, and Steel Condition

Bridge	Core	Elevation AHT (m)	Crack/ Spall	Crack Width/ Spall Area	Cs (mg_{Cl}/g_{dry})	D (m^2/s)	Projected C (mg/g)[a]		Cover Xc (cm) and Steel Condition[b]		
							Spiral	Bar	Spiral	Bar	Strand
Hathaway	H-8-2-1	0.15			c	c	0.19		3.3 NC	-	-
	H-8-2-2	0.11			11.6	5.92E-14			-	-	-
	H-8-2-3	-0.14			9.75	2.86E-13			-	-	-
	H-8-2-4	-0.14			9.6	9.20E-14	1.16		2.5 NC	-	-
	H-8-2-5	1.52			7.37	3.02E-14	0.08		3.3 NC	-	-
	H-8-2-6	1.52			c	c	0.10		2.7 NC	-	-
	H-29-3-1	0.15			c	c			-	-	5.0 NC
	H-29-3-2	0.15			8.36	8.41E-14	0.25		3.5[e] NC	-	-
	H-29-3-3	1.52	Crack	0.3 mm	4.69	7.41E-14		0.44	-	2.5 LC	4.4 LC
	H-29-3-4	1.52			c	c	0.14		3.5 NC	-	-
Pensacola Bay	P-4-1-1	0.32			7.4	2.40E-13	3.42		1.9 NC	-	-
	P-4-1-2	0.32	Crack	0.3 mm	12.8	4.38E-14	3.14[g]		2 NC	-	-
	P-4-1-3	0.76			8.64	7.79E-14	0.81		2.5 NC	-	-
	P-4-1-4	0.79			c	c	0.93		2.4 NC	-	5.1 LC
	P-110-2	0.30	Spall	$100cm^2$	g	g	1.87		2.7[e] LC	-	-
	P-110-2-1	0.38			c	c	1.26		2.7[e] NC	-	-
	P-110-2-2	0.38			8.35	1.25E-13	1.26		2.7 NC	-	6.4 LC
	P-110-2-4	1.52			9.38	6.07E-14			-	-	6.4 NC

Table A3 (continued)

Bridge	Core	Elevation AHT (m)	Crack/ Spall	Crack Width/ Spall Area	Cs (mg_{cl}/g_{dry})	D (m^2/s)	Projected C (mg/g)[a]		Cover Xc (cm) and Steel Condition[b]		
							Spiral	Bar	Spiral	Bar	Strand
Pensacola Bay	P-149-2	0.66	Spall	270cm^2	g	g	1.90		1.4[f] SC	-	-
	P-185-4	0.81	Spall	100cm^2	g	g	2.04	1.15[d]	2.6[e] SC	3.2[e] NC	-
	P-185-4-1	0.48			14.7	9.6E-14	1.0		3 NC	-	-
	P-185-4-2	0.48			12.3	5.52E-14	1.13		2.1 NC	-	-
	P-196-1-1	0.33			g	g	2.4		2.4 NC	-	-
	P-196-1-2	0.33			g	g	2.22		2.5 NC	-	-
	P-213-4-1	1.42			6.05	8.66E-14	0.10[g]		3.9 NC	-	-
	P-213-4-2	1.42	Crack	0.3 mm	5.0	6.81E-14		0.11	-	3.8 NC	-
	P-219-4-1	0.29			9.47	6.38E-14	0.84		2.3 NC	-	-
	P-219-4-2	0.29			c	c	1.92		1.7 NC	-	-
	P-237-1-1	0.28			7.82	3.12E-13	4.07[g]		2.6 NC	-	-
	P-237-1-2	0.28			c	c	3.25		2.4 NC	-	4.8 NC
	P-252-1-1	0.30			c	c	5.88	4.77[d]	1.0 NC	1.6 NC	4.7 NC
	P-252-1-2	0.28			7.89	3.43E-13	4.08		1.9 NC	-	-
Brooks	Br-3-2-3	0.62	Crack	0.2 mm	3.76	2.81E-13			-	-	-
	Br-3-2-4	0.62			3.66	2.46E-13			-	-	-
	Br-3-2-5	0.15			4.69	1.97E-13	1.18	0.47	2.6 LC	3.8 LC	-
	Br-3-2-6	0.15	Crack	0.2 mm	5.33	2.88E-13	1.28		3.2 NC	-	-

Table A3 (continued)

Bridge	Core	Elevation AHT (m)	Crack/ Spall	Crack width/ Spall Area	Cs (mg_{cl}/g_{dry})	D (m^2/s)	Projected C (mg/g)[a]		Cover Xc (cm) and Steel Condition[b]		
							Spiral	Bar	Spiral	Bar	Strand
St. George Island	162ws1	0.15	Crack	< 0.05 mm	8.96	7.84E-14	0.08		7.9 NC	-	-
	162ws2	0.15			8.22	5.02E-14	0.08		8 NC	-	-
	162ws3	0.30	Crack	< 0.05 mm	6.70	4.39E-14	0.08		8.3 NC	-	-
	162ws4	0.30			6.97	2.87E-14	0.08		8 NC	-	-
	163ws1	0.15	Crack	< 0.05 mm	4.33	5.02E-13	0.08		8.9 NC	-	-
	163ws2	0.15			4.08	3.09E-13	0.08		8.1 NC	-	-
	163ws3	0.30	Crack	< 0.05 mm	4.11	1.74E-13	0.08		7.2 NC	-	-
	163ws4	0.30			4.24	2.40E-13	0.08		8.3 NC	-	-

a. Except as indicated, value listed is projected chloride concentration at depth of spiral wire and/or spacing bar (Xc) at time of inspection using equation (1), listed diffusion parameters, and assuming Co=0.08mg/g. In cores where direct comparison with data in Table A3 was possible, projected value was found to be between those listed for slices immediately above and below steel position. Exceptions are noted under (g).
b. NC- no corrosion. LC- light surface rust. SC- severe corrosion. See Section 3.
c. Diffusion parameter values of companion core extracted at the same elevation. See Figure A1.
d. Cover data taken from companion core.
e. Cover value estimated using spall and core fragments.
f. Assumed typical diffusion parameter values for cores at low elevation. D=1.5e-13m^2/s, Cs=10mg/g.
g Listed value is by linear interpolation from concentrations of slices immediately above and below steel position as listed in Table A4.

Table A4 Chloride Concentration Profile Data and Analysis Results

Bridge	Core	Time in service (yrs)	C (mg/g)	Midpoint (cm)	Thickness (cm)	C_s (mg/g)	D (m^2/s)
Hathaway	H8-2-2	43	11.05	0.10	0.20	11.6	5.92e-14
			7.53	0.55	0.70		
			3.33	1.41	0.64		
			0.90	2.47	1.12		
			0.16	4.22	1.00		
			0.148	5.26	1.69		
	H8-2-3	43	8.8	0.15	0.3	9.75	2.86e-13
			8.41	0.57	0.54		
			7.24	1.24	0.44		
			3.92	2.19	1.07		
			1.57	3.85	1.88		
	H8-2-4	43	9.05	0.15	0.30	9.6	9.20e-14
			6.62	0.57	0.54		
			4.60	1.24	0.44		
			1.46	2.19	1.07		
			0.27	4.00	2.18		
	H8-2-5	43	6.33	0.13	0.25	7.37	3.02e-14
			4.76	0.41	0.32		
			1.31	1.21	0.45		
			0.50	1.86	0.92		
			0.64	3.12	1.21		
	H29-3-2	43	11.46*	0.10	0.20	8.36	8.41e-14
			6.07	0.50	0.61		
			3.72	1.27	0.54		
			1.52	2.23	1.01		
			0.01	3.67	1.48		
	H29-3	43	4.02	.27	.55	4.69	7.41e-14
			2.29	1.07	.66		
			0.31	2.63	.78		
			0.12	3.48	1.22		

Table A4 (continued)

Bridge	Core	Time in service (yrs)	C (mg/g)	Midpoint (cm)	Thickness (cm)	C_s (mg/g)	D (m^2/s)
Pensacola Bay	P4-1-1	43	7.05	0.18	0.35	7.4	2.40e-13
			5.69	0.71	0.72		
			3.89	1.51	0.48		
			2.25	3.00	2.12		
			0.43	4.71	1.31		
			0.18	6.14	1.17		
	P4-1-2	43	12.16	0.10	0.20	12.8	4.38e-14
			8.22	0.47	0.54		
			4.09	1.14	0.44		
			0.99	3.96	2.30		
	P4-1-3	43	8.39	0.10	0.20	8.64	7.79e-14
			6.08	0.47	0.19		
			3.64	1.14	0.45		
			1.48	2.40	1.72		
			0.08	3.98	1.08		
			0.07	5.83	2.25		
	P110-2-2	43	13.09	0.14	0.28	8.35	1.25e-13
			6.48	0.49	0.43		
			4.45	1.23	0.46		
			1.69	2.41	1.73		
			0.25	3.88	1.20		
			0.12	5.38	1.41		
	P110-2-4	43	6.34	0.57	1.13	9.38	6.07e-14
			2.57	1.52	0.78		
			0.18	2.64	1.08		
			0.11	4.71	0.87		
	P185-4-1	43	7.91	0.18	0.35	14.7	9.6e-14
			10.45	0.62	0.54		
			6.39	1.29	0.45		
			1.74	2.70	1.99		
			0.03	4.39	1.40		

Table A4 (continued)

Bridge	Core	Time in service (yrs)	C (mg/g)	Midpoint (cm)	Thickness (cm)	C_s (mg/g)	D (m^2/s)
Pensacola Bay	P185-4-2	43	10.73	0.20	0.40	12.3	5.52e-14
			7.66	0.59	0.38		
			0.38	3.31	1.73		
			0.16	4.90	1.07		
			0.12	6.00	0.75		
	P213-4-1	43	3.75	0.79	1.58	6.05	8.66e-14
			1.30	2.04	0.91		
			0.11	3.22	1.07		
			0.09	4.48	1.07		
	P213-4-2	43	4.23	0.32	0.63	5.0	6.81e-14
			1.98	1.10	0.94		
			0.87	1.98	0.44		
			0.45	2.60	0.44		
			0.33	3.23	0.44		
	P219-4-1	43	7.87	0.30	0.60	9.44	6.61e-14
			4.73	0.87	0.54		
			2.65	1.54	0.44		
			0.19	2.80	1.71		
			0.13	4.91	2.13		
	P237-1-1	43	6.99	0.30	0.60	7.86	3.12e-13
			5.85	0.87	0.54		
			5.00	1.54	0.44		
			3.33	2.80	1.71		
			0.59	4.38	1.07		
			0.16	6.25	2.29		
	P252-1-2	43	6.31	0.23	0.45	7.89	3.43e-13
			6.80	0.72	0.54		
			4.51	1.39	0.45		
			3.79	2.34	1.08		
			2.03	3.61	1.08		
			0.54	5.71	2.73		

Table A4 (continued)

Bridge	Core	Time in service (yrs)	C (mg/g)	Midpoint (cm)	Thickness (cm)	C_s (mg/g)	D (m^2/s)
Brooks	Br3-2-3	39	5.84*	0.14	0.27	3.76	2.81e-13
			3.40	0.54	0.54		
			2.12	1.21	0.44		
			1.59	2.16	1.07		
			0.86	3.84	1.92		
	Br3-2-4	39	6.83*	0.10	0.20	3.66	2.46e-13
			3.20	0.39	0.39		
			2.46	1.09	0.63		
			1.46	2.07	0.95		
			0.66	3.73	1.99		
	Br3-2-5	39	10.22*	0.10	0.20	4.69	1.97e-13
			4.05	0.47	0.43		
			2.52	1.15	0.50		
			1.54	2.43	1.47		
	Br3-2-6	39	8.77*	0.13	0.25	5.33	2.88e-13
			4.45	0.54	0.58		
			3.51	1.27	0.50		
			1.44	2.97	2.54		
			0.59	4.89	1.30		
St. George Island	152TPN-2	2.18	9.48	0.06	0.11	10.3	2.26e-13
			8.32	0.16	0.10		
			6.67	0.28	0.13		
	162WS-1	2.6	7.75	0.04	0.08	8.96	7.84e-14
			6.38	0.13	0.09		
			4.76	0.23	0.11		
			2.81	0.33	0.10		
			1.57	0.42	0.09		
			1.18	0.58	0.23		
			0.65	1.08	0.61		

Table A4 (continued)

Bridge	Core	Time in service (yrs)	C (mg/g)	Midpoint (cm)	Thickness (cm)	C_s (mg/g)	D (m^2/s)
St. George Island	162WS-2	2.6	7.00	0.05	0.10	8.22	5.02e-14
			5.15	0.15	0.09		
			3.37	0.24	0.09		
			1.90	0.33	0.08		
			0.61	0.46	0.20		
			0.25	0.93	0.56		
	162WS-3	2.6	5.83	0.05	0.09	6.70	4.39e-14
			3.87	0.14	0.10		
			2.33	0.24	0.10		
			1.28	0.34	0.09		
			1.01	0.44	0.12		
			0.48	0.61	0.21		
			0.52	1.18	0.56		
	162WS-4	2.6	5.58	0.05	0.10	6.97	2.87e-14
			3.94	0.15	0.10		
			1.67	0.25	0.10		
			0.75	0.35	0.10		
			0.27	0.49	0.17		
			0.11	1.09	0.51		
	163WS-1	2.14	4.03	0.07	0.13	4.33	5.02e-13
			3.81	0.18	0.09		
			3.25	0.29	0.12		
			2.79	0.41	0.12		
			1.82	0.73	0.33		
			0.45	1.20	0.25		
			0.09	8.47	0.40		
	163WS-2	2.14	3.76	0.05	0.10	4.08	3.09e-13
			3.28	0.17	0.14		
			2.89	0.31	0.14		
			2.01	0.46	0.10		
			0.82	0.62	0.23		
			0.30	1.09	0.36		
			0.08	8.12	0.30		

Table A4 (continued)

Bridge	Core	Time in service (yrs)	C (mg/g)	Midpoint (cm)	Thickness (cm)	C_s (mg/g)	D (m^2/s)
St. George Island	163WS-3	2.14	3.77	0.06	0.12	4.11	1.74e-13
			3.34	0.17	0.12		
			2.41	0.28	0.10		
			1.77	0.38	0.10		
			1.23	0.55	0.24		
			0.54	1.00	0.32		
			0.14	8.30	0.29		
	163WS-4	2.14	3.90	0.05	0.09	4.24	2.4e-13
			3.57	0.13	0.07		
			2.75	0.22	0.11		
			2.26	0.33	0.10		
			1.66	0.48	0.20		
			0.99	0.67	0.19		
			0.68	0.87	0.21		
			0.35	1.07	0.20		
			0.08	8.29	0.25		
	1404-3	1.83	5.45	0.052	0.10	5.95	1.44e-13
			4.19	0.15	0.08		
			3.19	0.23	0.09		
			2.49	0.32	0.08		
	1404-4	1.80	8.50	0.03	0.07	9.53	1.09e-13
			6.48	0.13	0.12		
			4.770	0.21	0.12		
			4.33	0.28	0.09		
			2.72	0.39	0.14		
	943-3	1.89	7.39	0.077	0.94	8.37	4.03e-13
			7.14	1.45	1.03		
			6.04	2.49	0.75		
			5.04	3.47	1.21		
			4.36	4.55	1.25		

* Data for sample closest to surface not used to fit chloride concentration and depth to Eq. 1 (see Section 4.3).

Table A5 Field Potential Mapping

Bridge	Pile	Reinforcement	Elevation AHT (ft)	E vs CSE (mV)		Remarks
Hathaway	H-8-2-1	wire	Water	-361	-376	
			0	-151	-167	
			1	-143	-160	
			2	-40	-68	
			3	73	38	
			4	172	141	
			5	191	160	
			6	180	147	
	H-29-3-1	strand	Water	-656	-625	
			0	-426	-389	
			1	-328	-312	
			2	-251	-240	
			3	-154	-151	
			4	-111	-100	
			5	-103	-100	
			6	-90	-82	
	H-29-3-2	wire	Water	-425	-425	
			0	-245	-238	
			1	-179	-194	
			2	-116	-113	
			3	-14	-11	
			4	9	9	
			5	40	40	
			6	72	55	
	H-29-3-3	spacing rebar	Water	-520	-524	Minor rusting on rebar. Coincident with crack.
			0	-376	-382	
			1	-264	-260	
			2	-161	-161	
			3	-96	-140	
			4	-99	-96	
			5	-60	-68	
			6	-3	-12	

Table A5 (continued)

Bridge	Pile	Reinforcement	Elevation AHT (ft)	E vs CSE (mV)		Remarks
Hathaway	H-29-3-4	wire	Water	-530	-508	
			0	-364	-348	
			1	-240	-244	
			2	-181	-187	
			3	-120	-127	
			4	-111	-108	
			5	-88	-69	
			6	-43	-40	
Pensacola Bay	P-4-1-1	wire	0	-535		
			1	-499		
			2	-420		
			3	-276		
			4	-240		
	P-4-1-2	strand	0	-379		
			1	-306		
			2	-260		
			3	-167		
			4	-112		
	P-4-1-3	wire	0	-302	-331	
			1	-282	-282	
			2	-269	-248	
			3	-157	-150	
			4	-75	-119	
	P-4-1-4	strand	0	-380		
			1	-299		
			2	-285		
			3	-148		
			4	-130		
	P-110-2	wire	0	-270	-250	Core extracted from spalled concrete. Corroded wire.
			1	-301	-256	
			2	-182	-160	
			3	-134	-79	
			4	-100	-54	
			5	-5	7	

Table A5 (continued)

Bridge	Pile	Reinforcement	Elevation AHT (ft)	E vs CSE (mV)		Remarks
Pensacola Bay	P-110-2-1	wire	0	-263		
			1	-283		
			2	-129		
			3	-70		
			4	-84		
			5	3		
	P-110-2-2	wire	0	-270		
			1	-179		
			2	-134		
			3	-87		
			4	-84		
			5	-52		
	P110-2-2	strand	0	-333	-240	-330
			1	-232	-87	-247
			2	-73	-14	-184
			3	-17	-143	-152
			4	-38	-104	-116
			5	-109	-124	-129
	P-149-2	wire	Water	-456		Core extracted from spalled concrete. Corroded wire.
			0	-325		
			1	-230		
			2	-214		
			3	-160		
			4	-69		
			5	-85		
	P-185-4	spiral	Water	-590		Core extracted from spalled concrete. Corroded wire.
			0	-402	-434	
			1	-343	-396	
			2	-420	-462	
			3	-238	-342	
			4	-334	-400	
			5	-187	-194	

Table A5 (continued)

Bridge	Pile	Reinforcement	Elevation AHT (ft)	E vs CSE (mV)		Remarks
Pensacola Bay	P-185-4	Strand				Core extracted from spalled concrete. Corroded wire.
			Water	-585		
			0	-404	-401	
			1	-352	-342	
			2	-404	-396	
			3	-241	-248	
			4	-335	-312	
			5	-197	-196	
	P-213-4-1	wire	Water	-530		
			0	-448		
			1	-290		
			2	-269		
			3	-205		
			4	-207		
			5	-178		
			6	-154		
	P-213-4-2	strand	Water	-530		
			0	-444		
			1	-305		
			2	-275		
			3	-262		
			4	-227		
			5	-187		
			6	-181		
	P-219-4-1	wire	0	-409		
			1	-381		
			2	-298		
			3	-260		
			4	-240		
	P-237-1-1	wire	Water	-490	-489	
			0	-410	-380	
			1	-290	-302	
			2	-196	-214	
			3	-138	-145	
			4	-115	-135	

Table A5 (continued)

Bridge	Pile	Reinforcement	Elevation AHT (ft)	E vs CSE (mV)		Remarks
Pensacola Bay	P-252-1-1	wire	Water	-460		
			0	-417		
			1	-351		
			2	-180		
			3	-150		
			4	-109		
	P-252-1-1	spacing rebar	0	-365		
			1	-287		
			2	-70		
			3	-109		
			4	-119		
	P252-1-1	strand	Water	-500		
			0	-42		
			1	-362		
			2	-194		
			3	-37		
			4	-212		
	P-252-1-2	wire	Water	-499		
			0	-324		
			1	-160		
			2	-84		
			3	-153		
			4	-44		
Brooks	Br-3-2-5	spiral	Water	-684	-693	
			0	-638	-645	
			1	-359	-395	
			2	-109	-154	
			3	-116	-153	
			4	-69	-92	
	Br-3-2-5	spacing rebar	Water	-670	-693	
			0	-624	-643	
			1	-376	-378	
			2	-162	-153	
			3	-140	-125	
			4	-129	-95	

Table A5 (continued)

Bridge	Pile	Reinforcement	Elevation AHT (ft)	E vs CSE (mV)		Remarks
Brooks	Br-3-2-6	spiral	Water	-640	-643	
			0	-584	-549	
			1	-337	-300	
			2	-93	-81	
			3	-50	-26	
			4	-30	-8	
St. George Island	152TPN-2	wire	Water	-489		
			0	-360		
			1	-241		
			2	-168		
			3	-68		
			4	-55		
			5	-72		
	162WS-1	wire	Water	-567		
			0	-415		
			1	-267		
			2	-159		
			3	-110		
			4	-153		
			5	-155		
	162WS-4	wire	Water	-568		
			0	-382		
			1	-241		
			2	-134		
			3	-134		
			4	-163		
			5	-174		
	163WS-3	wire	Water	-410		
			0	-382		
			1	-275		
			2	-232		
			3	-131		
			4	-68		
			5	-57		

Table A5 (continued)

Bridge	Pile	Reinforcement	Elevation AHT (ft)	E vs CSE (mV)		Remarks
St. George Island	163WS-4	wire	Water	-407		
			0	-405		
			1	-321		
			2	-148		
			3	-136		
			4	-42		
			5	-42		

Table A6 Field IRH Measurements

Bridge	Pile	Elevation AHT (ft)	Time	IRH (%)		Temperature (°C)	Remarks
				Measured	Calibrated		
Hathaway	H-8-2	0.44	10:30	82.8	84.7	15	Sealed probe into fitting.
			10:31	78.9	80.6	16.5	
			10:33	76.3	77.9	17.2	
			10:39	74.6	76.1	17	
			10:47	73.9	75.4	16.7	
			10:52	73.5	75.0	16.6	
			11:00	72.9	74.4	16.5	
			11:12	72.1	73.5	16.4	
			11:19	71.8	73.2	16.4	
			11:29	71.4	72.8	16.3	Ambient conditions 85%RH 15°C
	H-8-2	5	10:31	83.5	75.1	15.1	Sealed probe into fitting.
			10:33	82.3	73.7	15.1	
			10:39	81.1	72.4	15.2	
			10:47	79.9	72.1	15.1	
			10:52	79.6	71.7	14.9	
			11:00	79.2	71.1	14.9	
			11:12	78.7	71.0	15	
			11:19	78.6	70.7	15	
			11:29	78.3	70.6	15	Ambient conditions 85%RH 15°C
	H-29-3	0.5	11:41	74.9	76.4	14.9	Sealed probe into fitting.
			11:42	83.6	85.6	14.8	
			11:45	84	86.0	14.5	
			11:50	84.6	86.6	14.3	
			12:00	84.9	86.9	14.3	
			12:05	84.8	86.8	14.4	
			12:10	84.8	86.8	14.5	
			12:15	84.8	86.8	14.5	
			12:20	84.7	86.7	14.6	
			12:26	84.7	86.7	14.6	
			12:30	84.7	86.7	14.7	
			12:35	84.6	86.6	14.7	

Table A6 (continued)

Bridge	Pile	Elevation AHT (ft)	Time	IRH (%)		Temperature (°C)	Remarks
				Measured	Calibrated		
Hathaway	H-29-3	5	11:41	85.1	79.0	15.7	Sealed probe into fitting.
			11:42	83.5	76.4	15.1	
			11:45	82.6	75.4	14.7	
			11:50	81.2	73.9	14.7	
			12:00	80.5	73.9	13.0	
			12:05	79.9	73.3	14.7	
			12:10	79.4	72.7	14.8	
			12:15	79.3	72.6	15.0	
			12:20	79	72.3	15.0	
			12:26	78.5	71.7	15.1	
			12:30	78.5	71.7	15.1	
			12:35	78.4	71.6	15.3	
Pensacola Bay	P110-2	1.17	4:00	-	-	-	Sealed probe into fitting.
			4:02	71	66.7	18.7	
			4:04	71.6	67.4	18.8	
			4:06	72.2	68.1	18.7	
			4:10	73.2	69.3	18.8	
			4:26	73.5	69.6	19.3	
			4:33	73.7	69.9	19.4	
			4:41	73.7	69.9	19.4	
			4:46	73.8	70.0	19.4	
			4:51	73.9	70.1	19.4	Ambient 63.7%RH 19.6°C
	P110-2	5	4:02	-	-	-	Sealed probe into fitting.
			4:04	68.6	64.2	19.7	
			4:06	69.4	65.2	19.6	
			4:10	70.3	66.3	19.3	
			4:26	71.1	67.2	19.4	
			4:33	71.3	67.5	19.4	
			4:41	71.4	67.6	19.5	
			4:46	71.5	67.7	19.5	
			4:51	71.5	67.7	19.4	Ambient 63.7%RH 19.6°C

Unit Conversions Table

CONVERSION FACTORS, US CUSTOMARY TO METRIC UNITS

Multiply	by	to obtain
inch	25.4	mm
foot	0.3048	meter
square inches	645	square mm
cubic yard	0.765	cubic meter
pound/cubic yard	0.593	kg/cubic meter
$inch^2$/year	$2.046\ 10^{-11}$	m^2/sec
gallon/cubic yard	4.95	liter/cubic meter
standard cubic feet/hour	466.67	ml/minute
ounces	28.35	gram
pound	0.454	kilogram
pound (lb)	4.448	newtons
kip (1000 lb)	4.448	kilo newton (kN)
pound/in^2	0.0069	MPa
kip/in^2	6.895	MPa
ft-kip	1.356	kN-m
in-kip	0.113	kN-m